RICE UNIVERSITY

Studying the Interactions of Biomacromolecular Assemblies with Surfaces Using the Microcantilever Sensor and Quartz Crystal Microbalance

By

Kai-Wei Liu

A THESIS SUBMITTED
IN PARTIAL FULFILLMENT OF THE
REQUIREMENTS FOR THE DEGREE

Doctor of Philosophy

APPROVED, THESIS COMMITTEE:

Sibani Lisa Biswal, Assistant Professor
Chemical and Biomolecular Engineering

Laura Segatori, Assistant Professor
Chemical and Biomolecular Engineering

Robert Raphael, Associate Professor
Bioengineering

Huey W. Huang, Professor Physics & Astronomy

HOUSTON, TEXAS
MAY 2011

ABSTRACT

This thesis uses surface sensitive tools to characterize the effect of a solid surface on immobilized biomacromolecules. This includes understanding how adhesion to the surface can change the affinity of these macromolecules to small molecules compared to bulk studies. Two classes of immobilized biomacromolecules, the supported lipid bilayer (SLB) and the *Lac* repressor protein (LacI), are characterized using microcantilever sensors and quartz crystal microbalance with dissipation (QCM-D).

The first part of this thesis reports the use of microcantilever beams, an ultrasensitive sensor for measuring the surface free energy changes on a substrate induced by molecular adsorptions, to probe the interaction between a solid surface and a phospholipid bilayer. This sensing method integrates two well-developed techniques: solid-supported lipid bilayers (SLBs) and the microcantilever (MC) sensors. Studying the adsorption free energy of lipid bilayers on a solid surface allows better characterizing of the formation and stability of SLBs. Microcantilever converts the Gibbs free energy change taking place on its surface into a mechanical deformation. As molecules physisorb or chemisorb onto the surface of the microcantilevers, the microcantilevers bend, either due to induced compressive or tensile stresses, which result from the surface free energy change. By monitoring the deflection values of the microcantilevers, the real-time surface free energy change during the SLB formation can be detected. This thesis has led to the development of a novel biosensor – lipid membrane coated microcantilevers – to detect the adsorption, insertion, aggregation and solubilizing effect of membrane-active substances, such as surfactants and peptides, on the phospholipid membranes.

To better characterize the surface free energy, SLBs doped with charged lipids or cholesterol are shown to alter the surface free energy. We can predict this change in surface free energy using a thermodynamic model. Application of this membrane-coated cantilever is put into use for detecting how amphiphilic molecules interact with SLBs, as well as for probing the abrupt conformational change of SLBs during a temperature induced phase-transition. This study systematically demonstrates various usage aspects of microcantilever to characterize the SLBs, and how this technique may advance the biophysical knowledge of the lipid membrane, one of the essential building blocks of life.

The second part of this thesis reports the use of both microcantilever sensors and QCM-D to measure the adsorption free energy and mass of a model protein, the *Lac* repressor (LacI), and compare how a modified T334C mutant that includes a cysteine group to orient the protein on the gold surface through a covalent sulfur bonds retains its binding capabilities over that of wild type LacI.

The main challenge of this work is to unravel how the adsorption of biomacromolecules at the solid/liquid interface leads to surface free energy changes and ultimately changes the stress of the underlying solid surface (the cantilever). The uses of microcantilever sensors and QCM to probe the interactions that take place on SLBs and surface-bound proteins have the advantage of being a sensitive, real-time, and label-free technique.

Acknowledgement

I would like to thank my Ph.D. advisor, Dr. Sibani Lisa Biswal, for her guidance on my study in the past four years. She provides me a research environment of abundant resources, not only the hardware needed to realize new ideas but also constant opportunities to widen my horizon in national and international conferences. I have learned from my advisor how to approach a problem in my experiments and how to do good presentations. Many thanks to my committee members, Dr. Laura Segatori, Dr. Robert Raphael and Dr. Huey W. Huang, for their kind discussions about my research and giving me advices on my thesis.

During my Ph.D. study, I have been helped and stimulated to brainstorm by many professors in Rice. Dr. Marc Robert has always encouraged me in many occasions and given clear and useful advices. Dr. Huey Huang helped me to figure out the problems in the field of lipid membrane physics in my research. Dr. Robert Raphael taught me in person how to make lipid vesicles, when my research is still a seed idea. Dr. Kathleen Matthews gave insights and possible solutions to the experiments of the interdisciplinary project on studying *Lac* repressor. Dr. Qilin Li assisted me in using the QCM-D equipment. Special thank to Dr. Janice Hewitt, who spent a lot of time training me how to write good research articles in English. This is a take-home skill that I can continue to sharpen for the rest of my life.

I want to thank my labmates for bringing happiness and spice to my life in the group. They are Dr. Madhuri Tahker, Dr. Yoon-Su Choi, Kung-Po Chao, Julie Byrom, Jinghui Wang, Dichuan Li, Gautam Kini, Kun Ma, Charles Conn and Di Du. I have also had a good time with several alumni group members, Weijia Xie and Nan Du. I have many good friends in other groups in Rice, who share ideas, update what is new in research, and help me a lot in my experiments.

They are Dr. Hitesh Bagaria, Dr. Shyam (Benny) Benegal, Dr. Yu-Lun Fang, Dr. Jie Yu, Dr. Yen Sun, Dr. Jia Xu, Chun-Jen Lin, and Dr. Ping Zhang.

During the five years of study in Rice, I appreciate the warm support from my family in Taiwan and from my granduncle and grandaunt right here in Houston. I want to thank my future husband Hsi-Chun Liu, who has understood me and accompanied me for more than seven years. The completion of this Ph.D. degree is a great effort made not only by myself but also by so many people who support me and care about me. I sincerely dedicate this thesis to my dear family and friends.

Kai-Wei Liu

2011 May, Rice University

Table of Contents

List of Tables

List of Figures

Chapter 1

Introduction

1.1.Objectives

Immobilization of biomolecules on solid surfaces is of considerable interest because it is required for a number of important biotechnology applications. These applications include purifying molecules by selective binding surface-grafted antibodies, access to analytical assays that are performed at liquid-solid or gas-solid interfaces, and modifying either inorganic or organic materials to be biocompatible. [1] Lab-on-a-chip and microarray devices are practical applications of biomolecular immobilization (this includes DNA, protein and lipid membrane) for rapid disease diagnostics [2-4] However, immobilizing the biomolecules without losing their function is a critical issue. For example, surface–bound proteins have different conformations from free proteins in solution. This is due to the protein preferential interacting with solid surfaces through electrostatic, hydrophobic, and entropic forces, which cause the protein to lose its native folded structure. Fixing biomolecules onto solid surfaces while maintaining their native function remains a contemporary challenge to many biosensing platforms. To overcome these challenges, fast and facile tools to study the properties of the immobilized biomolecular layer are of great interest. The main objective of this thesis is to understand how surface-sensitive sensors, which are commonly used for detecting and characterizing biomolecules, influence the biophysical properties of these surface-bound molecules. In particular, this thesis focuses on the microcantilever and the quartz-crystal microbalance with dissipation (QCM-D) to study two major macromolecular assemblies: lipid membranes and proteins.

Supported lipid bilayers (SLBs) are an extensively studied topic of macro-biomolecular

immobilization onto solid surfaces due to their ability to form a model membrane and offer biocompatibility to a surface. SLBs exhibit properties that are different from free–standing lipid bilayers but are stable when adsorbed on solid surfaces. SLBs oftentimes remain fluid, similar to that of a free-standing lipid bilayer, thanks to a lubrication water layer between the SLB and the solid surface. Efforts have been made to characterize the lipid film itself as well as the SLB–surface interactions. One objective of this thesis is to use the microcantilever sensors to probe the SLB–surface interactions. Further studies will focus on the ability to characterize the interactions between membrane-active substances and SLBs that take place on the microcantilever sensor surfaces. The second topic covered in this thesis will be the structure of a DNA binding protein, *Lac* repressor, which has importance in metabolism of lactose in bacteria *Escherichia coli* (*E. coli*). One of the objects of the thesis is to use surface-sensitive tools to examine the denaturing and surface binding process of the *Lac* repressor, as well as *Lac* repressor's ability to bind DNA when it is immobilized on solid surfaces.

1.2. Outline

The first topic of this thesis is integrating the knowledge of SLBs with microcantilever sensors. The original idea of using microcantilevers for sensing applications can be traced back to observations on the cantilever beams in the force spectroscopy setup in the 1980s. Previous literature of the microcantilevers and the supported lipid bilayers, are reviewed in Chapter 2 and Chapter 3, respectively. The working principles and the development of the microcantilever as a chemical and biological sensor since the invention in 1980s will be introduced. The original work of the supported lipid bilayer (SLB) platform is reviewed in Chapter 3. SLBs share most of the fundamentals with the free-standing lipid bilayer, thus a good understanding of both the

biological and model membrane is necessary.

Integrating the SLBs with microcantilever sensors is the major contribution made in this thesis. Chapter 4 reports the use of free-standing microcantilever beams to probe the interactions between a solid surface and a phospholipid bilayer. The observed deflection of a cantilever is related to the changes in the surface free energy of the solid surface that supports the phospholipid bilayer. A systematical characterization of factors that influence the bending, such as electrostatic, hydrophobic and other intermolecular interactions between the bilayer with the substrate, are examined. In addition, this chapter explains how the adsorption of lipid membranes can compress the microcantilevers. The work presented in Chapter 4 is published in *Analytical Chemistry*. [5]

Chapter 5 presents a method to characterize the phase transitions in SLBs using microcantilever sensors, similar to calorimetry. By ramping the temperature near the transition temperature of the lipid film adsorbed on the microcantilevers, detection of the gel-liquid phase transition temperatures (T_m) of a supported lipid bilayer (SLB) and monolayer is possible. During the phase transition, the supported lipid membrane undergoes a conformational change in which the lipid alkyl chains transform between an ordered and disordered phase. This process is accompanied with changes in free energy which leads to changes in the surface stress of the underlying solid support. Phase transitions of both SLBs and Langmuir-Blodgett transferred lipid monolayer are measured.

After a good understanding of the lipid membrane-coated microcantilever is obtained, a practical application for probing interactions between the SLBs and other membrane-active substances is demonstrated in Chapter 6 and Chapter 7. Specifically in Chapter 6, a group of simple amphiphilic surfactants known for intercalating into lipid membranes, lys-lipids, is used.

In Chapter 7, an alpha helical peptide, PEP1, which has been proved to be an effective drug for inhibiting Hepatitis C Virus (HCV) infection, is used. These two amphipathic molecules interact with SLBs and cause the SLB-coated microcantilevers to experience compressive or tensile stresses. These stress results elucidate the interactions between the SLB and these small molecules. These two chapters demonstrate that the microcantilever sensor is a useful surface-sensitive tool for sensing how amphipathic molecules insert and disrupt lipid membranes supported on solid surfaces.

In addition to the SLBs, surface bound proteins at solid–liquid interface are another immobilized biosystem that is challenging to characterize. In addition to microcantilever, which is a stress sensor useful for detecting thin film stress, another useful biosensor based on mass, QCM-D, is chosen to study the surface–immobilization process of biomolecules. To highlight the novelty and high sensitivity of QCM-D in recognize the minute differences of biomolecules' structures and function, a protein which involves in the lactose metabolism, the *Lac* repressor (*LacI*), is tested. In particular, surface binding behavior of wild-type and a mutant of the *LacI* are compared. The mutant is a *LacI* analogue which has a designed to have a covalent binding site by which to orient the protein so that we can prevent the analogue from being denatured. The "covalent stabilization" strategy allows selective reaction with ligands. This work is collaboration with Jia Xu, who is a postdoctoral research in Matthews group (Department of Biochemistry and Cell Biochemistry, Rice University). This work presented in Chapter 8 is published in *Langmuir*. [6]

Finally, in Chapter 9 a brief summary of the work conducted in this thesis is presented. Suggestions for future work in applying these sensing techniques to probe the biomolecular forces and interactions are presented. In the Appendix A, several supplemental techniques are

documented to support the experimental results reported in this thesis.

1.3. References

(1) Vandenburg, E. T.; Brown, R. S.; Krull, U. J. In *Immobilized Biosystems - Theory and Practical Applications*; Veliky, I. A., Mclean, R. J. C., Eds.; Blackie Academic & Professional, 1994.

(2) Zhu, H.; Snyder, M. *Curr. Opin. Chem. Biol.* **2003**, *7*, 55-63.

(3) Bayley, H.; Cremer, P. S. *Nature* **2001**, *413*, 226-230.

(4) Wang, J. *Nucleic Acids Res.* **2000**, *28*, 3011-3016.

(5) Liu, K. W.; Biswal, S. L. *Anal. Chem.* **2010**, *82*, 7527-7532.

(6) Xu, J.; Liu, K.-W.; Matthews, K. S.; L., B. S. *Langmuir* **2011**, *27,* 4900–4905.

Chapter 2

Review on Microcantilever Sensors

2.1. Introduction

This thesis develops a strategy for using the lipid membrane-coated microcantilever for future biosensing applications. The motivation of this work comes from unsolved problems in two research fields: the sensing mechanism of microcantilever sensors and the conformation of supported lipid bilayers on solid surfaces. Are minute conformational changes of lipid membranes detectable using microcantilever sensors?

To understand the sensing mechanisms of microcantilever sensors, researchers have characterized the microcantilevers with well-studied and simple chemical components, such as gas adsorption of alkanethiols, self-assembled monolayers (SAMs), polymer brushes, DNA hybridization or target-ligand recognitions. [1-6] In this chapter the important contributions of these pioneering research work will be reviewed. Reviews on microcantilevers used for chemical and physical sensing will be first introduced followed by biomolecular sensing. The novelty of the research of this thesis, the integration of lipid membranes with microcantilever sensors, is based on these previous works and adds insights into the sensing mechanisms of microcantilevers. Following the reviews, a brief section to illustrate the physical fundamentals of the sensing mechanisms of the microcantilevers is provided.

2.2. Development of Microcantilever Sensors for Physical and Chemical Sensing

Cantilevers are beam structures, with one end fixed to a wall and the other end standing freely without a support. Civil engineers and architects use the cantilever structures for

constructions such as bridges, balconies or decks to carry loads and to distribute weight evenly along the beam. If the material is not rigid enough or simply not designed to reach a force balance, the cantilevers may deform and bend as a result of the loading or stress on the free end. A simple visualized example is the diving board which curves downward as a result of an end loading of a divers' body weight. As the size shrinks from meters to microns or sub-microns, the cantilevers become very sensitive to the environment and can bend and vibrate not only in response to the mass on the beam but also superficial chemical disturbances. (See Fig. 2.1) This phenomenon was actually unfavorable in its use as the commonly used stylus-tipped microcantilever in atomic force microscopy (AFM). At room temperature the thermally-induced vibration of microcantilever can reduce the force sensitivity of AFM by three orders of magnitude compared to the microcantilever cooled under 300 mK, and the adsorption of ambient air molecules on the microcantilever surface can lower its stability by two orders of magnitude compared to that mounted in an ultra-vacuum chamber. [7] However, this sensitive response to molecular adsorption on the microcantilever surface turns out to be a tremendous advantage for sensor applications. Fig. 2.2 shows that the microcantilever responds to the binding of target molecules to the surface-bound probe molecules by bending away from the molecular layer.

There are two modes of operation. The first is a static mode in which the cantilever obtains a new equilibrium position in response to a chemical signal caused by a surface stress change. Several detection methods are used to transduce signals from the microcantilever sensors into a measureable chemical signal. [1, 2, 8] One common method is the optical lever technique, which is used to measure the cantilever deflection in the static mode. In this method, low power laser diodes are focused onto the tip of each cantilever, which is usually coated with metal films to increase the reflectivity, and the reflected laser beams are captured onto a position sensitive photodetector (PSD). When the cantilever bends, the reflected laser beams change the reflection

angle. The moving trajectories of the reflected light are captured by the PDS. Since the displacement of the reflective laser beam is linear to the deflection, the deflection value of each cantilever is known. The other mode of operation is the dynamic mode, which measures the resonance frequency variation of the cantilever to obtain the loaded mass. The vibration of the free cantilever end is similar to a spring oscillator. The suspended mass and the spring constant of the cantilever are related to a fundamental resonance frequency. Thus, changes in the loaded mass can be detected by reading the fundamental frequency shift. However this dynamic measurement is limited to weakly damped environment, such as in air; while in liquid, the viscous damping dissipates most of the energy and suppresses the resonance. This drawback can be overcome by enhancing the quality factor of the cantilever (Q-factor). Several other methods, such as interferometry, piezoelectric cantilevers and capacitive cantilevers, are also developed for convenient detection in AFM; however, these methods lack in either sensitivity or feasibility for extensive sensor applications. In this thesis, mainly the static type – surface stress measurement using optical level method is the study focus.

The use of microcantilever sensors to measure surface stress was first discovered by a group in IBM Zurich Research Laboratory in 1994 and later by a group in Oak Ridge National Laboratory. [9-11] Gimzewski et al. used the micromechanical cantilevers to probe the heat released from a Pt-catalyzed chemical reaction of H_2 and O_2 mixture to form H_2O_2 with a sensitivity of 1 pJ. Thundat et al. reported that a scanning force microscope cantilever can respond to the ambient heat and humidity change. Berger et al. measured the surface stress induced by the self-assembly monolayers of alkanethiols on a gold surface using the microcantilevers. [5] The authors inspected the alkanethiol monolayers of five different alkyl lengths formed on the gold surface of the microcantilevers and concluded that the extent of the cantilever's bending is proportional to the length of the alkyl chain. This was an important quantitative analysis, relating

the adsorbed molecular structures with the readout of the cantilever sensor. Godin et al. continued the work of alkanethiol monolayers on small and large grain size of gold surfaces and presented a kinetic scheme of the surface stress on microcantilever surfaces during the monolayer formation. [12] Watari et al. later expanded the studies on the self-assembled alkanethiols' properties from structural to electrostatic. [13, 14] They found that the stronger the lateral electrostatic repulsion is in the monolayer, the more the cantilever bends, confirming that the microcantilever is sensitive to in-plane intermolecular forces. Sushko et al. later added a model to explain Watari's experiments. [15] In their analysis, the surface stress of a microcantilever is divided into two categories: the contribution from the chemical $\Delta\sigma_{chem}$ (the force which enforces cantilever bending) and the elastic $\Delta\sigma_{elast}$ (the force which resists cantilever bending). Gas sensing using microcantilevers can be achieved by adsorbing gases on either pure metal films or chemically selective polymer films. [16] Gas phase analytes, such as organic compound (tolune vapor, benzene), explosive trace (TNT), and inorganic vapor (mercury, hydrogen), have been probed with a sensing resolution of ppm ~ ppt. [2, 17-20]

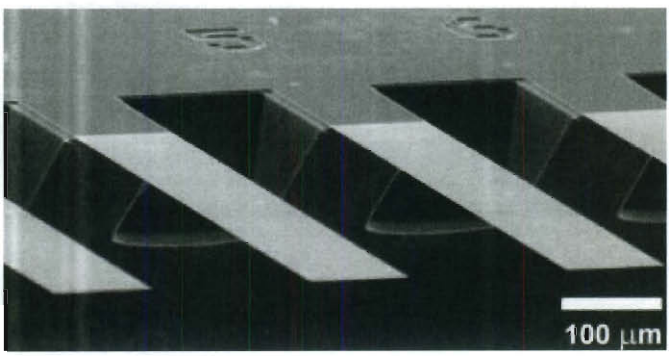

Figure 2.1. SEM image of a microfabricated silicon cantilever array. The dimension of each cantilever is 500 μm long, 100 μm wide and 1 μm thick. (Fritz et al. [4])

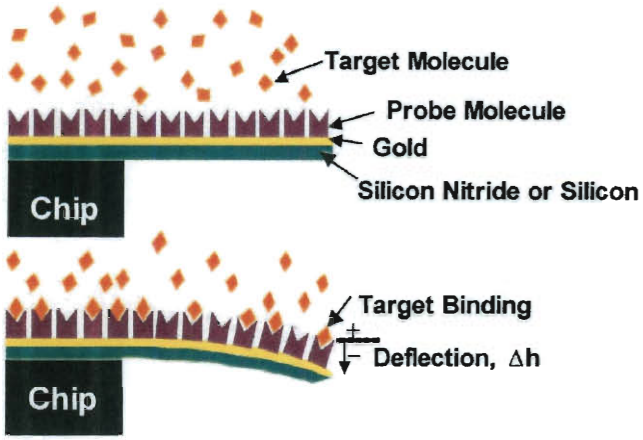

Figure 2.2. Specific binding of target molecules to the probe molecules immobilized on the gold surface is translated into the observable mechanical bending of the microcantilever. (Wu et al. [6])

Three different kinds of biomacromolecular assemblies, DNA, proteins and lipid membranes, are of special interest in studying with the use of microcantilevers. These biomacromolecules change their conformations and structures when ambient stimuli are present. Specific biomolecular recognition/binding is also a key to new drug design and toxin screening. Microcantilevers have been used as biosensors for these types of probing. Important literature is reviewed in the following section.

2.3. Microcantilever as Biosensors

2.3.1. Sensing DNA using Microcantilevers

Several attempts have been made to bring the microcantilevers into biosensing. One example is to monitor the DNA. Fritz et al. reported the cantilever response to DNA hybridization and showed its receptor-ligand binding mechanism, as shown in Fig. 2.3. [4] Wu et al. presented a qualitative theory to explain the origin of the cantilever bending generated from ssDNA immobilization and complementary DNA hybridization. The authors remarked that the

compressive bending (bending to the opposite side of the adsorbed layer) comes from an entropic driving force, which works to minimize the steric and electrostatic repulsion between grafted ssDNAs. [6] Contradictorily, the experimental results of Fritz and Wu were different. Upon DNA hybridization, the former showed a tensile surface stress (the cantilever bent toward the DNA film), while the latter a compressive surface stress (the cantilever bent away from the DNA film). Fritz's experimental result was backed up with a few published papers [21-24] Though these experiments were conducted in different conditions, such as buffer, ssDNA grafting density, and the hybridized DNA sequence and length, the differences in measured bending direction was possibly due to the different bending mechanisms. If the bending due to DNA hybridization is entropy-driven, the bending direction is likely to be tensile; if it is steric-driven, the bending direction is likely to be compressive. This assumption is tested by hybridizing the DNAs with target DNAs which contains either internal or terminal mismatches. [25] Hagan provided a model to describe how the inter-DNA forces translate to the mechanical bending of microcantilevers, by dividing the force interactions into four categories: the electrostatic free energy, F_{ELEC}, the conformational entropy and non-electrostatic free energy, F_{POLY}, the osmotic pressure of the counterions, F_{OSM}, and the mechanical energy penalty, E_{CANT}. [21] By individually analyzing and summing up the free energies from different type of interactions, the origin of the cantilever motion generated from the biomolecular film can be rationally designed.

Some other free energy analyses and models for DNA brushes on microcantilever surfaces have also reported. [26, 27] Other experiments on sensing DNA molecular structure changes were conducted by several groups. Shu et al. observed that the when grafted hydride dsDNA chains (duplex) fold to form quadruplex structures, the microcantilevers responds to the conformational transition by bending away from the dsDNA-grafted surface. [28] A reverse of DNA hybridization, Biswal et al. showed that the melting of dsDNA can be detected by ramping the temperature. [29]

At the transition temperature, complementary DNA dehybridize and break the hydrogen bonds from the immobilized DNA, creating a sharp transition of the surface stress. However, hybridization of DNA needs an optimized ssDNA monolayer and proper grafting density for successful sensing in surface stress. [24, 30] In addition to static surface stress measurement, dynamic probing for DNA hybridization also showed that the resonant frequency shift to higher frequency during the hybridization with complementary DNAs, meaning the mass detection during DNA hybridization is also direct and feasible. [31]

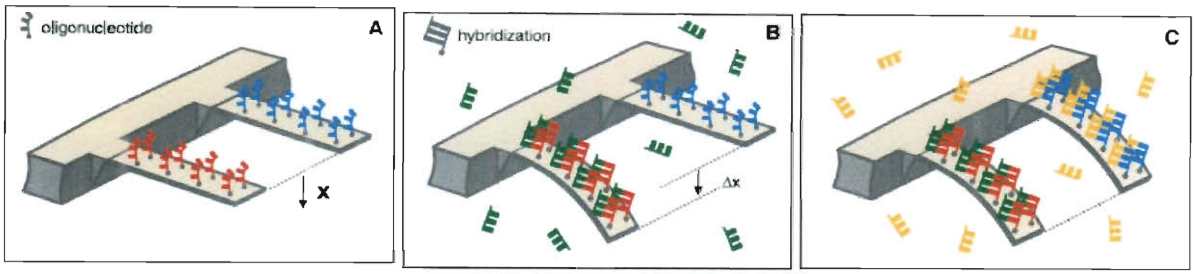

Figure 2.3. Hybridization of DNA on microcantilever surfaces. (Fritz et al. [4])

2.3.2. Sensing Proteins Conformations with Cantilevers

Proteins are also of great interest in investigations performed on microcantilevers because the rich hierarchical structures and folding motions of proteins make this type of sensing attractive. Protein adsorption onto the microcantilever surfaces can either induce compressive or tensile stress, depending on what is the resultant interaction of protein-protein and protein-surface. (Moulin et al. [32, 33] ; Shu et al. [34]; Wu et al. [35]) The protein adsorption-induced bending of microcantilevers is still obscure due to a number of force interplays and is difficult to predict the bending direction and bending magnitude. Efforts to ensure that surface-bound proteins do not denature and a deeper quantitative investigations on the bending mechanism are greatly needed.

After proteins or peptides adsorb to surfaces, understanding the aggregation and growth process is important. Several severe health disorders, such as Alzheimer's and Parkinson's diseases, have proven to be caused by the formation of amyloid plaques in the patient's brains. However the detection of amyloid fibrillation and growth in bulk solution is a challenging task. Knowles et al. have detected surface stress changes induced by insulin amyloid growth from seed fibrils which are bound on the gold surface of microcantilevers, shown in Fig. 2.4. [36, 37] Kiselev et al. reported the pH-induced fibrillation in a surface-bound lysozyme protein film, in which the proteins aggregate with their neighbor proteins, on both gold and SiO_2 surfaces. [38] Interestingly, both Knowles and Kiselev's findings indicates that the fibrillation process induced "tensile stresses" on solid surfaces for these two different molecules. The tensile stress is likely to be a result of the in-plane attractive forces between aggregated proteins.

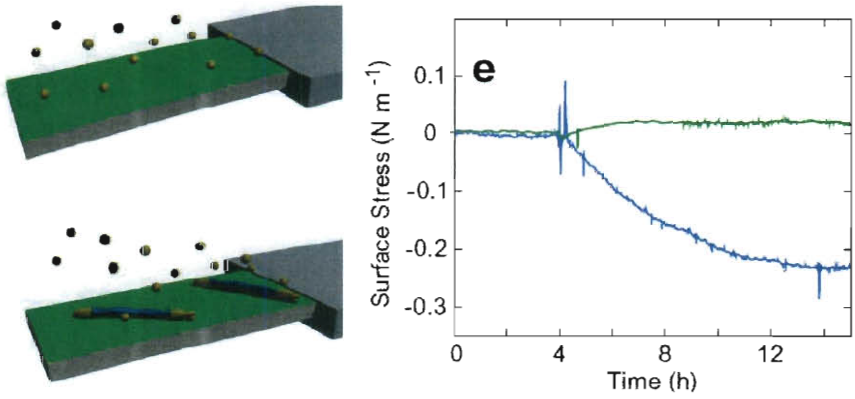

Figure 2.4. Insulin fibrillation monitored by static-mode microcantilevers. (Knowles et al. and White et al.[36, 37])

Catalytic activity of proteins can be quantitatively measured by microcantilever sensors. [39] Raorane et al. showed that ligand-receptor type binding of the substrate to the protease follows the Michaelis–Menten equation. They found that the reaction constant, or the Michaelis–Menten

constant, of the surface-bound protease is one-order lower than that of the reaction in solution phase. Regardless of their experimental findings, their model is simplified using the Langmuir adsorption equation to obtain the reaction constant without considering intermolecular interactions, which might account for the inaccuracy in their analysis.

Specific recognition between antibiotic drugs with mucopeptide precursors on the bacterial cell wall were explored by Ndieyira et al., as shown in Fig. 2.5. [40] They detected a stronger binding between the antibiotic drug, vancomycin, with Alanin-terminated mucopeptide precursors ($_{D}Ala$) over the mutated analogue $_{D}Lac$, thus determined that the former is vancomycin–sensitive and the latter is vancomycin–resistant. Instead of fitting the surface stress versus concentration using simple Langmuir equation, they introduced a critical percolation threshold to modify the Langmuir equation for the fitting. Only at the surface coverage of the mucopeptides higher than the threshold will the microcantilevers be able to sense the antibiotic transduction.

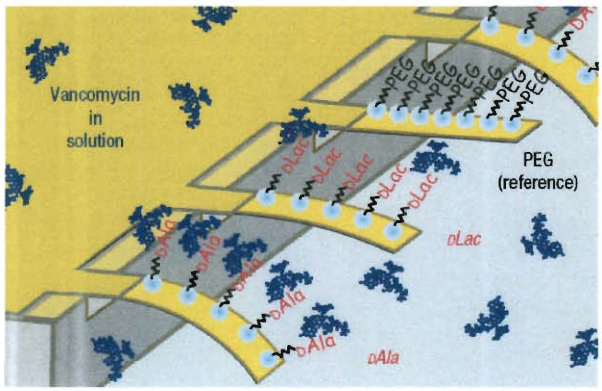

Figure 2.5. Detection of vancomycin-mucopeptide analogue interactions on microcantilever arrays. (Ndieyira et al. [40])

2.3.3. Sensing Lipid Membranes Using Microcantilevers

Another category of interest in biomacromolecules is the lipid membrane. By taking advantage of the well characterized technique of the supported lipid bilayers (SLBs), coating the cantilever with a thin lipid membrane of 5 nm in thickness is possible. Pera et al. made a first attempt to coat the microcantilever with a SLB on either gold or silicon dioxide surface of the microcantilever and monitor the cantilever bending of this coating process. [41] However, their experimental results showed an inconsistency of the bending directions without further interpretations and a large overshoot noise signal for the lipid film coated on gold and silicon surfaces (Fig. 2.6). One possible improvement to their experiment is to modify the lipid vesicle preparation method, so that much more homogeneous and monodispersed lipid vesicles can fuse onto the surface and ensure the SLB with fewer defects. This thesis will describe the improvement and better characterizations of the membrane coated cantilever, based on Pera's findings.

One third of all the known proteins in living organisms are associated with cell lipid membranes, in which the proteins are properly folded in the lipid membranes and retain their native structures. [42, 43] Preparing a robust surface-supported lipid membrane to accommodate membrane proteins is one of the strategies of lab-on-chip design for membrane protein sensing. Peptides inserting into the lipid membrane were observed on microcantilevers by Pera et al. [41] Ghatnekar-Nilsson et al. and Ghatkesar et at. [44, 45] These groups showed the melittin insertion leads to membrane expansion and cause the microcantilevers to bend toward the side opposite of that coated with the lipid membrane. Light-exposure induced conformational change of a membrane protein, bacteriorhodopsin (bR), was monitored on the microcantilever by Braun et al. [46] However, the bRs cystein mutant coated on the microcantilevers in Braun's experiments was a partially dry film made from fusing the bR proteoliposomes onto gold surfaces through cystein-gold bonds, and the experiments were conducted in an air chamber with humidity control.

This setup posed two problems: on gold surfaces the proteoliposomes may not fuse to form a single lipid film even with the cystein-gold assisted binding. The AFM image of their gold surface shows patchy membranes with heights ranging from 5~15 nm. The lipid-protein mixtures may cause inaccurate interpretation of the data. In addition, the ideal protein medium is in aqueous solution with the physiological condition, while they instead used an air chamber with >95% humidity. Ghatkesar et al. improved the setup by depositing the liposomes to adsorb on the gold surface rather than to rupture and fuse to a single lipid film, before the peptides were added for binding with the membrane. [44, 47] However, the vesicles were partially suspended in the aqueous medium and partially physisorbed on the gold surface. The peptide binding sites on the vesicles were limited to the side where the vesicles were partially suspended in the aqueous medium. In other words, the binding signal was far away from the microcantilever surface and may not be accurately detected. Tark et al. deposited lipid nanodisks, which are lipid bilayers surrounded by an amphipathic protein belt, on the gold side. [48] Though the nanodisks were stable and can stabilize membrane proteins on solid surfaces, preparing the lipid-protein complex is more complicated than fusing lipid vesicles on the SiO_2 surfaces. The systematic characterization and the better preparation of the supported lipid bilayers introduced in this thesis work will greatly improve those shortcomings mentioned above.

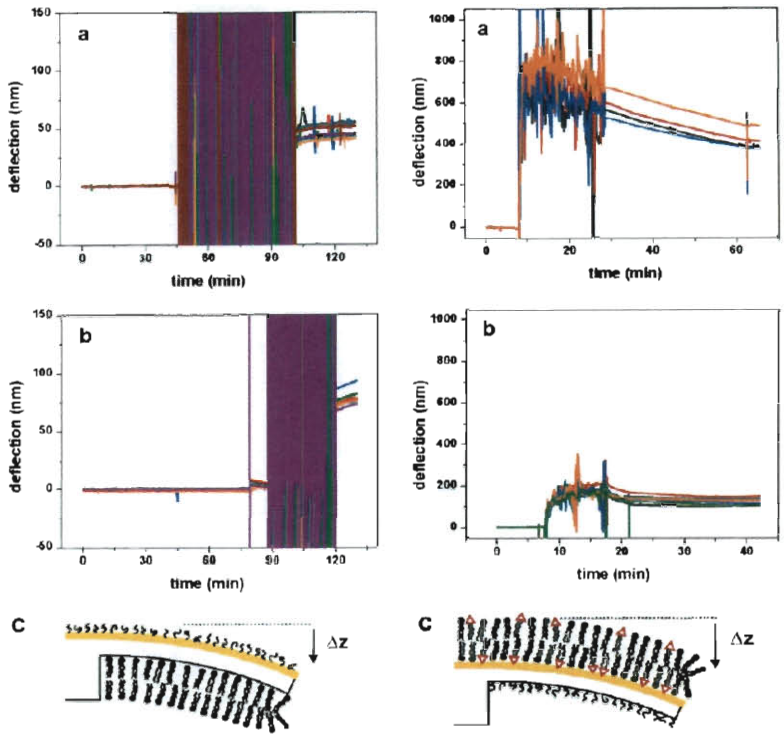

Figure 2.6. Left: Lipid bilayer physisorbed on the silicon dioxide surface of the cantilever induced a tensile cantilever bending (a) DOPC lipid membrane formation. (b) DMPC lipid membrane formation. (c) Illustration of the membrane coated cantilever. Right: thiolated Lipid bilayer chemisorbed on gold surface of the cantilever induced a compressive cantilever bending (a) 100% thiolated lipid (DPPTE) membrane formation. (b) 10% DPPTE and 90% DOPC lipid membrane formation. (c) Illustration of the membrane coated cantilever. (Pera et al. [41])

2.4. Free Energy Transduction through Microcantilever

2.4.1. Origin of Surface Stress of Solid Materials

Providing a number of examples of microcantilevers in sensing biomolecular assemblies, the cause and the magnitude of the bending motions of the microcantilevers is still not explicitly understood. The general principle of the sensing mechanism of the microcantilevers is described

here. This section employs the concept of solid physics and material science to explain the stress and the bending motion of the microcantilever sensors.

As molecules in the bulk solution preferentially attach and are confined to a solid surface, the total free energy in the system is lowered. The lowered free energy can be described by the difference between the chemical potential of the adsorbates in the bulk solution and that adsorbed on the surface ($\mu_s - \mu_b = \Delta\mu$), or simply the standard Gibbs free energy of adsorption (ΔG_{ads}). [49] Adsorbates adsorbing, including physisorption and chemisorption, onto the solid surfaces can exert a superficial surface stress to the solid lattices. The induced surface stress originates from the redistribution of the electric charges at the interface of the solid phase, and is an integral of all the in-plane components of the force per unit length along the normal direction, minus that force in the bulk. Thus, the measurable surface stress can be thought as the difference of electric charge distribution between the solid surface and the bulk. As shown in Figure 2.7 (a), at the metal surface without adsorbates which have absent upper atoms, the interfacial charge (as shown as the empty ellipse) redistributes and enhances the bonding between the first and the second atom layers and between the atoms in the superficial layer. As a result, the surface charge density increases, and so does the attractive force between the surface metal atoms. This surface encounters a tensile stress, or a positive stress, meaning that a positive work is required to elastically stretch the surface. For clean surfaces of metals, the surface stress is usually tensile; while for clean surfaces of semiconductors, it can be either tensile or compressive. For Si surfaces, the sign of the surface stress depends on the size of the doping atoms, the type of the substituted atoms, and the lattice direction (for example, surface stress of clean surface of Si(111) is tensile, while that of Si(100) is compressive). [50, 51]

As adsorbates adsorb to the surface as shown in Figure 2.7 (b), the surface stress changes. If the adsorbates are electronegative, the electrons in the surface atoms tend to be attracted by the

adsorbates, thus the charge density between the substrate atoms decreases. The decrease in the charge density between surface atoms causes a compressive surface stress because less bonding electrons can hold the adjacent surface atoms together, compared to the clean surface. However, if the adsorbates are electropositive, the phenomenon is reversed, and the resulted surface stress is usually tensile.

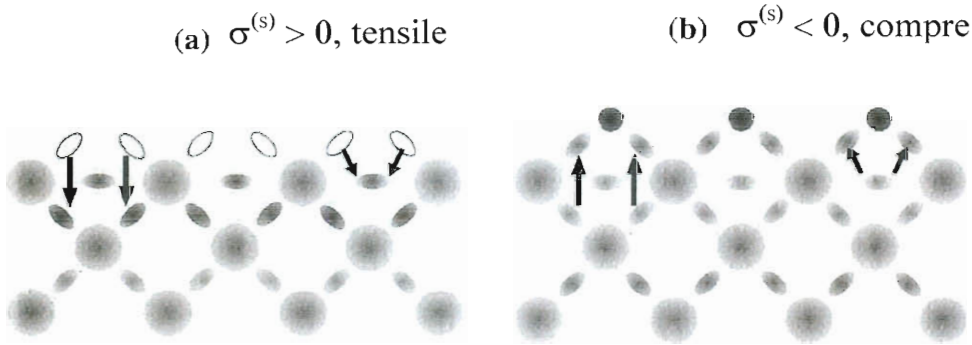

Figure 2.7. The charge distribution at the metal surfaces (a) without and (b) with electronegative adsorbates (shown as dark solid circles). (Ibach, H. [50])

2.4.2. Relating Surface Stress with Surface Free Energy of Solids

In the previous section, the adsorption-induced surface stress of solids is discussed. However it is the Gibbs free energy of the chemical reaction that takes place on the solid surface. Therefore, the relation between surface stress and free energy should be established before using the surface stress measured by microcantilevers as an indicator of a surface chemical reaction.

To relate the two physical properties, the surface free energy γ is given as a reversible work (W) done to increase a surface area increment dA on the solid surface. That is, to strain a surface, the needed work is: [52]

$$\gamma dA = dW = d(E_S N) = E_S \frac{\partial N}{\partial A} dA + N \frac{\partial E_S}{\partial A} dA . \qquad (2.1)$$

E_s is the specific free energy (energy per molecule), and N is the number of total surface molecules. This work includes both the elastic and plastic contributions: the elastic contribution means that the elastic stretching of the surface forces the molecules to increase the area per molecule, denoted as surface stress, σ. While the plastic contribution can be thought as the expansion of liquids, which expand the surface area by supplementing the surface with more molecules and keeping the area per molecule constant. This plastic contribution of the surface free energy can be said as the surface tension of solid, γ_s. Essentially, this reversible work, dW or γdA, is required to expand a solid surface against the surface stress (σ) and surface tension of the solid (γ_s).

$$\gamma dA = dW = \sigma \, dA_{elastic} + \gamma_s dA_{plastic} \tag{2.2}$$

The surface stress of a solid surface is generally the elastic part of surface free energy change, also known as the reversible work per area to stretch the surface elastically. Thus, $\gamma_{elastic} = \sigma$. For more detailed derivation, the surface stress is defined as:

$$\begin{aligned} \gamma_{elastic} &= \left(E_s \frac{\partial N}{\partial A} + N \frac{\partial E_s}{\partial A} \right)_{elastic} \\ &= \mathbf{0} + N \frac{\partial E_s}{\partial A} = N \frac{\partial \left(\gamma_s A / N \right)}{\partial A} = \gamma_s + \frac{\partial \gamma_s}{\partial A / A} \\ &= \gamma_s + \frac{\partial \gamma_s}{\partial \varepsilon_{elastsic}} \equiv \sigma \end{aligned} \tag{2.3}$$

This expression of surface stress is first derived by Shuttleworth in 1950. [53] In addition, the plastic form of the surface free energy is the surface tension of solids, that is, $\gamma_{plastic} = \gamma_s$.

$$\gamma_{plastic} = \left(E_s \frac{\partial N}{\partial A} + N \frac{\partial E_s}{\partial A} \right)_{plastic}$$
$$= E_s \frac{\partial N}{\partial A} + \mathbf{0} = \frac{E_s}{A/N} \tag{2.4}$$
$$= \gamma_s$$

For liquid, the total work required to increase an area is equal to the surface tension of liquids, as seen in Eq. (2.4). As for solid, the total work required (surface stress) contains the surface tension and a derivative of surface tension with respect to the resulted strain, as seen in Eq. (2.3).

Since the integral of the γ_s over a solid surface corresponds to the amount of surface free energy for a stress-free solid surface, the surface tension can be seen as a local surface free energy. Thus, in Eq. (2.3), the σ at a certain location contains a local surface free energy, plus the increment of the local surface free energy divided by the local strain. This equation will be used to explain the sensing mechanism of microcantilever sensors throughout this thesis.

2.4.3. Microcantilevers to Probe Surface Free Energy at Solid/Liquid Interface

The cantilever bending method is commonly used and well established for measuring the internal stress of thin films. [54, 55] Not only for measuring the internal stress of the bulk material during heating or film growth, but also the adsorption-induced stress at solid interfaces can be accurately measured using cantilevers.

The cantilever deflection is related to changes in the surface free energy associated with physi- or chemisorption of molecules to its surface [56, 57]. It is the difference in the surface stress between the upper and lower surface of the cantilever that causes the cantilever to bend. This induced surface stress is related to the interfacial properties of the coating layer, whether it be rigidly bonded layers, adsorbed molecules, or in our case, a thin lipid bilayer film. The relationship between the change in cantilever deflection, Δz, and change in surface stress, $\Delta\sigma$ (units N/m), has been commonly described using Stoney's equation: [58]

$$\Delta\sigma = \frac{Et^2}{3(1-\nu)L^2}\Delta z \tag{2.5}$$

where ν is Poisson's ratio of the cantilever material, E is the Young's modulus, L is the cantilever length, and t is the cantilever thickness. The key assumptions in Stoney's equation are that (i) the bending of the cantilever is small, (ii) the length of the cantilever is large compared to its width, which are both large compared to its thickness, (iii) the thickness of the coating layer is negligible compared to the cantilever thickness, and (iv) that the load is uniform. In cases where the above assumptions do not hold, there have been corrections made to Stoney's equation, however, in the case of a thin lipid bilayer of 5 nm in thickness, Stoney's equation is reasonably accurate.

The change is surface stress is greatly influenced by the presence of adsorbates on the cantilever. As molecules adsorb to a solid surface, there is a release in the adsorption free energy, ΔG_{ads}, at the solid-liquid interface. As described by Pinnaduwage, et al., if this energy is absorbed by the solid surface, it is converted to surface free energy, γ: $-\Delta G_{ads} = \Delta\gamma = \gamma(\varepsilon) - \gamma(\varepsilon=0)$, where ε is the surface strain. [57] For a solid surface, the surface free energy is coupled to its surface stress, which leads to deformation of the solid surface. The Shuttleworth equation relates σ, γ, γ_s, and ε [59, 60], as described in the section 2.4.2:

$$\sigma = \gamma_s + \frac{\partial\gamma_s}{\partial\varepsilon} = \gamma_{elastic} \tag{2.6}$$

The second term accounts for the change in the interatomic distance as the surface is elastically strained. From Eq. (2.5) and (2.6), surface stress changes can be directly related to changes in the surface free energy upon SLB adsorption:

$$\Delta\sigma \sim -\Delta G_{ads} \tag{2.7}$$

As a compressive stress in the SiO_2 surface is generated, the cantilever bends toward the direction of gold coated surface. A stronger affinity between the solid and SLB results in a larger

(more negative) ΔG_{ads} [61, 62].

In the following chapter, a detailed background into supported lipid bilayers is provided.

2.5. Reference:

(1) Datskos, P. G., Lavrik, N. V., and Sepaniak, M. J. In *Smart Sensors and MEMs,* 1 ed.; Yurish, S. Y., Ed.; Springer, 2005, pp 331-379.

(2) Thundat, T.; Majumdar, A. In *Sensors and Sensing in Biology and Engineering*; Springer-Verlag: New York, 2003.

(3) Arlett, J. L.; Myers, E. B.; Roukes, M. L. *Nature Nanotechnology* **2011**, *Published online 27 March 2011*

(4) Fritz, J.; Baller, M. K.; Lang, H. P.; Rothuizen, H.; Vettiger, P.; Meyer, E.; Guntherodt, H. J.; Gerber, C.; Gimzewski, J. K. *Science* **2000**, *288*, 316-318.

(5) Berger, R.; Delamarche, E.; Lang, H. P.; Gerber, C.; Gimzewski, J. K.; Meyer, E.; Guntherodt, H. J. *Science* **1997**, *276*, 2021-2024.

(6) Wu, G. H.; Ji, H. F.; Hansen, K.; Thundat, T.; Datar, R.; Cote, R.; Hagan, M. F.; Chakraborty, A. K.; Majumdar, A. *Proceedings of the National Academy of Sciences of the United States of America* **2001**, *98*, 1560-1564.

(7) Binnig, G.; Quate, C. F.; Gerber, C. *Physical Review Letters* **1986**, *56*, 930-933.

(8) Raiteri, R.; Grattarola, M.; Butt, H. J.; Skladal, P. *Sensors and Actuators B-Chemical* **2001**, *79*, 115-126.

(9) Gimzewski, J. K.; Gerber, C.; Meyer, E.; Schlittler, R. R. *Chemical Physics Letters* **1994**, *217*, 589-594.

(10) Thundat, T.; Warmack, R. J.; Chen, G. Y.; Allison, D. P. *Appl. Phys. Lett.* **1994**, *64*, 2894-2896.

(11) Sepaniak, M.; Datskos, P.; Lavrik, N.; Tipple, C. *Analytical Chemistry* **2002**, *74*, 568A-575A.

(12) Godin, M.; Williams, P. J.; Tabard-Cossa, V.; Laroche, O.; Beaulieu, L. Y.; Lennox, R. B.; Grutter, P. *Langmuir* **2004**, *20*, 7090-7096.

(13) Watari, M.; Galbraith, J.; Lang, H. P.; Sousa, M.; Hegner, M.; Gerber, C.; Horton, M. A.; McKendry, R. A. *Journal of the American Chemical Society* **2007**, *129*, 601-609.

(14) Watari, M.; Ndieyira, J. W.; McKendry, R. A. *Langmuir*, *26*, 4623-4626.

(15) Sushko, M. L.; Harding, J. H.; Shluger, A. L.; McKendry, R. A.; Watari, M. *Advanced Materials* **2008**, *20*, 3848-+.

(16) Hagleitner, C.; Hierlemann, A.; Lange, D.; Kummer, A.; Kerness, N.; Brand, O.; Baltes,

H. *Nature* **2001**, *414*, 293-296.

(17) Zuo, G. M.; Li, X. X.; Zhang, Z. X.; Yang, T. T.; Wang, Y. L.; Cheng, Z. X.; Feng, S. L. *Nanotechnology* **2007**, *18*.

(18) Hu, Z. Y.; Thundat, T.; Warmack, R. J. *Journal of Applied Physics* **2001**, *90*, 427-431.

(19) Xu, X. H.; Thundat, T. G.; Brown, G. M.; Ji, H. F. *Analytical Chemistry* **2002**, *74*, 3611-3615.

(20) Thundat, T.; Wachter, E. A.; Sharp, S. L.; Warmack, R. J. *Applied Physics Letters* **1995**, *66*, 1695-1697.

(21) Hagan, M. F.; Majumdar, A.; Chakraborty, A. K. *Journal of Physical Chemistry B* **2002**, *106*, 10163-10173.

(22) Biswal, S. L.; Raorane, D.; Chaiken, A.; Birecki, H.; Majumdar, A. *Analytical Chemistry* **2006**.

(23) McKendry, R.; Zhang, J. Y.; Arntz, Y.; Strunz, T.; Hegner, M.; Lang, H. P.; Baller, M. K.; Certa, U.; Meyer, E.; Guntherodt, H. J.; Gerber, C. *Proceedings of the National Academy of Sciences of the United States of America* **2002**, *99*, 9783-9788.

(24) Marie, R.; Jensenius, H.; Thaysen, J.; Christensen, C. B.; Boisen, A. *Ultramicroscopy* **2002**, *91*, 29-36.

(25) Hansen, K. M.; Ji, H. F.; Wu, G. H.; Datar, R.; Cote, R.; Majumdar, A.; Thundat, T. *Analytical Chemistry* **2001**, *73*, 1567-1571.

(26) Sushko, M. L. *Faraday Discussions* **2009**, *143*, 63-80.

(27) Bergese, P.; Oliviero, G.; Alessandri, I.; Depero, L. E. *Journal of Colloid and Interface Science* **2007**, *316*, 1017-1022.

(28) Shu, W. M.; Liu, D. S.; Watari, M.; Riener, C. K.; Strunz, T.; Welland, M. E.; Balasubramanian, S.; McKendry, R. A. *Journal of the American Chemical Society* **2005**, *127*, 17054-17060.

(29) Biswal, S. L.; Raorane, D.; Chaiken, A.; Birecki, H.; Majumdar, A. *Analytical Chemistry* **2006**, *78*, 7104-7109.

(30) Alvarez, M.; Carrascosa, L. G.; Moreno, M.; Calle, A.; Zaballos, A.; Lechuga, L. M.; Martinez-A, C.; Tamayo, J. *Langmuir* **2004**, *20*, 9663-9668.

(31) Zheng, S.; Choi, J. H.; Lee, S. M.; Hwang, K. S.; Kim, S. K.; Kim, T. S. *Lab on a Chip*, *11*.

(32) Moulin, A. M.; O'Shea, S. J.; Badley, R. A.; Doyle, P.; Welland, M. E. *Langmuir* **1999**, *15*, 8776-8779.

(33) Moulin, A. M.; O'Shea, S. J.; Welland, M. E. *Ultramicroscopy* **2000**, *82*, 23-31.

(34) Shu, W. M.; Laue, E. D.; Seshia, A. A. *Biosensors & Bioelectronics* **2007**, *22*, 2003-2009.

(35) Wu, G. H.; Datar, R. H.; Hansen, K. M.; Thundat, T.; Cote, R. J.; Majumdar, A. *Nature*

Biotechnology **2001**, *19*, 856-860.

(36) Knowles, T. P. J.; Shu, W.; Huber, F.; Lang, H. P.; Gerber, C.; Dobson, C. M.; Welland, M. E. *Nanotechnology* **2008**, *19*.

(37) White, D. A.; Buell, A. K.; Dobson, C. M.; Welland, M. E.; Knowles, T. P. J. *Febs Letters* **2009**, *583*, 2587-2592.

(38) Kiselev, G. A.; Kudrinskii, P. V.; Yaminskii, I. V.; Vinogradova, O. I. *Protection of Metals* **2008**, *44*, 535-541.

(39) Raorane, D. A.; Lim, M. D.; Chen, F. F.; Craik, C. S.; Majumdar, A. *Nano Letters* **2008**, *8*, 2968-2974.

(40) Ndieyira, J. W.; Watari, M.; Barrera, A. D.; Zhou, D.; Vogtli, M.; Batchelor, M.; Cooper, M. A.; Strunz, T.; Horton, M. A.; Abell, C.; Rayment, T.; Aeppli, G.; McKendry, R. A. *Nature Nanotechnology* **2008**, *3*, 691-696.

(41) Pera, I.; Fritz, J. *Langmuir* **2007**, *23*, 1543-1547.

(42) Fernandez, C.; Hilty, C.; Wider, G.; Wuthrich, K. *Proceedings of the National Academy of Sciences of the United States of America* **2002**, *99*, 13533-13537.

(43) Nelson, D. L.; Cox, M. M. *lehninger principles of biochemistry*, 4th edi ed., 2005.

(44) Ghatkesar, M. K.; Lang, H.-P.; Gerber, C.; Hegner, M.; Braun, T. *PLoS One* **2008**, *3*, e3610.

(45) Ghatnekar-Nilsson, S.; Lindahl, J.; Dahlin, A.; Stjernholm, T.; Jeppesen, S.; Hook, F.; Montelius, L. *Nanotechnology* **2005**, *16*, 1512-1516.

(46) Braun, T.; Backmann, N.; Vogtli, M.; Bietsche, A.; Engel, A.; Lang, H.; Gerber, C.; Hegner, M. *Biophysical Journal* **2006**, *90*, 2970-2977.

(47) Braun, T.; Ghatkesar, M. K.; Backmann, N.; Grange, W.; Boulanger, P.; Letellier, L.; Lang, H. P.; Bietsch, A.; Gerber, C.; Hegner, M. *Nature Nanotechnology* **2009**, *4*, 179-185.

(48) Tark, S.-H.; Das, A.; Sligar, S.; Dravid, V. P. *Nanotechnology*, *21*, 435502.

(49) Castellan, G. W. *Physical Chemistry*, 3rd ed.; The Benjamin/Cummings Publ. Co., 1983.

(50) Ibach, H. *Physics of Surfaces and Interfaces*; Springer, 2006.

(51) Ibach, H. *Surface Science Reports* **1997**, *29*, 195-263.

(52) Butt, H.-J.; Kappl, M. *Surface and Interfacial Forces*; Wiley-VCH, 2010.

(53) Shuttleworth, R. *Proceedings of the Physical Society of London Section A* **1950**, *63*, 444-457.

(54) Koch, R.; Abermann, R. *Thin Solid Films* **1985**, *129*, 63-70.

(55) Ohring, M. *Materials Science of Thin Films - Deposition and Structure*, 2nd ed.; Academic Press, 2002.

(56) Bergese, P.; Oliviero, G.; Alessandri, I.; Depero, L. E. *J. Colloid Interface Sci.* **2007**, *316*,

1017-1022.

(57) Pinnaduwage, L. A.; Boiadjiev, V. I.; Hawk, J. E.; Gehl, A. C.; Fernando, G. W.; Wijewardhana, L. C. R. *Nanotechnology* **2008**, *19*.

(58) Stoney, G. G. *Proceedings of the Royal Society of London Series a-Containing Papers of a Mathematical and Physical Character* **1909**, *82*, 172-175.

(59) Shuttleworth, R. *Proc. Phys. Soc., London Sec. A* **1950**, *63*, 444-457.

(60) Sushko, M. L. *Faraday Discuss.* **2009**, *143*, 63-80.

(61) Rubingh, D. N., Holland P. M., Ed. *Cationic Surfactant: Physical Chemistry*; Dekker, 1990.

(62) Parfitt, G. D., Rochester, C. H., Ed. *Adsorption from Solution at the Solid/Liquid Interface*; Academic Press Inc., 1983.

Chapter 3

Review on Supported Lipid Bilayers

3.1. Introduction

This chapter provides a technical background on supported lipid bilayers that is needed to follow the context of this thesis. Understanding the physical and chemical properties of lipid bilayers is key to characterizing how to to study membranes using the microcantilever sensor. A brief background of the lipid bilayers is first introduced. The review will then move from biological membranes to in-vitro artificial membranes, as known as model membranes, and finally to specifically one of the most popular model membranes: the supported lipid bilayer (SLB). This chapter will focus mostly on the SLBs, which is the membrane type of interest in this thesis. Moreover, the surface analytical tools, which are frequently used to characterize the SLBs in the past decade, will be introduced, and related published literatures will be reviewed.

3.2. Lipid Bilayers

Biological membranes are composed of a bilayer of amphiphilic lipid molecules which separates intracellular contents of cells from the extracellular matrix. As a permeability barrier, the membrane also acts as a gate for ions and nutrients through the cells. A typical membrane is a thin film of only 5 nm in thickness and is a very dynamic structure. The constant movement of substances on and through the bilayer, as well as the organization of the membrane structure is commonly described by the fluid mosaic model, proposed by Singer and Nicolson in 1972 [1] (Fig. 3.1). The two leaflets of lipid molecules are fluid with a viscosity similar to that of olive oil, so that individual lipids float laterally with a typical mobility of ~1 $\mu m^2/s$. [2] To understand the

physical and chemical properties of biomembranes, one has to trace back to the basic building blocks which constitute the biomembranes, the lipid molecules. Each lipid molecule has a hydrophilic headgroup, and two hydrophobic tails. As the lipid molecules self-assemble together to form a bilayer, the force that holds the lipid molecules together varies with lipid types as well as temperature. The differences in the forces result in lipid polymorphic phases, as listed in Table 3.1.

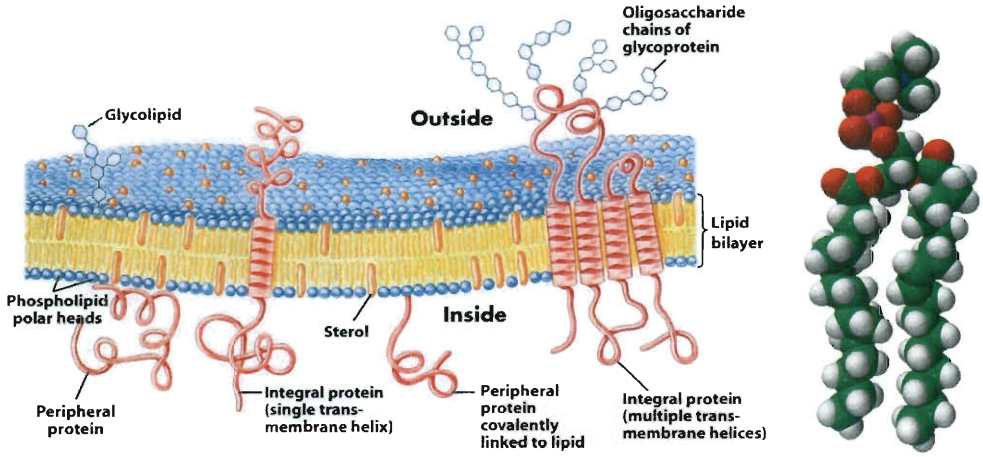

(a) (b)

Figure 3.1. (a) A widely accepted look of a biological membrane, described by the Fluid Mosaic Model. A biomembrane mainly consists of lipids, cholesterols, transmembrane proteins, and carbohydrates. (*Lehninger Principles of Biochemistry,* chapter 11 [3]) (b) One of the typical synthetic lipid molecules, 1-palmitoyl-2-oleoyl-*sn*-glycero-3-phosphocholine (POPC), has two alkyl chains and one phosphatidylcholine headgroup.

Besides lipids, biological membranes also consist of proteins, cholesterol, and carbohydrates as depicted in Fig. 3.1. These components are embedded, float in the sea of the lipids and add diversity to the polymorphic phases to the membrane. Given the complexity of

biomembranes, it is essential to single out the substance in the membrane that is of interest. Model membranes are artificial and are composed of no more than three or four kinds of lipids. The focus of this thesis is on assembling and characterizing the model membranes; therefore, reviews for important literatures on the model membranes will be given through this chapter.

- Lamellar Phase (L)
  - Without cholesterol
    - L_α: fluid; liquid crystalline (L_c); liquid disordered (L_d)
    - L_β: gel; solid ordered (S_o)
    - L_β': some pure phospholipid show minor phase transition between L_β and L_α; L_β phase of tilted chains
    - P_β: rippled phase; some pure phospholipid show minor phase transition between L_β and L_α
  - With cholesterol
    - L_o: liquid ordered
  - Monolayer in Langmuir isotherm
    - Fluidic phases $<T_m$:
      - ❖ Liquid expanded (L_E)
      - ❖ Liquid condensed (L_C)
- Hexagonal (H)
    - H_I: lipid layer with positive curvature; cylinders with nonpolar centers, water outside
    - H_{II}: lipid layer with negative curvature; cylinders with water inside, nonpolar groups outside
- Cubic (Q)
    - Q^{224}: bicontinuous two networks of rods.
    - Q^{227}: quasi-spherical micelles packed into cubes

TABLE 3.1. Common representations of lipid polymorphism phases.

3.3. Model Membranes

3.3.1. Vesicle Lipid Bilayers

Lipid vesicles, or liposomes, are spherical lamellar lipid bilayers. The lipid vesicle is a highly-ranked form of self-assembly, considering organizing billions of lipid molecules into one structure because the lipid's amphiphilic property provides the hydrophobic driving force for self-assembly. The self-assembly of lipids to form a spherical shape in water, or called spontaneous vesiculation, is energetically favored. This assembly mechanism is important as to speculate the origin of the first cell on Earth.

Categorized by size, unilamellar lipid vesicles are categorized as small, large and giant unilamellar vesicles. Small Unilamellar Vesicles (SUVs) have sizes ranging from 20 nm to 50 nm. In SUVs, the lipid alkyl chains are less tightly packed than LUVs or GUVs because of the high curvature of SUVs, thus the interfacial tension (in lateral plane direction) of SUV surfaces is lower than their larger analogs. SUVs can be made by extrusion or sonication methods. Large Unilamellar Vesicles (LUVs) range from100 nm to 2 μm. LUVs can be made by extrusion method. Giant Unilamellar Vesicles (GUVs) range from 2 μm to 300 μm. Electroformation is a convenient way to produce GUVs, however the method is limited to phosphatidylcholine or to lipid mixtures containing mainly phosphatidylcholine. [4]

3.3.2. Supported Lipid Bilayers (SLBs)

Supported lipid bilayers (SLBs) are planar lipid bilayers that are supported on solid substrates, such as mica and glass, and they have become a useful model for studying the processes that take place in the cell membrane. Pioneered by Brian, Tamm and McConnell in mid 1980s, SLBs have been developed into a field that blends surface, polymer and biological sciences. [5, 6] Fixing the soft membrane to a solid substrate allows access to surface analytical tools (such as atomic force microscopy (AFM) and total internal reflection fluorescence microscopy (TIRF)) for direct visualization. To monitor the lipid assembly deposition on the

solid substrates, researchers have successfully used a number of quantitative surface analysis tools, such as quartz crystal microbalance with dissipation (QCM-D) [7-10], surface plasmon resonance (SPR) [7, 11, 12], and imaging ellipsometry [13, 14] to follow the bilayer formation process. In particular, SLBs have proven to be useful in understanding the interactions that govern the force distribution of lipids and membrane proteins, as well as the association of small molecules with the membrane. [15-20] The material used for the supporting surface for SLBs could be a solid (Solid-SLBs), or soft matters such as polymer cushions, polymer tethers or alkanethiol self-assembled monolayers (SAMs). Fig. 3.2 depicts several common SLBs supported on a variety of surface modifications.

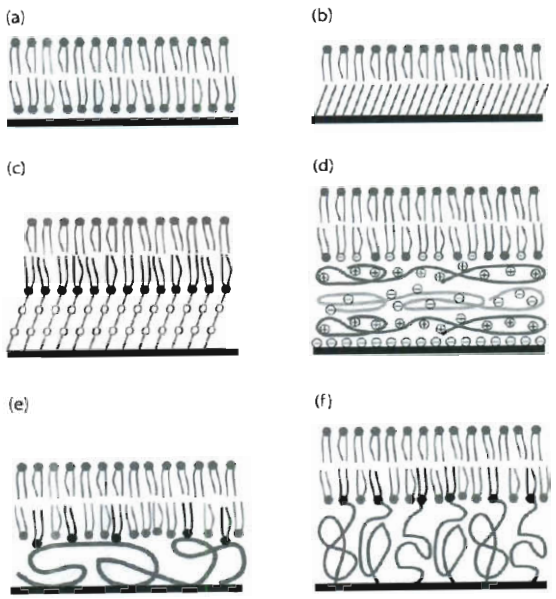

Figure 3.2. Several common surface model lipid membranes. SLBs supported on a variety of surface modifications, such as (a) solid surfaces (glass slides, silicon wafer or mica), (b) self-assembled monolayers (SAMs, usually alkanethiol on gold surfaces) hybrid, (c) oligomer hybrid, (d) polyelectrolyte cushion supported, (e) tethered random copolymer, and (f) tethered telechelic polymer. (Ph.D. thesis of Munro, J. C. [21])

Among many methods for preparing SLBs, vesicle fusion is one of the most convenient ways. By contacting SUVs or LUVs with the solid surface, vesicles fuse onto the solid surfaces and form SLBs spontaneously. This method has the advantage of convenience, ease of being able to reconstitute membrane proteins, and in-situ preparation. This method is chosen to prepare the SLBs in this thesis.

The mechanism SLB formation via vesicle fusion is extensively studied both theoretically (Seifert and Lipowsky [22, 23], Efremov et al. [24], Zhdanov and Kasemo [25]) and experimentally. [8, 26, 27] The widely accepted model of vesicle fusion follows four steps: adsorption, fusion, rupture, and merger (Fig. 3.3). [26, 28] During the fusion and rupture process, the vesicles first adsorb to the surface and fuse with other vesicles to form larger vesicles. The vesicle adsorption is irreversible and diffusion-controlled. Many models proposed that the vesicle adsorption on glass follows Langmuir type adsorption. [29] Until a critical size of the adsorbed vesicles is reached, the adhesion force between the membrane and the surface is strong enough to break the surface-bound vesicles. Thus, the rupture of an adsorbed vesicle is size-dependent. Lipowsky and Seifert established a model and predicted the critical adsorbed phospholipid vesicle size to be 0.2 μm. [22, 23, 30, 31] Once the vesicles rupture, they are converted to supported bilayer disks. To reduce membrane tension at the membrane edges, the isolated membrane patches merge to form complete bilayer coverage of the surface.

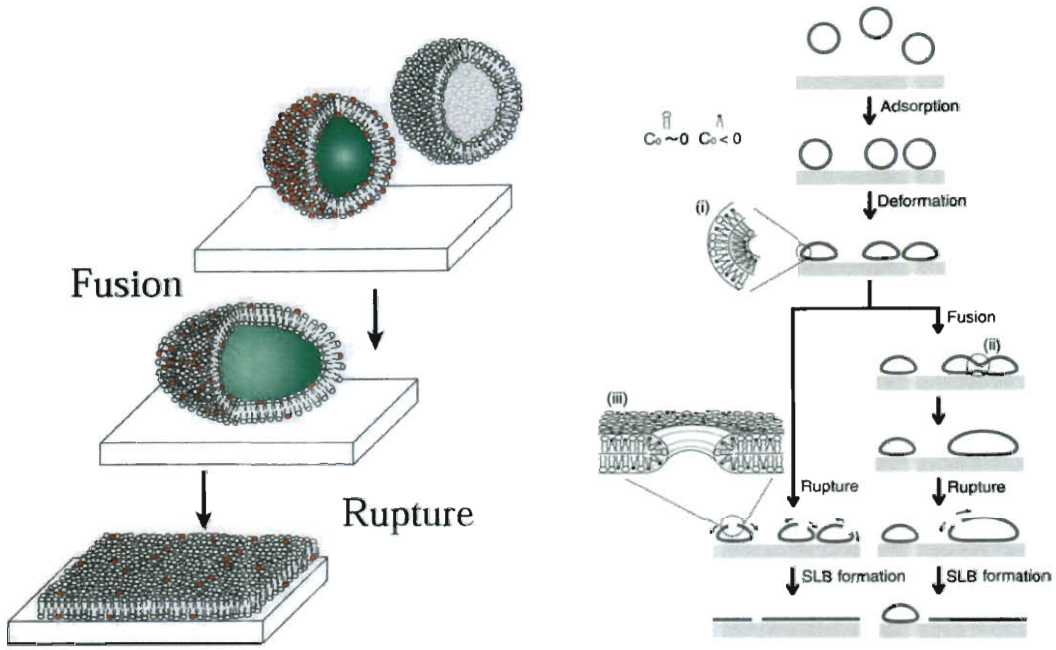

(a) (b)

Figure 3.3. Proposed mechanisms of vesicle fusion on surfaces. (a) A general schematic steps of vesicle fusion. (Johnson et al. [26]) (b) Detailed mechanism of vesicle fusion on surfaces. An intermediate of fused vesicles occurs when the vesicle size dose not reach a critical rupture radius, as shown in the pathway of (ii). (Hamai et al. [28])

The other common method for assembling SLB is lipid monolayer transfer by the Langmuir-Blodgett (LB) technique, followed by vesicles fusion on the first lipid monolayer. Briefly, the lipid molecules are dispersed at the air/water interface in a Teflon trough and confined in a specified surface area by one or two Teflon barriers. The Teflon barrier(s) also control the surface area of the lipid film by slowly compressing the film. The surface pressure, measured by a Wilhelmy plate, is an indicator of packing density and strength of lateral interaction of the lipid film. Due to the lipid's amphiphilicity, the lipids self-assemble to an ordered film when being compressed to a packing density at which the lipids start to interact with

each other, with their polar headgroups immersing in water and two apolar alkyl chains exposed to air. The more the barriers compress the lipid film, the higher the lipid packing density. At a proper surface pressure, which is usually close to the biological lipid lateral pressure around 20~35 mN/m, the lipid monolayer is lifted vertically from the air/water interface by a substrate pre-immersed in the water. [32, 33] After preparing the first lipid leaflet, the second layer can be prepared by the vesicle fusion method as previously mentioned. This method has advantages over vesicle fusion for its convenience to adjust the lipid lateral pressure in-situ and to control the surface grafting density of polymer tethers if the tethers are needed as in Fig. 3.2(f). However LB technique does not apply to incorporating membrane proteins in the monolayer because most of the proteins re-configure and loss their native structures at the air/water interface.

Substrate properties can greatly influence the formation of SLBs. The methods used to prepare glass substrates also influences the quality of SLBs. Seu et al. compared SLBs formed on the glass slides pretreated with piranha-etching, baking, and detergent-cleaning. [34] They found that detergent-cleaning and baking methods provide the SLBs a higher lateral mobility than those prepared by piranha-etching method due to different surface roughness. In addition, different substrate materials to form SLBs have been explored. Attempts to fuse SUVs to form SLBs on substrates other than silica-based surface are explored on TiO_2, [35] indium tin oxide (ITO) [36] and gold, however those surfaces cannot provide enough adhesion energy to break the adsorbed lipid vesicles. Stable adsorption of lipid vesicles onto those surfaces was analyzed as an alternative of surface-bound membrane. [37-39] Additionally, modifying gold surfaces with hydrophobic SAMs to form hybrid bilayers is the other way. [40, 41] Hybrid bilayers formed on hydrophobic self-assembled monolayers (SAMs) of various surface free energy show different formation kinetics. [11, 42, 43] Several studies have shown how surface properties, such as surface charge density, surface free energy and surface modifications with hydrophilic/hydrophobic polymer

tethers or SAMs, affect the interactions between the lipid vesicles and the solid support. [11, 44, 45] Despite the insights on the formation and stability of lipid membranes gained from these experiments, the differences between the free-standing membranes and membranes near a solid surface remain unclear.

The elastic properties of lipid membranes such as local curvature stress and bilayer deformation from hydrophobic mismatch have emerged as important parameters that govern the function of embedded ion channels, receptors, and other integral membrane proteins. [46-48] Faller et al. have demonstrated using coarse-grained simulations that there is a strong tension associated with the proximal lipid leaflet in a SLB resulting in a lateral pressure profile that deviates greatly from that of a free-standing lipid bilayer. [49, 50] That is, the membrane bilayer is no longer tension-free as a free-standing membrane. [51]

Surface patterned SLBs can be achieved by photolithography. The Boxer group has created patterned bilayers with each bilayer patch separated by rectangular photoresist corrals or protein barriers (Fig. 3.4(a)(b)). [52-55] Another method uses patterned PDMS stamp to transfer lipid patches from dry lipid films to the target substrate (also called soft lithography), thus leaving patterned lipid film features. [56, 57] In addition, SLBs have also been introduced to microfluidic devices (Fig. 3.4(c)). Bilayer arrays with specific composition variations in different micro-patterned corrals can be achieved by directing each composition into individual laminar stream created in microfluidic channels. [54, 58] Daniel et al. explored the electrophoresis of charged dyes in the membrane by integrating the SLBs which contain two different negatively charged dyes in a microfluidic channel and applying an electric field parallel to the channel. [59] They observed that the two different dyes in the SLBs were separated into two bands on the SLBs as a result of the electrophoretic phenomena.

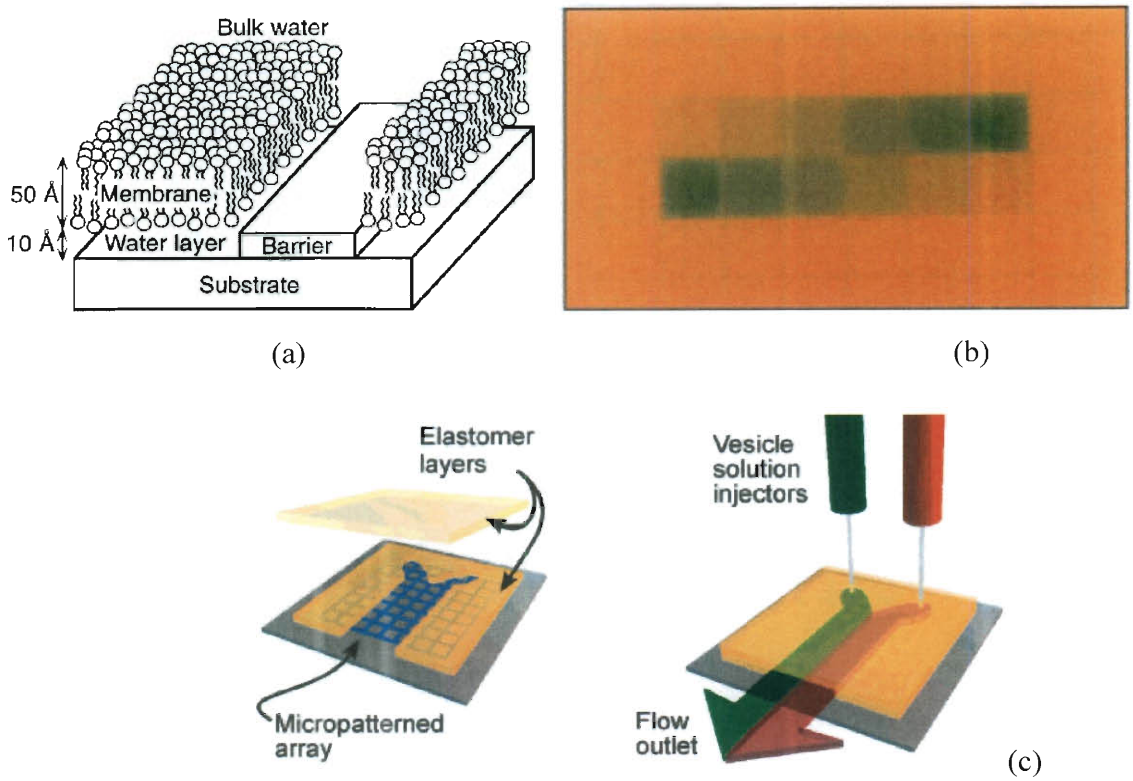

Figure 3.4. Integrating supported lipid bilayers to microfabrication techniques. (a) Supported lipid bilayer partitioned by microfabricated barriers. (b) Epifluorescence of patterned lipid membranes (50μm by 50 μm) separated by corrals 2 μm wide. (c) Covering the patterned arrays of SLBs with microfludic channels. Different vesicle solutions were directed into individual laminar flow streams. (Groves, Ulman and Boxer. [53]; Kam and Boxer [54])

3.4. Techniques for Characterizing SLBs

A number of surface analytical technologies are used to probe the physical and chemical properties of the SLBs and interactions that take place on the SLBs. Besides the microcantilever sensor used in this thesis, several other popular surface technologies are described in this section.

3.4.1. Mass and Viscoelastic Characterization of SLBs Using the Quartz Crystal Microbalance with dissipation (QCM-D)

QCM-D is useful for monitoring surface reactive process, and it extracts the surface mass change from the intrinsic vibration properties of quartz itself. Quartz is a piezoelectric material and mechanically deforms when an electric potential is applied. If an oscillating voltage is applied across the quartz, the quartz vibrates at a specific frequency, which is determined by the thickness of the crystal. Surface adsorption of molecules to the quartz crystals alters the effective crystal thickness, so as the resonance frequency. The adsorbed mass alters the resonance frequency linearly. That is, by observing the changes in the resonance frequency, the adsorbed mass is known. Sauerbrey equation relates the mass change (Δm) and the frequency change over the overtone (Δf) by a constant C:

$$\Delta m = -\frac{C}{t}\Delta f$$

The physical property of quartz itself, such as the density, shear modulus, transverse wave velocity in quartz, and the active surface area, decides the constant C. More information about the working principles and usage of QCM-D is described in Chapter 8 and Appendix A.

Keller and Kasemo were the first to detect the lipid mass deposited on SiO_2-coated quartz crystal surfaces to confirm the SLB formation using the QCM-D. In their experiments, a SLB on a SiO_2 surface results in the frequency shift of the quartz crystal by 26.0 Hz, or 468 ng/cm^2. Assuming the density of a lipid membrane close to 1 g/cm^3, the film thickness is 4.68 nm, which is close to the value of a SLB. This value of frequency change has become an indicator of a good SLB formation. As the frequency and dissipation evolve with time during the SLB formation, a two-step process observed. In the first few minutes, the vesicles adsorb to the surface, creating a large frequency and dissipation change. Shortly after the adsorption, the vesicles rupture and spread into a thin film, so the dissipation decrease to be smaller than $1 \cdot 10^{-6}$ (See Fig. 3.5). [8]

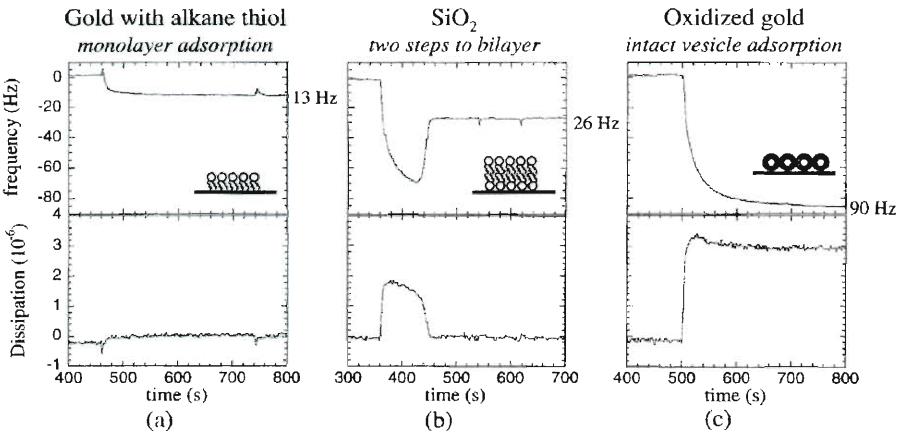

Figure 3.5. QCM-D measurement for formation of different lipid assemblies on three different surfaces from SUVs. (a) A lipid monolayer was formed on hydrophobic alkane-modified gold surface. (b) On a SiO_2 surface, a dense thin layer of SLB forms within minutes. (c) Plain gold surface attracts lipid membranes to adsorb on the surface but not strongly enough to break lipid vesicles into a SLB. (Keller and Kasemo. [8])

3.4.2. Measuring Thickness of SLBs Using Ellipsometry

The optical thickness of a thin SLB film can be determined by ellipsometry. [13, 60-63] , as shown in Fig. 3.7. Howland et al. determined the SLB thickness with an accuracy of 0.2 nm, and they observed a lateral phase separation of a two-component SLB with dendritic domains. [13] Furthermore, they used imaging ellipsometry, which combines the microscopy and ellipsometry techniques, to visualize the topographic thickness map of patterned lipid membrane patches supported on different surface modifications. [13, 64] Munro and Frank used ellipsometry to determine the thickness of polymer-SLBs with various polymer tether density and polymer adsorption time. [44] Stroumpoulis et al. used ellipsometery to follow vesicle fusion onto SiO_2 surfaces. [65] They developed a kinetic equation to describe the time-dependent lipid film thickness during the SLB growth and derived the diffusion coefficient for lipid vesicles to diffuse near the

surfaces.

Based on measuring the changes of the polarization of monochromatic light reflected from the surface of interest, an ellipsometer is used to determine the thickness and refractive index properties of a thin film on a surface. It is capable of measuring film thickness ranging from 10^{-10} to 10^{-6} m. From electromagnetic theory, when polarized monochromatic light reflect at an oblique incidence, the polarization properties change in both the p (parallel to the plane of incidence) and s (the light oscillating perpendicular to the plane of incidence) components of the light. The changes in the (i) phase difference (δ_p- δ_s) between the p and s components of the reflected light and (ii) the ratio of the reflective light intensity of p (R_p) to s (R_s) can be written as: [66]

$$\Delta = \delta_p - \delta_s, \text{ and } \tan\Psi = \frac{|R_p|}{|R_s|}. \tag{3.1}$$

R_p and R_s are the complex reflection coefficients for light polarized parallel and perpendicular to the plane of incidence, respectively. Thus, upon reflection, there are independent changes in the phase (Δ) and intensity (Ψ) between the two polarization component s and p. Δ, Ψ are frequently referred to as ellipsometry angles. The relation between Δ and Ψ can be summarized by the equation:

$$\frac{R_p}{R_s} = \text{Re}\,(R) + \text{Im}\,(R) = \tan\Psi \cdot \exp[j\Delta]. \tag{3.2}$$

With a thin film on the surface, there are more than one interfaces; the collected reflected light is composed not only the direct reflective light but also the lights that transmit across the film and then reflect at the bottom of the film. Thus, the R_p and R_s has to count reflections at interfaces of ambient/film and film/substrate (See Fig. 3.6) and can be written as:

$$R_p = \frac{r_p^{12} + r_p^{23}\exp[-2j\beta]}{1 + r_p^{12} r_p^{23}\exp[-2j\beta]}, \text{ and } \quad R_s = \frac{r_s^{12} + r_s^{23}\exp[-2j\beta]}{1 + r_s^{12} r_s^{23}\exp[-2j\beta]}, \tag{3.3}$$

$$\text{where } \quad \beta = 2\pi\left(\frac{d}{\lambda}\right) N_2 \cos\phi_2 \tag{3.4}$$

r^{12} and r^{23} are reflective intensity of light reflected at interfaces of medium 1,2 and 2,3. N is the reflective index, and θ is the reflective angle. λ is the wavelength. The thickness of the film, d, then can be derived by solving the equations.

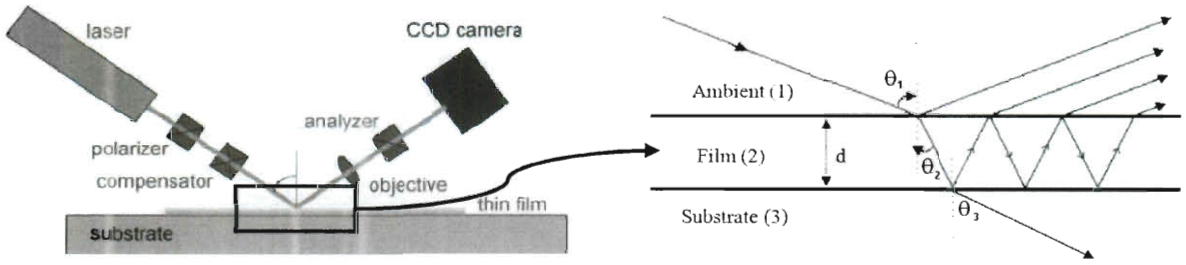

(a) (b)

Figure 3.6. (a)Schematic diagram for nulling type imaging ellipsometer (EP3 model, Nanofilm, German). (b) Zoom-in representative of the reflections and transmissions at two interfaces. The total resultant reflected light is composed of the direct reflected beam and the infinite series of beams which are transmitted from the film back to the ambient.

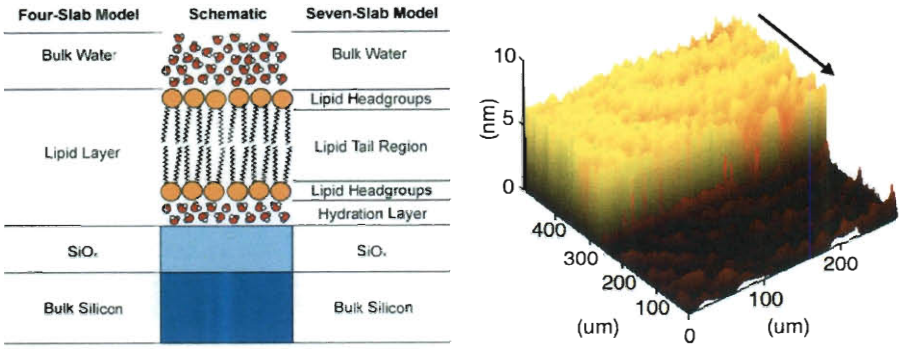

(a) (b)

Figure 3.7. (a) The optical models for the SLB. The seven slab model on the right side is closer to a real scenario, but it is too complicated to fit the data. The four slab model is a simplified version of the seven layer one and consists of bulk water, SLB, SiO_2, and Si. Each layer is defined with refractive index. Fitting the optical model to the Δ and Ψ results in a thickness map as shown in (b). (Howland, et al. [13])

3.4.3. Fluidity Characterization of SLBS by Fluorescence Recovery After Photobleaching (FRAP)

Fluorescence Recovery After Photobleaching (FRAP) is a well-received method for determining the fluidity and lateral mobility of lipid membranes. Particularly, the fluidity of SLBs is an indicator whether the membrane can be used to properly accommodate membrane proteins. If lacking good fluidity, the membrane is thought to be "pinned" to the solid through the added tether molecules or proteins. In this case, the incorporated membrane proteins or channels have no space for further folding and stretching and lose their biological function. The working principle is, by monitoring the rate of the unbleached fluorescent tags diffuse into the area where the fluorescent tags are previously bleached, the diffusion coefficient can be derived quantitatively. The fluorescence fraction f(t) in the pre-bleached area is defined as:

$$f(t) = \frac{F(t) - F(0)}{F(\infty) - F(0)}, \tag{3.5}$$

where F(t) is the fluorescence intensity as a function of time. F(0) is the fluorescence intensity before bleaching, and F(∞) is the final recovered intensity. Thus, the recovery half time, $\tau_{1/2}$, can be determined as the time where f(t)=1/2. Knowing the radius, r, of the bleached area, the diffusion coefficient is derived by the equation:

$$D_f = \frac{0.22\, r^2}{\tau_{1/2}}. \tag{3.6}$$

In addition, FRAP can be used to determine the fluidity of each individual leaflet with respective fluorescent tags. [6] Other than the mobility of lipids, FRAP can also tell the mobility of protein incorporated in a SLB, so that whether the protein is fixed or not. [67] This is particularly useful for testing if a polymer cushion supported or tethered lipid bilayer is successful or not. [44, 60] (see Fig. 3.8)

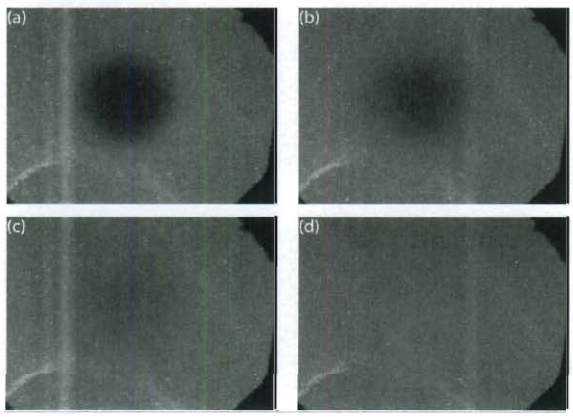

Figure 3.8. Fluorescence recovery of Texas red doped SLB supported on a 10% tethered PEG film. The images were taken at (a) 0, (b) 1, (c) 3 and 15 minutes after photobleaching. The diffusion coefficient was determined 2.1 $\mu m^2/s$. (Munro et al.[60])

3.5. Adsorption Free Energy of Vesicles on Solid Surfaces

Despite many models and mechanisms proposed, it is the adsorption free energy that participates in the surface free energy change at the solid–liquid interface and can be measured by the microcantilever sensors. Since the vesicles are composed of amphiphilic lipids, which are similar to surfactants, the adsorption behavior of ionic surfactants on solid surfaces can be compared to the lipids.

This adsorption free energy of a surfactant-like amphipathic molecule on solid from solution is found to be related to the charge density of both the adsorbate (lipid) and adsorbent (SiO_2). Also it depends on the configurations of the physically adsorbed film. The adsorption free energy is usually written as a number of additive contribution terms. For adsorption of ionic surfactants on solid, the adsorption free energy is written as a sum of free energy terms from electrostatic interactions and a specific adsorption free energy term that comprises interactions that is non-electrostatic: [68, 69]

$$\Delta G_{ads} = \Delta G_{elec} + \Delta G_{spec}, \tag{3.7}$$

where the two terms include:

$\Delta G_{elec} = \Delta G_{coul} + \Delta G_{dip}$ (columbic interaction and dipole momentum changes)

$\Delta G_{spec} = \Delta G_{cc} + \Delta G_{cs} + \Delta G_{hs}$ (chain-chain, chain-surface and headgroup-surface and other factors)

These expressions describe SLB adsorption on the SiO_2 surface. For instance, for POPC lipid bilayer (zwitterionic) adsorption, the total adsorption free energy consists of both ΔG_{elec} and ΔG_{spec}, while the ΔG_{coul} in ΔG_{elec} is absent due to counterions on phosphate group and choline group of the headgroup. Thus when the POPC bilayer is replaced by a DOTAP bilayer (cationic lipid, similar aliphatic chain length with POPC), the main change is in ΔG_{elec}. Besides the electrostatic contribution, the addition of hydrophobic molecules to the bilayer, such as cholesterol, changes ΔG_{cc} because cholesterol molecules embed themselves in the hydrophobic

aliphatic chain part of the bilayer. Increasing the adsorption free energy of a SLB on the solid surface will lead to larger surface free energy of the solids, as described in Chapter 2. Thus, on a microcantilever surface, the stronger affinity between the lipids and the SiO_2 surface, the more the microcantilever bends.

For a scenario closer to a real SLB supported on solid surfaces, an interstitial water layer sandwiched between the SLB and the solid should be considered. The adsorption of the lipid membrane film can be depicted in Fig. 3.9. Because of the separation by a water layer of 1 nm thick, the interactions in the lipid film does not directly affect the surface free energy of the solid substrate. Compared to other surface–grafted molecules described in Chapter 2, such as alkanethiol SAMs and DNA brushes, the lipid membrane expansion or contraction may not mechanically drive the microcantilevers to bend. However, the overall interactions between lipid–lipid and lipid–solids all count and affect the affinity between the SLB and the solids. With higher lipid–lipid interactions, the lipid membrane is more stable on the surface, so the adsorption is more favored and will increase the total adsorption free energy. This theory will be examined by experimental measurement using microcantilevers in Chapter 4.

The total adhesion energy is a sum of energies from van der Waals force, electrostatic force, hydration force and steric force. If consider the adhesion of zwitterionic lipid membranes to solid surfaces a result of only the van der Waals attraction, and the interstitial water layer is 1 nm, the adhesion work is calculated to be $5.3 \cdot 10^{-4}$ J/m^2, or 0.53 mN/m (using the equation of van der Waals interaction energy for two adhered surfaces, $W=-A_H/12\pi D^2$, where A_H is the Hamaker constant and D the separation between the membrane and the surface. A_H is taken to be $2 \cdot 10^{-20}$ J). [70] This magnitude will be compared to the measured value to evaluate the contribution of van der Waals attraction to the adsorption free energy in Chapter 4. It is reported that the electrostatic energy dominates the overall adhesion energy for charged surfaces and membranes. [71]

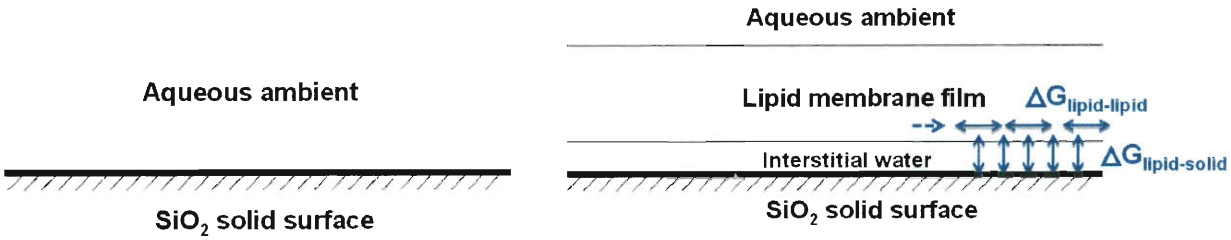

(a) (b)

Figure 3.9. Schematics of a SiO_2 surface (a) before, and (b) after the SLB is formed. Both lipid-lipid and lipid-solid interactions contribute to the free energy of adsorption.

3.6. Reference

(1) Singer, S. J.; Nicolson, G. L. *Science* **1972**, *175*, 720.

(2) Luckey, M. *Membrane Structural Biology - With Biochemical and Biophysical Foundations*; Cambridge University Press, 2008.

(3) Nelson, D. L.; Cox, M. M. *Lehninger Principles of Biochemistry*, 4 ed., 2004.

(4) Luisi, P. L. *Giant Vesicles*; Jone Wiley & Sons: Zurich, Switzerland, 2000.

(5) Tamm, L. K.; McConnell, H. M. *Biophysical Journal* **1985**, *47*, 105-113.

(6) Brian, A. A.; McConnell, H. M. *Proceedings of the National Academy of Sciences of the United States of America-Biological Sciences* **1984**, *81*, 6159-6163.

(7) Keller, C. A.; Glasmastar, K.; Zhdanov, V. P.; Kasemo, B. *Phys. Rev. Lett.* **2000**, *84*, 5443-5446.

(8) Keller, C. A.; Kasemo, B. *Biophys. J.* **1998**, *75*, 1397-1402.

(9) Richter, R.; Mukhopadhyay, A.; Brisson, A. *Biophys. J.* **2003**, *85*, 3035-3047.

(10) Weng, K. C.; Kanter, J. L.; Robinson, W. H.; Frank, C. W. *Colloid Surf. B-Biointerfaces* **2006**, *50*, 76-84.

(11) Silin, V. I.; Wieder, H.; Woodward, J. T.; Valincius, G.; Offenhausser, A.; Plant, A. L. *J. Am. Chem. Soc.* **2002**, *124*, 14676-14683.

(12) Tawa, K.; Morigaki, K. *Biophys. J.* **2005**, *89*, 2750-2758.

(13) Howland, M. C.; Szmodis, A. W.; Sanii, B.; Parikh, A. N. *Biophys. J.* **2007**, *92*, 1306-1317.

(14) Sanii, B.; Parikh, A. N. *Soft Matter* **2007**, *3*, 974-977.

(15) Tanaka, M.; Sackmann, E. *Nature* **2005**, *437*, 656-663.

(16) Tanaka, M. *MRS Bull.* **2006**, *31*, 513-520.

(17) Tanaka, M.; Sackmann, E. *Phys. Status Solidi A-Appl. Mat.* **2006**, *203*, 3452-3462.

(18) Castellana, E. T.; Cremer, P. S. *Surf. Sci. Rep.* **2006**, *61*, 429-444.

(19) Rossi, C.; Chopineau, J. *Eur. Biophys. J. Biophys. Lett.* **2007**, *36*, 955-965.

(20) Sackmann, E. *Science* **1996**, *271*, 43-48.

(21) Munro, J. C., Stanford University, 2004.

(22) Seifert, U. *Phys. Rev. A* **1991**, *43*, 6803-6814.

(23) Seifert, U.; Lipowsky, R. *Physical Review A* **1990**, *42*, 4768-4771.

(24) Efremov, A.; Mauro, J. C.; Raghavan, S. *Langmuir* **2004**, *20*, 5724-5731.

(25) Zhdanov, V. P.; Kasemo, B. *Langmuir* **2001**, *17*, 3518-3521.

(26) Johnson, J. M.; Ha, T.; Chu, S.; Boxer, S. G. *Biophys. J.* **2002**, *83*, 3371-3379.

(27) Hamai, C.; Cremer, P. S.; Musser, S. M. *Biophysical Journal* **2007**, *92*, 1988-1999.

(28) Hamai, C.; Yang, T. L.; Kataoka, S.; Cremer, P. S.; Musser, S. M. *Biophysical Journal* **2006**, *90*, 1241-1248.

(29) Jackson, S.; Reboiras, M. D.; Lyle, I. G.; Jones, M. N. *Faraday Discuss.* **1986**, *81*, 291-301.

(30) Lipowsky, R.; Seifert, U. *Mol. Cryst. Liquid Cryst.* **1991**, *202*, 17-25.

(31) Lipowsky, R.; Seifert, U. *Langmuir* **1991**, *7*, 1867-1873.

(32) Peterson, I. R. *Journal of Physics D-Applied Physics* **1990**, *23*, 379-395.

(33) Kuhner, M.; Tampe, R.; Sackmann, E. *Biophys. J.* **1994**, *67*, 217-226.

(34) Seu, K. J.; Pandey, A. P.; Haque, F.; Proctor, E. A.; Ribbe, A. E.; Hovis, J. S. *Biophys. J.* **2007**, *92*, 2445-2450.

(35) Rossetti, F. F.; Textor, M.; Reviakine, I. *Langmuir* **2006**, *22*, 3467-3473.

(36) Kumar, K.; Tang, C. S.; Rossetti, F. F.; Textor, M.; Keller, B.; Voros, J.; Reimhult, E. *Lab on a Chip* **2009**, *9*, 718-725.

(37) Sofou, S.; Thomas, J. L. *Biosens. Bioelectron.* **2003**, *18*, 445-455.

(38) Kik, R. A., Wageningen Universiteit, 2007.

(39) Jung, H.; Kim, J.; Park, J.; Lee, S.; Lee, H.; Kuboi, R.; Kawai, T. *J. Biosci. Bioeng.* **2006**, *102*, 28-33.

(40) Richter, R. P.; Berat, R.; Brisson, A. R. *Langmuir* **2006**, *22*, 3497-3505.

(41) Plant, A. L. *Langmuir* **1999**, *15*, 5128-5135.

(42) Hubbard, J. B.; Silin, V.; Plant, A. L. *Biophys. Chem.* **1998**, *75*, 163-176.

(43) Lingler, S.; Rubinstein, I.; Knoll, W.; Offenhausser, A. *Langmuir* **1997**, *13*, 7085-7091.

(44) Munro, J. C.; Frank, C. W. *Langmuir* **2004**, *20*, 3339-3349.

(45) Cha, T.; Guo, A.; Zhu, X. Y. *Biophys. J.* **2006**, *90*, 1270-1274.

(46) Hong, H. D.; Tamm, L. K. *Proc. Natl. Acad. Sci. U. S. A.* **2004**, *101*, 4065-4070.

(47) Keller, S. L.; Bezrukov, S. M.; Gruner, S. M.; Tate, M. W.; Vodyanoy, I.; Parsegian, V. A. *Biophys. J.* **1993**, *65*, 23-27.

(48) Podgornik, R.; Parsegian, V. A. *Langmuir* **1992**, *8*, 557-562.

(49) Xing, C. Y.; Ollila, O. H. S.; Vattulainen, I.; Faller, R. *Soft Matter* **2009**, *5*, 3258-3261.

(50) Xing, C. Y.; Faller, R. *J. Phys. Chem. B* **2008**, *112*, 7086-7094.

(51) Jahnig, F. *Biophys. J.* **1996**, *71*, 1348-1349.

(52) Yoshina-Ishii, C.; Boxer, S. G. *Langmuir* **2006**, *22*, 2384-2391.

(53) Groves, J. T.; Ulman, N.; Boxer, S. G. *Science* **1997**, *275*, 651-653.

(54) Kam, L.; Boxer, S. G. *J. Am. Chem. Soc.* **2000**, *122*, 12901-12902.

(55) Kung, L. A.; Kam, L.; Hovis, J. S.; Boxer, S. G. *Langmuir* **2000**, *16*, 6773-6776.

(56) Xia, Y. N.; Whitesides, G. M. *Annual Review of Materials Science* **1998**, *28*, 153-184.

(57) Hovis, J. S.; Boxer, S. G. *Langmuir* **2001**, *17*, 3400-3405.

(58) Kam, L.; Boxer, S. G. *Langmuir* **2003**, *19*, 1624-1631.

(59) Daniel, S.; Diaz, A. J.; Martinez, K. M.; Bench, B. J.; Albertorio, F.; Cremer, P. S. *J. Am. Chem. Soc.* **2007**, *129*, 8072-+.

(60) Munro, J. C.; Frank, C. W. *Langmuir* **2004**, *20*, 10567-10575.

(61) Richter, R. P.; Brisson, A. R. *Biophysical Journal* **2005**, *88*, 3422-3433.

(62) Puu, G.; Gustafson, I. *Biochimica Et Biophysica Acta-Biomembranes* **1997**, *1327*, 149-161.

(63) Benes, M.; Billy, D.; Benda, A.; Speijer, H.; Hof, M.; Hermens, W. T. *Langmuir* **2004**, *20*, 10129-10137.

(64) Howland, M. C.; Sapuri-Butti, A. R.; Dixit, S. S.; Dattelbaum, A. M.; Shreve, A. P.; Parikh, A. N. *Journal of the American Chemical Society* **2005**, *127*, 6752-6765.

(65) Stroumpoulis, D.; Parra, A.; Tirrell, M. *Aiche Journal* **2006**, *52*, 2931-2937.

(66) Tomkins, H. G.; McGahan, W. A. *Spectroscopic Ellipsometry and Reflectometry: A User's Guide*; Wiley&Sons, Inc, 1999.

(67) Reits, E. A. J.; Neefjes, J. J. *Nature Cell Biology* **2001**, *3*, E145-E147.

(68) Rubingh, D. N., Holland P. M., Ed. *Cationic Surfactant: Physical Chemistry*; Dekker, 1990.

(69) Parfitt, G. D., Rochester, C. H., Ed. *Adsorption from Solution at the Solid/Liquid Interface*; Academic Press Inc., 1983.

(70) Israelachvili, J. N. *Intermolecular and Surface Forces: With Applications to Colloidal and Biological Systems*, 2 ed.; Elsevier Science & Technology Books, 1992.

(71) Wiegand, G.; Arribas-Layton, N.; Hillebrandt, H.; Sackmann, E.; Wagner, P. *J. Phys. Chem. B* **2002**, *106*, 4245-4254.

Chapter 4

Studying the Interactions of Lipid Bilayers with Solid Surfaces Using Microcantilevers

4.1.Introduction

This chapter reports the use of free-standing microcantilever beams, which have been used as an ultrasensitive method for measuring the surface free energy changes on a substrate induced by the adsorption of thin films as introduced in Chapter 2, to probe the interactions between a solid surface and a phospholipid bilayer. The surface stress induced on microcantilever surfaces by a 1-palmitoyl-2-oleoyl-*sn*-glycero-3-phosphocholine (POPC) planar supported lipid bilayer (SLB) is a direct measure of the surface free energy change upon lipid physisorption to a silicon dioxide (SiO_2) surface. Both lateral interactions in the membrane and that between the lipid membrane and the solid support are governed by a variety of intermolecular forces, such as van der Waals forces, [1] electrostatic interactions, [2, 3] and structural components. [4, 5] In this chapter, we report the surface stress measured in the solid support under conditions of (i) different SLB surface charge density, which can be associated with electrostatic partitioning in the adsorption free energy of the membrane. The deflection is influenced by electrostatic and intermolecular interactions of the bilayer with the substrate. Increasing the surface charge density in the supported lipid bilayer (SLB), by increasing the ratio of cationic to zwitterionic lipids in bilayer, resulted in an increase in cantilever deflection. (ii) Lipid transfer with oppositely charged membranes. The surface free energy changes due to lipid transfer between anionic unilamellar vesicles and a cationic supported bilayer were also observed using microcantilevers. And, (iii) the association of cholesterol with the lipid membrane. The

adsorption free energy of a mixed lipid and cholesterol bilayer was measured demonstrating a detectable decrease in affinity between the phospholipid bilayer and the solid surface as a result of the addition of cholesterol.

The findings yield a novel method of characterizing the affinity of planar lipid membranes with solid surfaces as a function of the interactions governing the structure of supported lipid membranes and shed light on how the electrostatic and structural interactions in the membrane change its interactions with a solid support.

4.2.Experimental Section

4.2.1.Lipid Vesicle Preparation

A zwitterionic lipid, 1-palmitoyl-2-oleoyl-*sn*-glycero-3-phosphocholine (POPC), was used to form a neutral lipid bilayer. A cationic lipid, 1,2-dioleoyl-3-trimethylammonium-propane (DOTAP), was used to generate mixed cationic–zwitterionic lipid bilayers to study electrostatic interactions within the bilayer. To study charge neutralization within the bilayer, an anionic lipid, 1- palmitoyl- 2- oleoyl- *sn*- glycero- 3- phospho- L-serine (POPS), was used. Finally, cholesterol was used to modify the interactions between lipid chains in the bilayer. The lipids and cholesterol were purchased from Avanti Polar Lipids (Alabaster, AL). All the lipids and chemicals were used as received without further purification. Vesicles were prepared by a standard extrusion method [6]. Briefly, pure and mixed lipid solutions of 0.25 ml were made at a concentration of 5 mg/ml in chloroform in a glass vial. The chloroform was evaporated and dried under a gentle ultra-pure nitrogen stream. The resulting lipid film was then desiccated in a vacuum chamber for a minimum of two hours and then hydrated with 0.25 ml of pH 7.4 phosphate buffered saline (PBS) buffer solution, with an ionic strength of 233.6 mM (Sigma-Aldrich, USA), followed by

vortexing the solution. The solution was then extruded 40 times through a polycarbonate membrane using a mini-extruder (Avanti Polar Lipids), resulting in a translucent solution of large unilamellar vesicles (LUVs) approximately 100 nm in diameter in PBS. The vesicle solution was further diluted with 9 parts of PBS to 1 part of the freshly extruded vesicle solution and stored at 4 °C until use. The estimated lipid concentration was 0.5 mg/ml. Note that the final vesicle solution concentration may be lower than initially desired due to lipid loss on filter membranes after extrusion, however the concentration was well above the SLB formation threshold needed to achieve full coverage.

4.2.2.Microcantilever Preparation

Cantilever chips were purchased from Concentris GmbH (Basel, Switzerland). The cantilevers are 500 μm in length, 100 μm in width, and 1 μm thick. Each chip contains eight rectangular silicon cantilevers, each with a spring constant of 0.026 N/m. In order to form clean hydrophilic surfaces for lipid bilayer formation, the microcantilever arrays were first treated with piranha solution (H_2SO_4:H_2O_2=7:1, heated to 120 °C). The cantilevers were then coated with 3 nm titanium followed by 20 nm gold layer via a high vacuum chamber (E-Beam Evaporator, Telemark.) resulting in a bimetallic structure. The cantilever arrays were placed in an UV ozone cleaner for 5 minutes under 5 psi oxygen. This resulted in a cantilever with a clean gold surface on the frontside and a hydrophilic silicon dioxide surface on the backside. Each cantilever was individually functionalized using glass microcapillaries. The surface functionalization typically proceeds for two hours. To prevent binding preferentially to either the silicon dioxide or gold side of the cantilever beam, hydrophilic polyethylene glycol (PEG) polymers were utilized. A dithiolaromatic-PEG molecule ($C_{25}H_{44}O_6S_2$, MW=504.74 g/mol, Sensopath Technologies, Bozeman, MT) was used to prevent vesicle adsorption to the gold surface of the cantilever. A

PEG-silane molecule, 2- [methoxy-(polyethyleneoxy)propyl]- trimethoxysilane ($C_{13}H_{30}O_7Si$, MW= 326.46 g/mol, Gelest Inc. Morrisville, PA), was used to prevent vesicle adsorption on the silicon dioxide surface of the cantilever. A reference cantilever was functionalized with both the dithiolaromatic-PEG and the PEG-silane. After use, the cantilevers were once again placed in the UV ozone cleaner for 5 minutes under 5 psi oxygen and then refunctionalized as described above.

4.2.3.Microcantilevers to Measure Surface Stress

All measurements were performed with a Cantisens Research System (Concentris GmbH, Basel, Switzerland). The cantilevers were mounted in a liquid chamber in which solutions were pumped past the cantilever chip via a syringe pump. The chamber was temperature controlled and for all reported experiments the chip was held at 25 °C. Prior to the introduction of vesicle solutions, the cantilever signals were set to a zero baseline value. Each sample injection consisted of flowing 0.2 mL of vesicle solution at a flow rate of 0.42 μL/sec. Excess liquid was pumped to the waste reservoir via a syringe pump. Real-time deflection of microcantilevers was monitored via a scanning laser diode aligned to the tip of the microcantilevers. The position of the reflected laser beam was captured using a position-sensitive-detector (PSD), with a sampling frequency of 1 Hz. The average thermomechanical sensitivity of the cantilevers was measured to be 73 ± 11 nm/K. [7] Due to small differences in material properties of the cantilevers such as stiffness or thickness variation of the evaporated gold layer, the deflections of the cantilevers were normalized using each cantilever's thermomechanical sensitivity. After normalization, the signal difference between the experimental cantilever and the reference cantilever was calculated to allow us to measure the cantilever deflection due to the vesicle rupture into a SLB. Each experiment was repeated 2~3 times on either the same or on a different chip, with a minimum of 4 cantilevers on the same chip used for each experiment. The signals were processed using

MATLAB. The regression model using a nonlinear least squares method with Gauss-Newton algorithm was used for the fits. Fitting coefficients were obtained within 95% confidence bounds.

4.3.Results

4.3.1. Lipid Deposition onto Functionalized Microcantilever Surfaces

Upon injection of the POPC vesicle solution into the flow chamber, the cantilevers undergo a surface stress change. For cantilevers modified with the dithiolaromatic-PEG, the cantilevers bend towards the gold surface. As shown in Fig. 4.2(a), a positive deflection of 73 ± 6.0 nm (17 ± 1.4mN/m) is observed due to the rupture of the lipid vesicles on the silicon dioxide surface. It is known that vesicles rupture to form a lipid bilayer of 5 nm in thickness on silicon dioxide. [8, 9] The origin of the deflection upon the lipid bilayer formation on the silicon oxide surface is the free energy change caused by the interaction of lipids with the cantilever surface. The cantilevers modified with both dithiolaromatic-PEG and PEG-silane, shown in Fig. 4.2(b), have little deviation from the baseline value indicating little vesicle adsorption or bilayer formation on the PEG films. For cantilevers modified with PEG-silane, a negative deflection of 420 ± 30 nm (98 ± 7.0 mN/m) is observed, shown in Fig. 4.2(c). It is well known that lipid vesicles adsorb intact onto gold surfaces rather than rupture to form SLBs. [8, 10, 11] The large negative deflection and the fact that the cantilevers bend away from the gold surface suggest steric repulsion between adsorbed vesicles. The signal equilibrates once a critical surface layer of vesicles is adsorbed. Note that the deflection due to bilayer formation is significantly smaller than the deflection generated due to vesicle adsorption. For a SLB adsorbed to a cantilever, there is an asymmetrical environment, with one leaflet facing an aqueous solution and the other a rigid substrate. The surface stress of SLB physisorption on SiO_2 surface is measured on

microcantilever to be 17 ± 1.4 mN/m, or an adsorption free energy of 3.3 ± 0.27 kJ/mol, assuming a POPC lipid cross-sectional area of 65 $Å^2$. When a lipid bilayer is physisorbed onto the cantilever, there is a compressive stress in the SiO_2 surface causing the cantilever to bend in the direction of gold-coated surface, as depicted in Fig. 4.1(a). The deflection of the cantilever is determined by an energy balance between the surface free energy contributed from lipid/lipid and lipid/solid interactions that tend to deflect the cantilever, as illustrated in Fig. 4.1(b), and the elastic energy of solid, that tends to counter the deflection of cantilever. [12-15] Note that the vesicle solution flowed for only 7 minutes (as indicated with shaded area in Fig. 4.2). After which, the valve was switched back to PBS buffer port. Since the bilayers adsorption is irreversible over this time scale, the cantilevers remain deflected, as shown in Fig. 4.2, from 780 sec to 1400 sec.

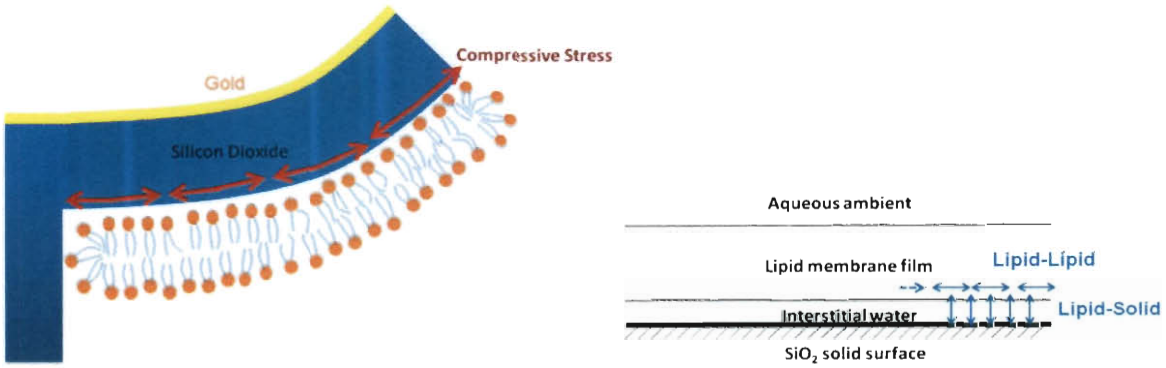

(a) (b)

Figure 4.1. A SLB physisorbs to a silicon dioxide surface of the cantilever. (a) Adsorption of a lipid membrane induces a compressive stress on the SiO_2 surface and results in cantilever bending toward the opposite side. (b) The commonly used sandwich model (membrane-water-solid) of a SLB. Both lipid/lipid and lipid/solid interactions contribute to the free energy of adsorption.

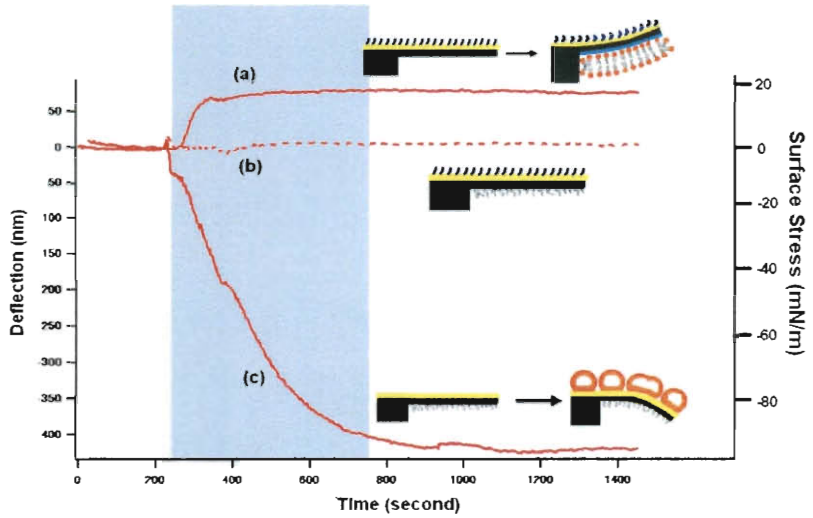

Figure 4.2. Deflection measurements upon injection of POPC vesicles onto functionalized SiO_2 and Au surfaces. Shaded area indicates when the vesicle solution is introduced into the measurement chamber. (a) Using a PEG-coated gold surface, a lipid bilayer forms on the silicon dioxide surface resulting in a positive deflection due to a compressive stress exerted on the silicon dioxide surface. (b) There is no significant response for a reference cantilever in which both the gold and silicon dioxide surfaces are functionalized with PEG. (c) For a cantilever in which the silicon dioxide is coated with PEG, intact vesicles adsorb onto the gold surface of the cantilever resulting in compressive stress exerted on the gold layer.

4.3.2.Surface Stress Generated for Mixed Cationic-Zwitterionic Lipid Bilayers

We examine the surface stress exerted by the charged lipid bilayers which is formed by rupturing vesicles composed of cationic DOTAP and zwitterionic POPC lipids. The positive charges on the headgroup of DOTAP enhance the headgroup-SiO_2 attraction, since SiO_2 is negatively charged at neutral pH. [16] The adsorption free energy can be tuned by varying the ratio of DOTAP to POPC. As shown in Fig. 4.3, as the DOTAP concentration changes from 0 to 100%, the measured surface stress increases from 17 ± 1.4 mN/m to 24 ± 1.5 mN/m. As the DOTAP ratio in the SLB is increased, the stronger electrostatic interactions between the headgroups and the SiO_2 surface increase the adsorption free energy, resulting in an increase in

the compressive stress. This result indicates that the surface stress can be tuned by modifying the ratio of charged lipids in a SLB. According to Eq. (2.6) and (2.7), the surface stress of solid surfaces is related to the adsorption free energy of adsorbate molecules. The electrostatic contribution of adsorption free energy per unit area is a function of the lipid bilayer charge density σ_{ele} and also the SiO_2 surface potential ψ_e of the inner Helmholtz plane: [16, 17]

$$\Delta G_{elec} = \sigma_{ele}\psi_e \text{ , where } \sigma_{ele} = \alpha e / a_1 \tag{4.1}$$

where a_1 is the average area per lipid molecule, α is the mole fraction of charged lipids, and e is the unit charge of a single electron. By varying the mole fraction of the cationic DOTAP to the zwitterionic POPC lipids, any changes in adsorption free energy due to charged lipids is proportional to the electrostatic contribution. We express the average lipid cross-sectional area in this two-component system using the following expression: $a_1 = a_{POPC}(1-\alpha) + a_{DOTAP}\,\alpha$, where $a_{POPC} = 0.65$ nm^2 and $a_{DOTAP} = 0.87$ nm^2 are the molecular areas for POPC and DOTAP as reported in the literature, [18-20] and α is the DOTAP mole fraction in the supported bilayer. The measured adsorption free energy (in the form of surface stress on cantilever substrate) of the cationic-zwitterionic lipid bilayer is then fitted to Eq. (4.1) where ψ_e is used as a fitting parameter. The fitted ψ_e value is -33mV with $R^2 = 0.83$, which is reasonably close to the literature value measured using streaming potential. [21]

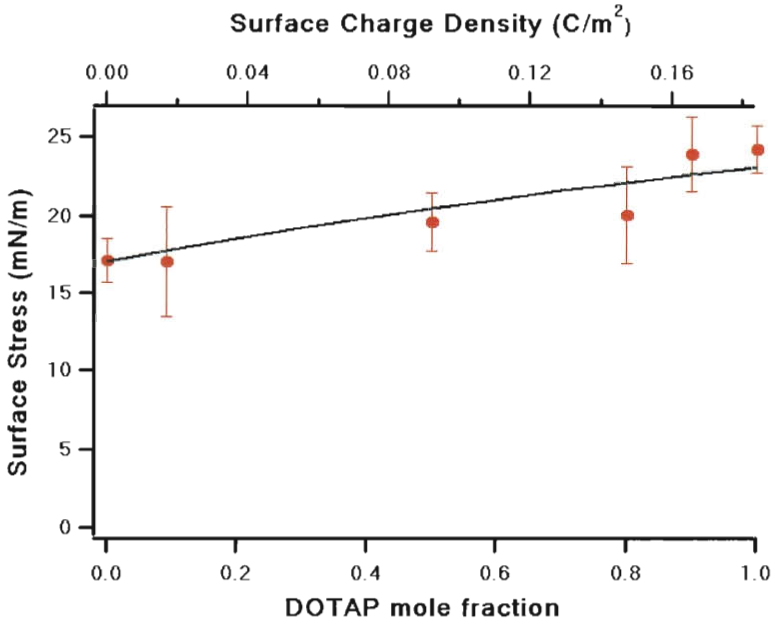

Figure 4.3. Surface stress induced by SLB composed of different DOTAP to POPC ratios as measured using microcantilevers. The solid line corresponds to the theoretical electrostatic partition of adsorption free energy of a lipid bilayer predicted in Eq. (4.1). The only fitting parameter is ψ_e = -33 mV with R^2 = 0.83.

4.3.3.Anionic LUV Lipids Transferring into Cationic SLBs

Researchers have demonstrated lipid transfer between a cationic SLB and anionic unilamellar vesicles, [22-24] but there is little understanding of how the adsorption free energy changes due to lipid transfer. To study the adsorption free energy changes due to lipid transfer on microcantilevers, a SLB composed of DOTAP lipids is first formed on the SiO_2 surface of the microcantilever, shown in Fig. 4.4 sample injection (i). A cationic SLB is chosen to ensure a strong driving force for lipid transfer with anionic vesicles. After SLB formation on the cantilever, vesicles composed of POPS and POPC are introduced to the flow chamber. As shown in Fig. 4.4 sample injection (ii), upon injection of neutral POPC vesicles, there is little change to the adsorption free energy of the SLB, indicating little lipid transfer between the cationic DOTAP

lipids and the zwitterionic POPC lipids. By introducing anionic vesicles composed of POPS and POPC, the adsorption free energy of the cationic SLB decreases, indicating charge neutralization occurs due to lipid transfer between the vesicles and the SLB. This decrease in adsorption free energy can be attributed to a decrease in the electrostatic affinity of the SLB to the SiO_2 surface due to lipid transfer between the cationic DOTAP lipids with either anionic POPS or zwitterionic POPC. As shown in Fig. 4.5, the surface stress decreases from 24 ± 1.5 mN/m for a bilayer composed entirely of DOTAP lipids to 8.4 ± 1.2 mN/m, for a bilayer mixed with DOTAP and POPS lipids. Though the final bilayer surface charge density after lipids remains undetermined, Kunze has reported a similar in-situ prepared cationic supported bilayer that contains 53% of the anionic donor lipids after electrostatic-driven lipid transfer, [22] which suggests that the SLB is neutralized after lipid transfer. It is interesting to note that the surface stress of a mixed DOTAP/POPS SLB is smaller than that of for a pure POPC SLB (17 ± 1.4 mN/m). One possible explanation is that lipids in a mixed DOTAP/POPS SLB are more tightly packed than a POPC SLB, which leads to a smaller average area per lipid and changes the charge density at the solid surface. Though both systems form neutral charged SLBs, dipole-dipole alignment between zwitterionic lipid headgroups results in localized repulsive interactions which lead to a larger average area per lipid compared to a mixed anionic/cationic SLB system. Again, this confirms that the adsorption free energy of a SLB can be tuned by modifying the electrostatic interactions between the lipids.

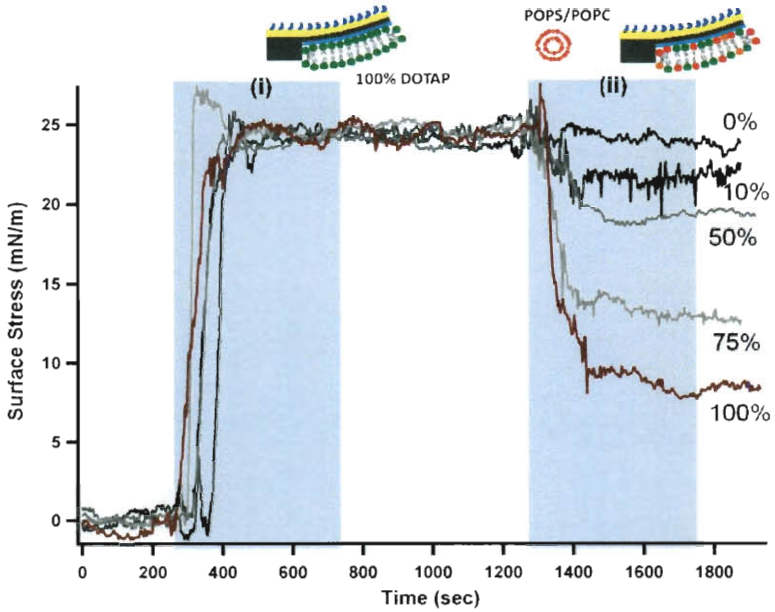

Figure 4.4. Surface stress changes due to electrostatic-induced lipid exchange between cationic DOTAP supported bilayer and anionic POPS (0, 10%, 50%, 75%, 100%)/POPC LUVs at 25 °C measured using microcantilevers. Shaded area (i) indicates injection of 0.5 mg/ml 100% DOTAP vesicles and formation of a cationic SLB, followed by (ii) injections of 0.5 mg/ml POPS(0, 10, 50, 75 and 100 mol%)/POPC LUVs.

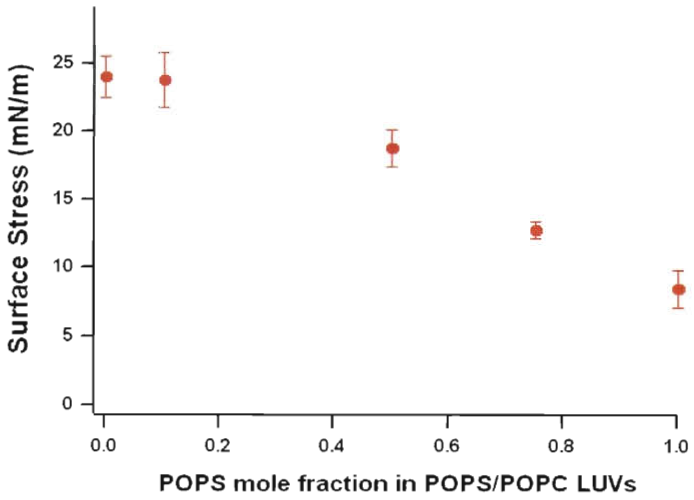

Figure 4.5. Surface stress measured after lipid exchange between a cationic DOTAP bilayer and anionic POPS/POPC LUVs as a function of the anionic POPS mole fraction in POPS/POPC LUVs.

4.3.4.Surface Stress Generated for Mixed Cholesterol-POPC Lipid Bilayers

To examine adsorption free energy changes due to the presence of cholesterol in a SLB, vesicles composed of POPC are made with varying ratios of cholesterol. The cholesterol content is varied from 0 to 50 mol%, after which the increased cholesterol content results in unstable vesicles. [25] As shown in Fig. 4.6, there is a decrease in the surface stress from 17 ± 1.4 mN/m to 9.9 ± 1.3 mN/m as the cholesterol content is increased to 50%, indicating that cholesterol perturbs the lipid chain configurations and packing geometry, which decreases the SLB adsorption free energy on the cantilever surface. Cholesterols in the bilayer is thought to mainly embed within the hydrophobic portion of the bilayer, exposing limited –OH groups at the lipid headgroup/chain interface. [25] Previous literature has shown that lipid membranes become more rigid and undergo a phase transition from liquid disordered (l_d) to liquid ordered (l_o) with increased cholesterol content from 5 to 30 mol%, resulting in a decrease in the van der Waals force between hydrophobic lipid chains. [26-28] The hydrophobic interactions between lipid chains are known to stabilize the membrane and enhance physisorption at liquid/solid interface, thus inclusion of cholesterol in the bilayer weakens the stabilizing energy, leading to a decreased adsorption free energy. We observe a nonlinear decrease in the surface stress of a mixed lipid-cholesterol film with increased cholesterol content, as shown in Fig. 4.6.

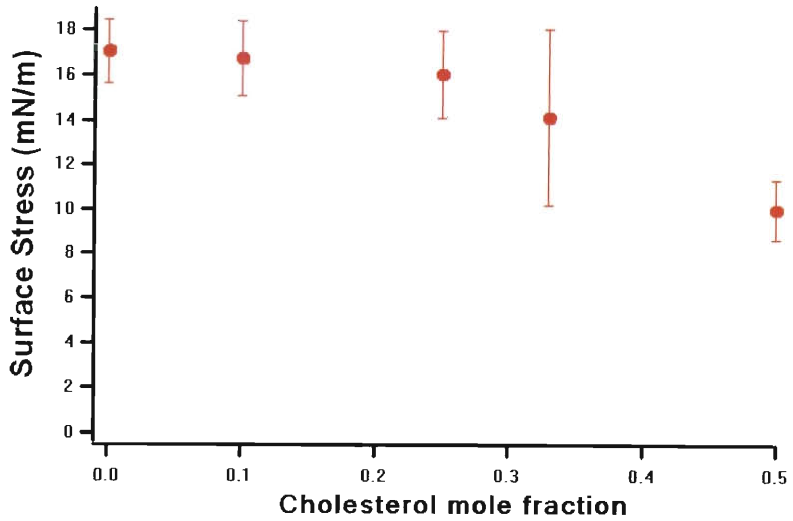

Figure 4.6. Surface stress induced by lipid bilayers composed of different cholesterol to POPC ratios measured at 25 °C from microcantilever experiments.

4.4.Discussion

As the SLB forms on the microcantilever surface, the origin of the cantilever bending is the adsorption free energy. The changes in surface free energy due to the adsorption of a thin film onto a solid from solution can be thought of as a surface film pressure. [29-31] In our system, at equilibrium, the surface free energy gives rise to a surface film pressure of the SLB, π_{SLB}. Note that the surface film pressure measured using microcantilevers is different from the surface pressure defined at air-water interface. Since the SLB is adhered to the solid surface through physisorption (mainly dipole-dipole, van der Waals forces and hydrogen bonding), part of the lateral inter-lipid interactions may not be incorporated into the surface free energy on solid. For systems such as alkanethiol self-assembled monolayers or DNA brushes fixed on gold, the lateral repulsions or attractions between molecules contribute to the substrate surface stress on cantilever without significant loss. [12, 14] In the SLB system, the physisorbed lipid bilayer must couple to the surface through a water layer of 1~1.5 nm. Additionally, being sandwiched by the

SLB and the solid substrate, this interstitial water layer is greatly affected by both the solid and the SLB. The water molecules must reorient to be crystalline-like and this ordering can influence the surface free energy at the liquid/solid interface. [16, 32, 33]

4.5.Conclusion

This chapter demonstrated that the adsorption free energy of SLBs on SiO_2 changes due to modifications in the electrostatic interactions, lipid transfer between oppositely charged membranes, and membrane mixing with cholesterol can be detected using microcantilevers. A surface stress change of 17 ± 1.4 mN/m (mJ/m^2) generated by a POPC SLB is measured. By adding cationic DOTAP lipids to the POPC membrane, there is an increase in the adsorption free energy due to increased electrostatic attraction between lipid headgroups in the SLB and the SiO_2 surface. To further affirm our model, lipid transfer between cationic SLBs and anionic lipid vesicles is performed to demonstrate a detectable surface stress change due to charge neutralization. Finally, the addition of cholesterol results in decrease in the surface stress. This work can lead to further studies of lipid membrane interactions with membrane-active peptides, transmembrane proteins, and in-situ modification of SLBs. Compared to other analytical techniques, such as Langmuir-Blodgett trough, which is limited to measurements of lipid monolayers at an air/water interface, microcantilevers can be utilized to detect real-time changes in the lipid membranes. This will lead to a better understanding of the function and formation of SLBs and the utilization of SLBs as mimics for biomembranes.

4.6.Reference

(1) Israelachvili, J. N. *Langmuir* **1994**, *10*, 3369-3370.

(2) Kim, Y. H.; Rahman, M. M.; Zhang, Z. L.; Misawa, N.; Tero, R.; Urisu, T. *Chem. Phys. Lett.* **2006**, *420*, 569-573.

(3) Cha, T.; Guo, A.; Zhu, X. Y. *Biophys. J.* **2006**, *90*, 1270-1274.

(4) May, S. *Eur. Phys. J. E* **2000**, *3*, 37-44.

(5) Lipowsky, R.; Seifert, U. *Mol. Cryst. Liquid Cryst.* **1991**, *202*, 17-25.

(6) Hope, M. J.; Bally, M. B.; Webb, G.; Cullis, P. R. *Biochim. Biophys. Acta,* **1985**, *812*, 55-65.

(7) Yue, M.; Lin, H.; Dedrick, D. E.; Satyanarayana, S.; Majumdar, A.; Bedekar, A. S.; Jenkins, J. W.; Sundaram, S. *J. Microelectromech. Syst.* **2004**, *13*, 290-299.

(8) Keller, C. A.; Kasemo, B. *Biophys. J.* **1998**, *75*, 1397-1402.

(9) Ajo-Franklin, C. M.; Kam, L.; Boxer, S. G. *Proc. Natl. Acad. Sci. U. S. A.* **2001**, *98*, 13643-13648.

(10) Nollert, P.; Kiefer, H.; Jahnig, F. *Biophys. J.* **1995**, *69*, 1447-1455.

(11) Sofou, S.; Thomas, J. L. *Biosens. Bioelectron.* **2003**, *18*, 445-455.

(12) Hagan, M. F.; Majumdar, A.; Chakraborty, A. K. *J. Phys. Chem. B* **2002**, *106*, 10163-10173.

(13) Sushko, M. L.; Harding, J. H.; Shluger, A. L.; McKendry, R. A.; Watari, M. *Adv. Mater.* **2008**, *20*, 3848-+.

(14) Sushko, M. L. *Faraday Discuss.* **2009**, *143*, 63-80.

(15) Dareing, D. W.; Thundat, T. *J. Appl. Phys.* **2005**, *97*.

(16) Papirer, E., Ed. *Adsorption on Silica Surfaces*; Marcel Dekker, Inc., 2000.

(17) Parfitt, G. D., Rochester, C. H., Ed. *Adsorption from Solution at the Solid/Liquid Interface*; Academic Press Inc., 1983.

(18) Bordi, F.; Cametti, C.; Gaudiuo, D.; Gili, T.; Sennato, S.; Biasio, A. D. In *Prog. Colloid Polym. Sci.* ; Springer Berlin / Heidelberg, 2004; Vol. 126, pp 47-50.

(19) Marsh, D. *Handbook of lipid bilayers*; CRC press, 1990.

(20) Bordi, F.; Cametti, C.; De Luca, F.; Gili, T.; Gaudino, D.; Sennato, S. *Colloid Surf. B-Biointerfaces* **2003**, *29*, 149-157.

(21) Bousse, L.; Mostarshed, S.; Vandershoot, B.; Derooij, N. F.; Gimmel, P.; Gopel, W. *J. Colloid Interface Sci.* **1991**, *147*, 22-32.

(22) Kunze, A.; Sjovall, P.; Kasemo, B.; Svedhem, S. *J. Am. Chem. Soc.* **2009**, *131*, 2450-2451.

(23) Kunze, A.; Svedhem, S.; Kasemo, B. *Langmuir* **2009**, *25*, 5146-5158.

(24) Liu, J. W.; Stace-Naughton, A.; Jiang, X. M.; Brinker, C. J. *J. Am. Chem. Soc.* **2009**, *131*, 1354-1355.

(25) Luckey, M. *Membrane Structural Biology - With Biochemical and Biophysical Foundations*; Cambridge University Press, 2008.

(26) Reyes Mateo, C.; Ulises Acuna, A.; Brochon, J. C. *Biophys J* **1995**, *68*, 978-987.

(27) Dynarowicz-Latka, P.; Hac-Wydro, K. *Colloid Surf. B-Biointerfaces* **2004**, *37*, 21-25.

(28) Dietrich, C.; Bagatolli, L. A.; Volovyk, Z. N.; Thompson, N. L.; Levi, M.; Jacobson, K.; Gratton, E. *Biophys. J.* **2001**, *80*, 1417-1428.

(29)Adamson, A. W., Gast, A. P. *Physical Chemistry of Surfaces*, 6 ed.; Wiley-Interscience, 1997.

(30) Schwartz, A. M. In *Absorbency*; Chatterjee, P. K., Ed.; Elsevier, 1985; Vol. 7, pp 85.

(31) Chatterjee, P. K., Ed. *Absorbency*; Elsevier, 1985.

(32) Milhaud, J. *Biochim. Biophys. Acta-Biomembr.* **2004**, *1663*, 19-51.

(33) Xing, C. Y.; Ollila, O. H. S.; Vattulainen, I.; Faller, R. *Soft Matter* **2009**, *5*, 3258-3261.

Chapter 5

Probing Temperature-induced Gel-liquid Phase Transition of Supported Lipid Bilayers and Monolayers

5.1. Introduction

Lipid bilayers and monolayers are known to exhibit many phases as a function of temperature. The thermally induced gel-fluid transition has been of particular importance due to its role in permeability and electric conductivity. [1-4] Attempts to understand the differences between supported and free-standing lipid membranes and how a solid support interacts and influences the stability of a SLB are undergoing. [5-11] One important parameter is the phase transition temperature T_m. It is believed that the gel-liquid transition of a lipid membrane is a first-order process at T_m where in the gel state the alkyl chains in the lipid molecules are organized into a crystalline-like lattice, whereas they are disordered in the liquid phase. [12, 13] However in a SLB, the two leaflets comprising the bilayer face different environments: one leaflet faces an ambient aqueous solution while the other side faces a rigid solid. This results in a membrane asymmetry, which is reported to cause differences in the surface tension, lipid lateral diffusion coefficient, and phase transition temperature between a SLB and a free standing membrane. Leonenko et al. reported that a mica-SLB demonstrates a broader gel-liquid phase transition than a free-standing one, accompanied with observable structural changes around the main T_m. [14] Feng et al. report that the gel-liquid phase transition for SLBs is a second-order process, with the primary transition at T_m and a secondary transition ~ 5 ^oC above T_m. [15] They propose that the proximal leaflet is stabilized by the ordered thin water film beneath it, which results in a secondary transition which occurs at a temperature higher than primary T_m. Oncins et

al. further confirmed the existence of the secondary T_m in the proximal leaflet by examining the phase transition of a Langmuir-Blodgett lipid monolayer. [16] All of these studies are observed by applying external forces such as force spectroscopy or atomic force microscopy, with their probe tips exerting external force to the soft films during scanning. [17] A less intrusive method to probe the order/disorder transition of lipid surface films is through the use of vibrational sum frequency spectroscopy (VSFS). [18, 19]

Chapter 4 demonstrates the use of microcantilevers to measure the adsorption free energy of lipid membranes on solid surfaces. [20] This chapter furthers the calorimetric sensing application of microcantilevers, to probe the subtle gel-liquid phase transition of phospholipid bilayers supported on a silicon dioxide surface. Conformational changes in the adsorbed molecular films and temperature-induced melting of dsDNA are readily observed using microcantilevers. [21-24] The recent success of microcantilevers is due to their ability to sensitively measure surface stress changes associated with liquid-solid interfacial behavior.

5.2. Materials and Methods

5.2.1. Lipid Vesicles

1-myristoyl-2-palmitoyl-sn-glycero-3-phosphocholine (MPPC, $T_m \sim 35$ °C) was purchased from Avanti Polar Lipids (Alabaster, AL). The lipids and chemicals were used as received without further purification. Lipid vesicles were prepared by the standard extrusion method and kept at least 15 °C above their phase transition temperature in hot water bath at all times. [25] Briefly, lipid was dissolved in 0.25 ml of chloroform at a concentration of 5 mg/ml in a glass vial. The chloroform was evaporated and dried under a gentle ultra-pure nitrogen stream. The resulting lipid film was desiccated in a vacuum chamber for at least two hours and then hydrated in 0.25 ml of a pH 7.4 phosphate buffered saline (PBS) buffer solution (Sigma-Aldrich, USA) at 50 °C, followed by vortexing the solution. The solution was then extruded 40 times

through a polycarbonate membrane with 100 nm pore-size using a mini-extruder (Avanti Polar Lipids), resulting in a translucent solution of large unilamellar vesicles (LUVs) approximately 100 nm in diameter in PBS. The vesicle solution was further diluted with 9 parts of PBS to 1 part of the freshly extruded vesicle solution and stored in warm water bath at 50 °C. The estimated lipid concentration was 0.5 mg/ml.

5.2.2. Microcantilevers Preparation

Cantilever chips were purchased from Concentris GmbH (Basel, Switzerland). The cantilevers are 500 μm in length, 100 μm in width, and 1 μm in thickness. Each chip contains eight rectangular cantilevers is which one surface is silicon and the other surface is coated with 3 nm titanium followed by 20 nm gold layer. Before functionalization, the cantilever arrays were placed in an UV ozone cleaner for 5 minutes under 5 psi oxygen to generate a silicon dioxide surface. To prevent vesicle binding to the gold surface of the cantilever, a dithiolaromatic-PEG ($C_{25}H_{44}O_6S_2$, MW=504.74 g/mol, Sensopath Technologies, Bozeman, MT) was used. The surface functionalization typically proceeds for two hours. PEG-silane, 2 - [methoxy-(polyethyleneoxy)propyl] - trimethoxysilane ($C_{13}H_{30}O_7Si$, MW= 326.46 g/mol, Gelest Inc. Morrisville, PA), was used to prevent vesicle from adsorbing on the silicon dioxide surface of the cantilever. A reference cantilever was functionalized with both the dithiolaromatic-PEG and the PEG-silane.

5.2.3. Langmuir Monolayer of Lipids

A supported lipid monolayer is prepared outside the measurement chamber. The lipid monolayer was deposited on the silicon dioxide surface using Langmuir-Blodgett transfer method (KSV 2000 series, KSV instruments Ltd., Helsinki, Finland). The cantilever is first pre-functionalized with dithiolaromatic-PEG to prevent lipid adsorption to the gold surface. The cantilever is then held on a Teflon clip and immersed into a DI water-filled Langmuir trough.

Lipid molecules were then dispensed onto the air-water surface, with the total surface area and surface pressure controlled by two barriers. At a surface pressure of 30mN/m (surface area of 50 $Å^2$ per MPPC molecule), the lipid monolayer was transferred onto the cantilever. The monolayer was dried in a desiccation chamber, and cantilever measurements were performed within 20 minutes.

5.2.4. Microcantilevers to Measure Surface Stress

All measurements were performed with a Cantisens Research System (Concentris GmbH, Basel, Switzerland). The cantilevers were mounted in a liquid chamber in which solutions were pumped past the cantilever chip via a syringe pump. SLBs were formed on silicon dioxide surface of microcantilevers through vesicle fusion at 10 °C above the primary T_m. Prior to the introduction of vesicle solutions, the cantilever signals were set to a zero baseline value. Each injection consisted of flowing 0.2 mL of vesicle solution at a flow rate of 0.42 μL/sec. A solution of MPPC vesicles was injected into the measurement chamber to form the SLB on silicon dioxide surface of microcantilever. Excess liquid was pumped to the waste reservoir via a syringe pump. Real-time deflection of microcantilevers was monitored via a scanning laser diode aligned to the tip of the microcantilevers. The position of the reflected laser beam was captured using a position-sensitive-detector (PSD), with a sampling frequency of 1 Hz.

The average thermomechanical sensitivity of the cantilevers was measured to be 73 ± 11 nm/K. [26] Due to small differences in material properties of the cantilevers such as stiffness or thickness variation of the evaporated gold layer, the deflections of the cantilevers were normalized using each cantilever's thermomechanical sensitivity. After normalization, the signal difference between the experimental cantilever and the reference cantilever was calculated to allow us to measure the cantilever deflection due to the vesicle rupture into a SLB. Phase transition curves were acquired by slowly ramping the temperature from 45 °C to 31 °C for the

bilayer or from 31 °C to 45 °C for the monolayer at a rate of ± 0.8 °C/min.

5.3. Results and Discussion

Fig. 5.1 shows the equilibrium deflection of microcantilevers upon the formation of a MPPC SLB at 45 °C. The vesicle solution flows through the measurement chamber from 240 sec to 720 sec. As vesicles fuse onto the SiO_2 surface and rupture to form a planar lipid bilayer, a compressive surface stress is induced, causing the cantilever to bend toward the gold side. The free energy of adsorption is transferred to the solid as a surface free energy at the solid-water-lipid interface (REFERENCE). This surface free energy disturbs the atoms of the solid surface, leading to a surface stress in the solid that deforms the material laterally. Due to a surface stress mismatch between the bulk and surface, the cantilever bends toward the gold surface. After switching back to buffer, the microcantilever remains deflected, confirming that a stable SLB has formed. The equilibrium deflection value (78 ± 2.6 nm) corresponds to a surface stress of 18 ± 0.62 mN/m induced by physisorption of a MPPC lipid film.

After the formation of the SLB, the temperature is decreased from 45 to 31 °C and the resulting cantilever responses are shown in Fig. 5.2(a). Due to the mismatch in the thermal expansion coefficients between gold and silicon, the reference cantilever decreases linearly with increasing temperature. For lipid bilayer coated cantilevers, a discontinuity in the linear bending profile is observed at ~35°C. The discontinuity, an abrupt step of ~ 20 nm, can be attributed to the gel-liquid phase transition of the lipid bilayer. By plotting the derivative of the deflection with respect to temperature in Fig. 5.2(b), a distinct peak can be detected from the d(Deflection)/dT plot, which corresponds to the phase transition temperature, T_m. It is found that the T_m value for the MPPC SLB measured with microcantilever (at 34.9 ± 0.1 °C) agrees well with the value reported for MPPC vesicles in the literature (35°C). Additionally, we see that at T_m,

the fluid phospholipids membrane undergoes a liquid disorder to gel ordered phase transition that generates an additional compressive surface stress of ~ 4.7 mN/m onto the solid support. It is well known that this phase transition is an exothermic process that results in an abrupt rise in change conformational order and reduced mobility of the lipid molecules. Interestingly, this transition is also associated with a reduction in molecular area, which is likely to laterally contract the lipid membrane, which should lead to a tensile surface stress, yet a compressive stress is observed. This observed surface stress may be a competition between the adsorption free energy induced compressive stress during the phase transition and the tensile stress induced by the membrane area reduction. Nevertheless, the overall surface stress is observed to be compressive.

We compare the supported MPPC bilayer phase transition with that of a MPPC monolayer. The MPPC monolayer prepared on the SiO_2 surface of microcantilevers using the Langmuir Blodgett transfer method is immersed at 31 ^{o}C. As the temperature is slowly increased to 45 ^{o}C, there is a change in the slope at ~41 ^{o}C in the deflection curve, as shown in Fig. 5.3(a). It is important to note that due to the different preparation method, the temperature ramping directions are different for bilayers and monolayers. The supported monolayers are transferred onto microcantilevers at room temperature; in the measurement, the temperature ramps from room temperature (25^{o}C) to 43^{o}C, thus the supported monolayers are heated from gel to liquid phase. While the supported bilayers are formed from rupturing vesicles in their fluid phase at 43^{o}C, so the SLBs are cooled from liquid to gel phase to find the T_m. Compared to the MPPC, SLB, the monolayer phase transition is seen as a slope change rather than an abrupt step. The plot of d(Deflection)/dT shows a clear change at 40.8 ± 0.10 ^{o}C for all monolayer coated cantilevers. The slope increases 0.26 ± 0.06 nm/^{o}C from ordered to disordered phase at T_m'. The increase in T_m for the monolayer is related to the difference between the interactions of a MPPC

monolayer and bilayer with the solid support. The stabilizing effect on the supported lipid monolayer is thought to come from electrostatic interaction, whereby negative charges on SiO_2 attract the polar lipid headgroups (the positively charged choline groups) [18] or from the crystalline-like water beneath the lipid layer [15], thus T_m shifts to higher temperature , from 34.9 ± 0.1 °C to 40.8 ± 0.10 °C.

Though many groups have reported a secondary transition temperature for SLBs, clear discontinuities are not observed at T_m' using microcantilevers. Furthermore, the ability for microcantilevers to probe the SLB phase transition may be limited if the conformational changes in the SLB do not generate enough change in the surface free energy to be converted into a surface stress, no deflection will be observed. In addition, the secondary phase transition appears as protrusion features or crack formations in the SLBs, which are observed by Feng et al. in their AFM images. They suggested that the protrusion and cracking features found at temperature near T_m on the SLBs are due to the interactions between the solid substrate and the bilayer. [15] SLBs constructed with defects may not exhibit the T_m + 5°C transition on microcantilevers because the surface free energy may not be a good indicator of these features of this phase transition. These features indicate discontinuity and defects in the SLBs near T_m.

In summary, we have demonstrated the use of microcantilevers to probe the gel-liquid phase transition of both supported lipid bilayers and monolayers. The primary transition temperature can be accurately detected for the MPPC SLB, but the secondary transition at T_m' is not obvious. T_m' for supported lipid monolayer is successfully detected at ~ + 5 °C higher than the primary T_m. This technique has been shown to precisely probe the conformational changes of phase transitions in macromolecular assemblies confined on surfaces. We offer this technique as a promising tool for future studies on the phase transition temperature of supported model lipid membranes.

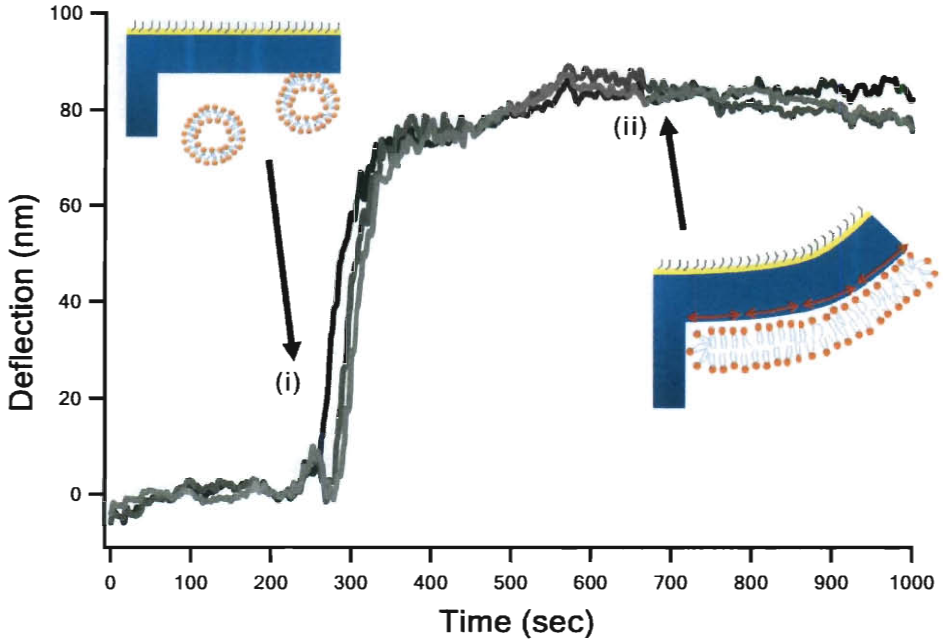

Figure 5.1. Real-time deflection measurement of the cantilever as a MPPC Supported Lipid Bilayer formed on the SiO_2 surface of the cantilever at 45°C. Arrow (i) indicates injection of MPPC vesicles into the measurement chamber. SLB forms on SiO_2 causing a deflection toward the gold side. Arrow (ii) indicates that the flow is switched from vesicle solution to PBS buffer. Three separate cantilevers on the same array are shown to confirm the formation of SLBs. Note that one cantilever (black curve) responds prior to other two (gray curves) because the vesicles reach it first in the measurement chamber.

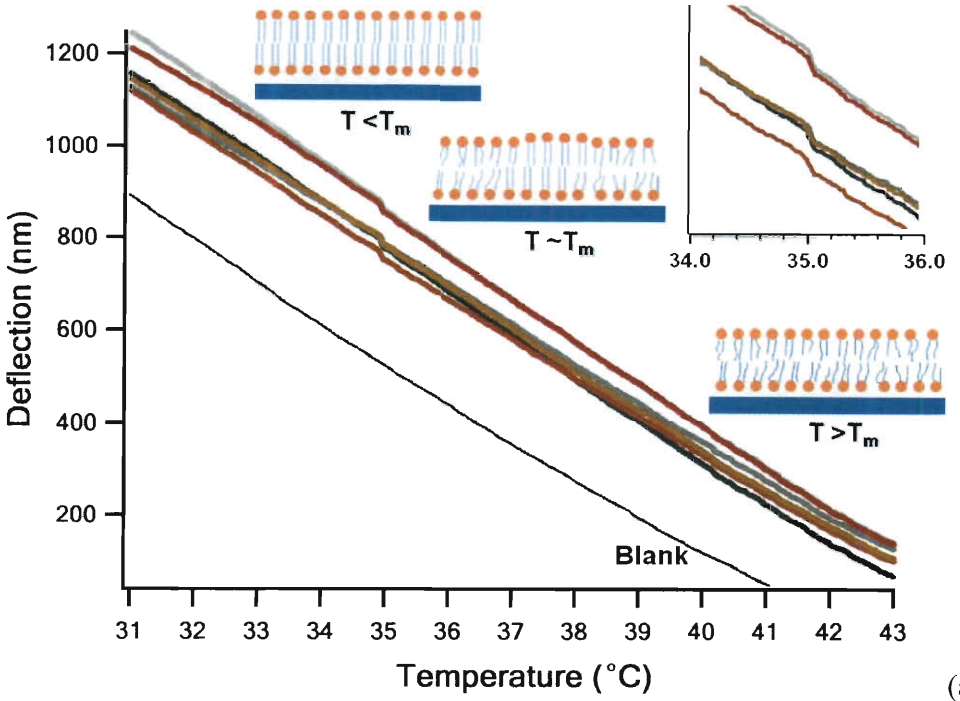

(a)

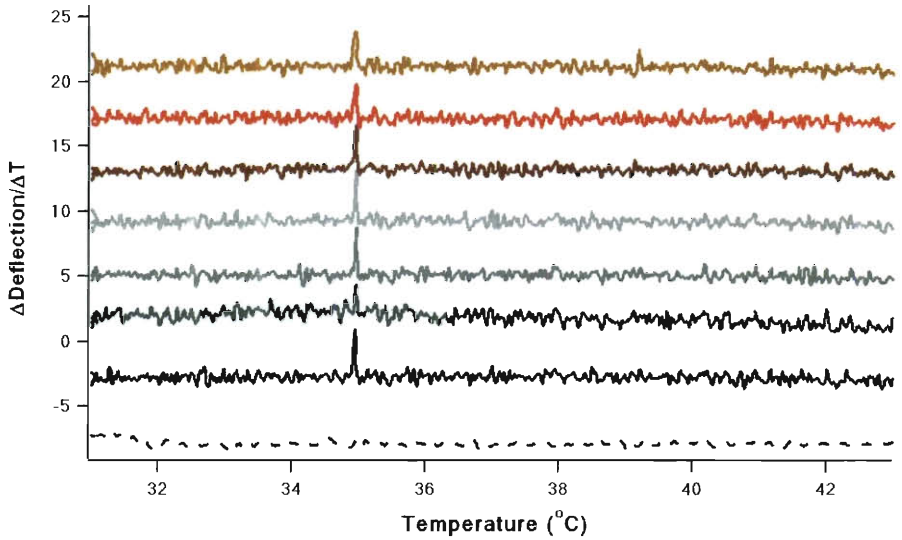

(b)

Figure 5.2. Phase Transition of MPPC Supported Lipid Bilayer. (a) Deflection of microcantilevers versus temperature. Inset figure provides finer resolution between 34 to 36 °C. (b) The derivative of the deflection with respect to temperature is shown. The T_m can be determined by the position of the peaks. Seven cantilevers on the same array are offset for clarity. The black dash line indicates a reference microcantilever without lipid membrane on the surface.

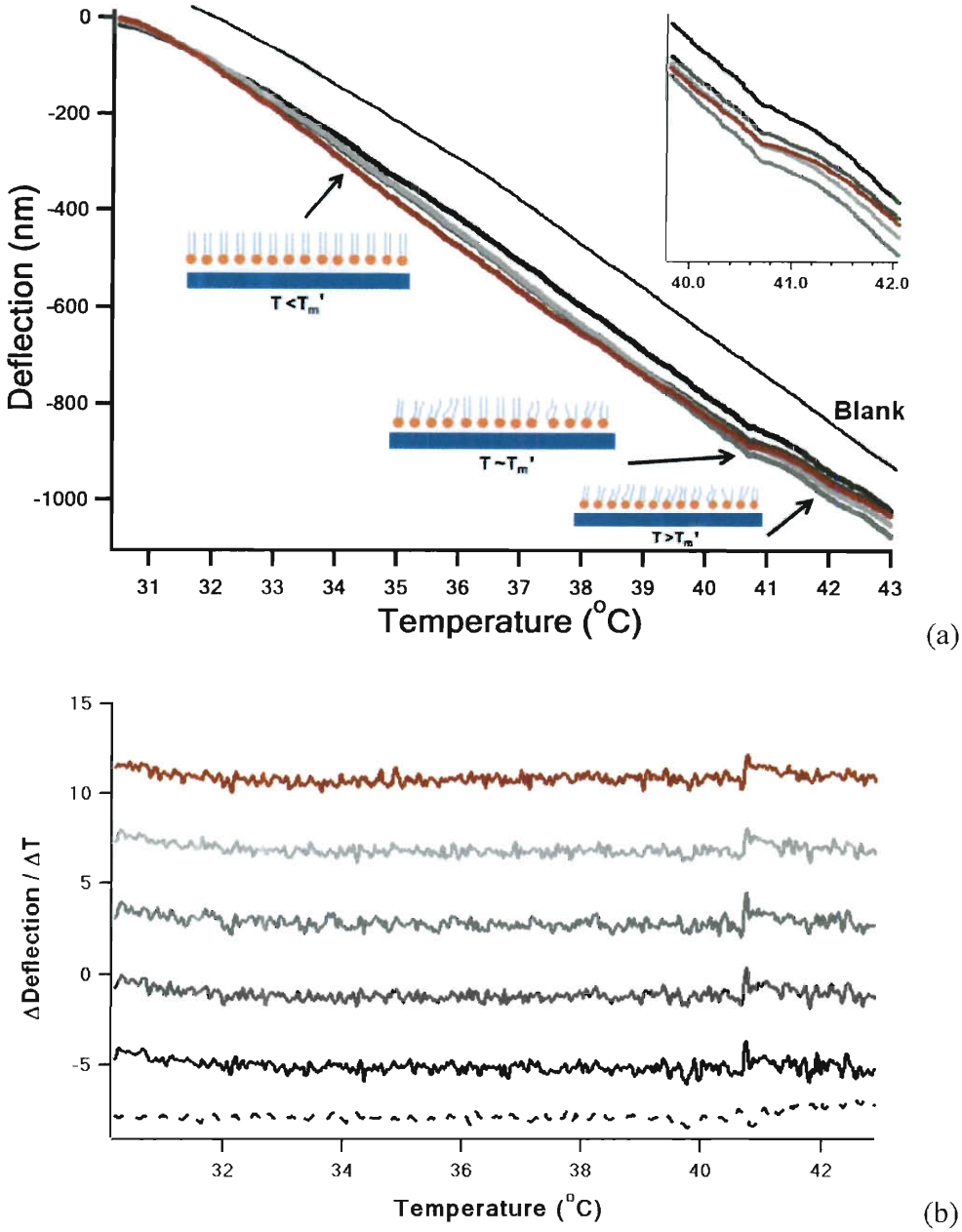

Figure 5.3. Phase Transition of MPPC Supported Lipid (Langmuir-Blodgett) Monolayer. (a) Deflection of microcantilevers vs. temperature. Inset figure provides finer resolution between 40 to 42 °C. (b) The derivative of the deflection with respect to temperature is shown. Five cantilevers on the same array are offset for clarity. The black dash line indicates a reference microcantilever without lipid membrane on the surface.

5.4. Conclusion

In summary, this short chapter demonstrated the novelty of using microcantilevers to probe the gel-liquid phase transition of both supported lipid bilayers and supported lipid monolayers. The measurements have unraveled a step further a recent controversial issue on multiple phase transition behaviors of SLBs originating from asymmetry. The primary transition T_m is accurately detected for the MPPC SLB, but the secondary transition at T_m' is not obvious. T_m' for supported lipid monolayer is successfully detected at ~ + 5 °C higher than the primary T_m. This technique has been shown to precisely probe the conformational changes of phase transitions in macromolecular assemblies confined on surfaces, and we highlight this technique as a promising tool for future studies on supported model lipid membranes.

5.5. References

(1) Papahadjopoulos, D.; Jacobson, K.; Isac, I. *biochim. Biophys. Acta - Biomembranes* **1973**, *311*, 330-348.

(2) Jendrasiak, G. L.; Mendible, J. C. *Biochim. Biophys. Acta* **1976**, *424*, 133.

(3) Boheim, G.; Hanke, W.; Eibl, H. *Proc. Natl. Acsd. Sci. USA* **1980**, *77*, 3403-3407.

(4) Smirnova, E. Y.; Kozhomkulov, E. T.; Vosnesensky, S. A.; Shevchenko, E. V.; Morozov, Y. V.; Antonov, V. F. *Chem. Phys. Lipids* **1986**, *41*, 173.

(5) Keller, C. A.; Glasmastar, K.; Zhdanov, V. P.; Kasemo, B. *Phys. Rev. Lett.* **2000**, *84*, 5443-5446.

(6) Keller, C. A.; Kasemo, B. *Biophys. J.* **1998**, *75*, 1397-1402.

(7) Richter, R.; Mukhopadhyay, A.; Brisson, A. *Biophys. J.* **2003**, *85*, 3035-3047.

(8) Chah, S.; Zare, R. N. *Phys. Chem. Chem. Phys.* **2008**, *10*, 3203-3208.

(9) Tawa, K.; Morigaki, K. *Biophys. J.* **2005**, *89*, 2750-2758.

(10) Xing, C. Y.; Faller, R. *J. Phys. Chem. B* **2008**, *112*, 7086-7094.

(11) Charrier, A.; Thibaudau, F. *Biophysical Journal* **2005**, *89*, 1094-1101.

(12) Nagle, J. F. *Annu. Rev. Phys. Chem.* **1980**, *31*, 157-195.

(13) Jacobson, K.; Papahadjopoulos, D. *Biochemistry* **1975**, *14*, 152-161.

(14) Leonenko, Z. V.; Finot, E.; Ma, H.; Dahms, T. E. S.; Cramb, D. T. *Biophys. J.* **2004**, *86*, 3783-3793.

(15) Feng, Z. V.; Spurlin, T. A.; Gewirth, A. A. *Biophys. J.* **2005**, *88*, 2154-2164.
(16) Oncins, G.; Picas, L.; Hernandez-Borrell, J.; Garcia-Manyes, S.; Sanz, F. *Biophys. J.* **2007**, *93*, 2713-2725.
(17) Seeger, H. M.; Marino, G.; Alessandrini, A.; Facci, P. *Biophys. J.* **2009**, *97*, 1067-1076.
(18) Anderson, N. A.; Richter, L. J.; Stephenson, J. C.; Briggman, K. A. *Langmuir* **2006**, *22*, 8333-8336.
(19) Liu, J.; Conboy, J. C. *J. Am. Chem. Soc.* **2004**, *126*, 8894-8895.
(20) Liu, K. W.; Biswal, S. L. *Anal. Chem.* **2010**, *82*, 7527-7532.
(21) Biswal, S. L.; Raorane, D.; Chaiken, A.; Birecki, H.; Majumdar, A. *Anal. Chem.* **2006**, *78*, 7104-7109.
(22) Zhou, F.; Biesheuvel, P. M.; Chol, E. Y.; Shu, W.; Poetes, R.; Steiner, U.; Huck, W. T. S. *Nano Lett.* **2008**, *8*, 725-730.
(23) Wu, G. H.; Ji, H. F.; Hansen, K.; Thundat, T.; Datar, R.; Cote, R.; Hagan, M. F.; Chakraborty, A. K.; Majumdar, A. *Proc. Natl. Acad. Sci. U. S. A.* **2001**, *98*, 1560-1564.
(24) Watari, M.; Galbraith, J.; Lang, H. P.; Sousa, M.; Hegner, M.; Gerber, C.; Horton, M. A.; McKendry, R. A. *J. Am. Chem. Soc.* **2007**, *129*, 601-609.
(25) Hope, M. J.; Bally, M. B.; Webb, G.; Cullis, P. R. *Biochim. Biophys. Acta,* **1985**, *812*, 55-65.
(26) Yue, M.; Lin, H.; Dedrick, D. E.; Satyanarayana, S.; Majumdar, A.; Bedekar, A. S.; Jenkins, J. W.; Sundaram, S. *J. Microelectromech. Syst.* **2004**, *13*, 290-299.

Chapter 6

Probing Insertion and Solubilization Effects of Lyso-lipids on Supported Lipid Bilayers Using Microcantilevers

6.1. Introduction

The interaction of lipid membranes with amphipathic molecules, such as surfactants, short-chain alcohols, and amphipathic peptides, plays an important role in the functionality and structure of lipid membranes.[1-3] Experimental evidence shows that model lipid membranes (for example, giant unilamellar vesicles, GUVs) can take up amphipathic molecules, leading to changes in the total membrane area, phase transitions, curvature and rigidity.[4] Amphipathic molecules in the bulk solution can insert to the external leaflet of the membrane and increase the total volume in the external leaflet. The resulting head group crowding in the external leaflet can cause the membrane to undergo surface area expansion or lateral compression, while the inner leaflet curves until the final bending momentum reaches zero. As a result, external and internal leaflets dilate to different extents, and the lateral pressure profile alters to reach a new balance.[5, 6] The ability to modulate the lateral pressure profile makes lyso-lipid and other amphipathic molecules good candidates for gating the on and off of mechano-sensitive ion channels.[2] Lyso-lipids are also proven to affect membrane protein folding in the rate and the folding yield by inducing an additional curvature stress after the incorporation of lyso-lipids.[5, 7] Compared to other surfactants commonly used for solubilizing membrane proteins, such as anionic sodium lauryl sulfate (SDS),[8, 9] lyso-lipids are much more similar to lipid molecules. The lyso-lipids are chosen because they share the same head group and similar tail group structure of the lipid in the target lipid bilayer; thus the only factor that dominates the interaction is the cone-like shape of

the surfactant. Therefore, lyso-lipids provide a simple model system for studying the mechanism of asymmetrical insertion into lipid membranes.

For surfactant concentration below the critical micelle concentration (CMC) in the bulk solution, the surfactants are present in the solution as monomers. In the form of monomers, the surfactants interact with lipid membranes mainly by partitioning reversibly into the membrane without disrupting the membrane integrity. As the concentration of surfactants increases and exceeds the CMC, the surfactants not only insert into lipid membranes, but also start to "lyse" or "solubilize" the lipid membranes. Solubilization of the lipid bilayer with surfactants is greatly affected by the concentration, charge, and hydrophile-lipophile-balance (HLB) of the surfactants. The process is commonly described in three stages as the surfactant concentration increases: (i) the membranes take up surfactant monomers; (ii) As the surfactants become saturated in the membrane, surfactants aggregate to form surfactant-lipid mixed micelles in the aqueous phase; and (iii) all the lipids are solubilized in the form of mixed micelles.[8, 10-13] To measure the changes in the lipid membrane in the presence of lyso-lipids, researchers have used the well-characterized micropipette aspiration techniques to study the membrane area dilation of GUVs upon the insertion of a lyso-lipid, MOPC.[14, 15] However, the membrane stretching is subject to an applied tension from the aspiration, which is argued to accelerate lyso-lipid flip-flop by several orders of magnitude, leading to membrane instability.[6, 16] The use of nuclear magnetic resonance (NMR) to detect phosphorus chemical shifts as an indication of a lateral pressure change induced by the lyso-lipid insertion was explored by Traïkia; however, an additional negatively-charged tracer lipid, DOPA, is required.[6] Henriksen et al. investigated the enthalpy, entropy and free energy parameters of lyso-lipid partitioning into model lipid membranes using isothermal titration calorimetry (ITC).[17] Little has been explored regarding how surfactants affect the supported lipid

bilayers (SLBs), which have now become a useful model for biological membranes. None of the above techniques can be easily used to study supported lipid membranes (SLBs).

This chapter demonstrates a new type of measurement, using lipid membrane-coated microcantilever sensors, for determining the changes in free energy in the lipid membranes when interacting with lyso-lipids. The microcantilever is a label–free technique that is not only able to probe minute changes in surface free energy, but also to monitor surface processes in real-time.[18-23] Since the interaction between lyso-lipids and lipid membranes is spontaneous and can lower the total system free energy, detection of the Gibbs free energy of adsorption via the cantilever deflection can provide thermodynamic insights into the partitioning of lyso-lipids into lipid membranes. Besides the free energy change obtained at equilibrium state, the mechanism of how lyso-lipids insert into or solubilize lipid membranes is also of great interest. The microcantilever also offers insight into the mechanism by which lyso-lipid insertion into lipid membranes result in membrane strain changes.

In Chapter 4, SLBs adsorption is systematically characterized on the microcantilever surface.[24] The microcantilever is shown a useful sensor for detecting the conformation and composition change of a SLB. In this chapter, the use of microcantilevers with a lipid membrane coating on the surface to probe the changes in free energy when lyso-lipids interact with SLBs is demonstrated. This chapter characterizes this system from two aspects: (i) lyso-lipids with different aliphatic chain lengths are tested to determine the role of hydrophobic effects in lyso-lipid interaction with SLBs. Longer chain length indicates a stronger hydrophobic match with the tail groups of the lipid molecules, so the chain length of lyso-lipids is a factor of detergency. Lipid membrane's resistivity to detergency of lyso-lipids is also analyzed. And (ii) lyso-lipids with concentrations ranging from below and above their CMC are tested on the SLBs. Both

reversible lyso-lipid adsorption and destructive solubilization of SLBs by lyso-lipids are observed and analyzed. These results reveal a promising sensing method for probing the interactions between lipid membranes and amphipathic molecules, such as toxins, drugs and amphipathic peptides, for future applications.

6.2.Experimental Section

6.2.1.Lipid Vesicle Preparation

Lipid vesicles were made from 1-palmitoyl-2-oleoyl-*sn*-glycero-3-phosphocholine (POPC). Lyso-lipids used in this paper are lyso-phosphocholine, denoted as lysoPC, with homologues of different aliphatic chain lengths: 1-stearoyl-2-hydroxy-*sn*-glycero-3-phosphocholine, (lysoPC 18:0), 1-palmitoyl-2-hydroxy-*sn*-glycero-3-phosphocholine (lysoPC 16:0), 1-myristoyl-2-hydroxy-*sn*-glycero-3-phosphocholine (lysoPC 14:0) and 1-lauroyl-2-hydroxy-*sn*-glycero-3-phosphocholine (lysoPC 12:0). All the lipids were purchased from Avanti Polar Lipids (Alabaster, AL) and used as received without further purification. Vesicles were prepared by the extrusion method.[25] Briefly, lyso-lipid solutions were dissolved at 5 mg/mL in chloroform. The chloroform was evaporated under a nitrogen stream. The resulting lipid film was then dried in a vacuum chamber for 2 h and then hydrated in 0.25 mL pH 7.4 phosphate buffered saline (PBS, Sigma-Aldrich) solutions made in ultrapure deionized water (Barnstead Nanopure system, Thermo Fisher Scientific), followed by vortexing the solution. The solution was then extruded 40 times through a 100 nm polycarbonate membrane using a miniextruder (Avanti Polar Lipids, AL), resulting in a translucent solution of large unilamellar vesicles (LUVs) approximately 100 nm in size. The vesicle solution was further diluted with 9 parts of PBS to 1 part of the freshly extruded vesicle solution and stored at 4 °C until use. Note that the final

vesicle concentration may be lower than initially desired due to lipid loss on filter membranes after extrusion; however, the concentration was well above the threshold needed to achieve full surface coverage of SLB. The preparation of lyso-lipid solution was a modification of the protocol of Needham.[14] Lyso-lipids were dissolved in chloroform and dried under a nitrogen stream. The dried lipid film was rehydrated in pH 7.4 PBS buffer solution and gently mixed using a vortex mixer. The sample was then diluted to give the final desired lyso-lipid concentration.

6.2.2.Microcantilever Preparation

Cantilever chips were purchased from Concentris GmbH (Basel, Switzerland). The cantilevers are 500 μm in length, 100 μm in width, and 1 μm thick. Each chip contains eight rectangular silicon cantilevers, each with a spring constant of 0.026 N/m. The cantilevers were coated with 3 nm titanium followed by 20 nm gold layer, resulting in a bimetallic structure. The cantilever arrays were placed in an UV ozone cleaner for 5 min under 5 psi oxygen to clean the gold surface on the front surface and generate a hydrophilic silicon dioxide surface on the back surface. Each cantilever was individually functionalized using glass microcapillaries. The surface functionalization typically proceeded for two hours. To prevent binding preferentially to either the silicon dioxide or gold side of the cantilever beam, polyethylene glycol (PEG) polymers were used. A dithiolaromatic–PEG molecule ($C_{25}H_{44}O_6S_2$, MW=504.74 g/mol, Sensopath Technologies, Bozeman, MT) was used to prevent vesicle adsorption to the gold surface of the cantilever. A PEG–silane molecule, 2-[methoxy-(polyethyleneoxy)propyl]-trimethoxysilane ($C_{13}H_{30}O_7Si$, MW= 326.46 g/mol, Gelest Inc. Morrisville, PA), was used to prevent lipid bilayer adsorption on the silicon dioxide surface of the cantilever. A reference cantilever was functionalized with both the dithiolaromatic–PEG and the PEG–silane. After use, the cantilevers

were once again placed in the UV–ozone cleaner for 5 min under 5 psi oxygen and then refunctionalized as described above.

6.3.Results

6.3.1. SLB Formation on SiO_2 Surface

The SLBs formed on SiO_2 surface of microcantilevers are characterized in Chapter 4. The gold surfaces of the microcantilevers are previously modified with the dithiolaromatic–PEG, so that the gold surfaces are made inert to lipid adsorption. Vesicles are attracted by the negatively charged SiO_2 surface of the microcantilevers and fuse onto the surface to form SLBs. Upon adsorption of the POPC vesicle to the SiO_2 surface, the cantilevers undergo a surface stress change. This surface stress change is compressive; therefore the cantilevers bend away from the side of SLB formation, as shown in Fig. 6.1 (a). The microcantilever bends with a deflection of 73 ± 6.0 nm. Thus, the measured surface stress, $\Delta\sigma_{ads,SLB}$, for SLB formation on SiO_2 is 17 ± 1.4 mN/m, or an adsorption free energy, $\Delta G^0_{ads,\,SLB}$, of 3.3 ± 0.27 kJ/mol, assuming a POPC lipid cross-sectional area of 65 $Å^2$.[24] Note that the vesicle solution flowed for 7 min (as indicated with shaded area in Fig. 6.2), after which, the valve was switched back to the PBS buffer port. Since the bilayer's adsorption is irreversible over this time scale, the cantilevers remain deflected, as shown in Fig. 6.2, from 300 to 650 s. The SLBs are stable for at least two hours of observation time and do not desorb after the solution is switched to buffer. After the SLBs are prepared on the SiO_2 surfaces of the microcantilevers, lyso-lipids with aliphatic chains of 18, 16, 14 and 12 carbons (lysoPC 18:0, 16:0, 14:0 and 12:0) are then introduced to the SLBs at bulk concentrations above and below their CMC.

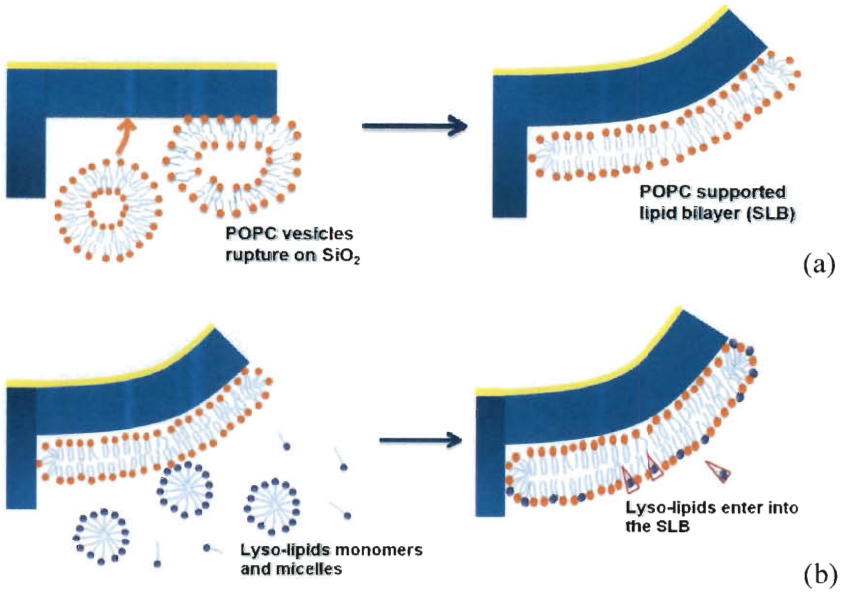

Figure 6.1. (a) Schematic of a SLB physisorbed to a silicon dioxide surface of the cantilever. Adsorption of a lipid membrane induces a compressive stress on the SiO_2 surface and results in cantilever bending toward the opposite side. (b) After the SLB is prepared, lyso-lipids (in the form of monomers or micelles) insert mostly into the external membrane leaflet, resulting in an increase in the surface free energy. The microcantilever responds to the change in surface free energy by bending away further from the side of membrane coating.

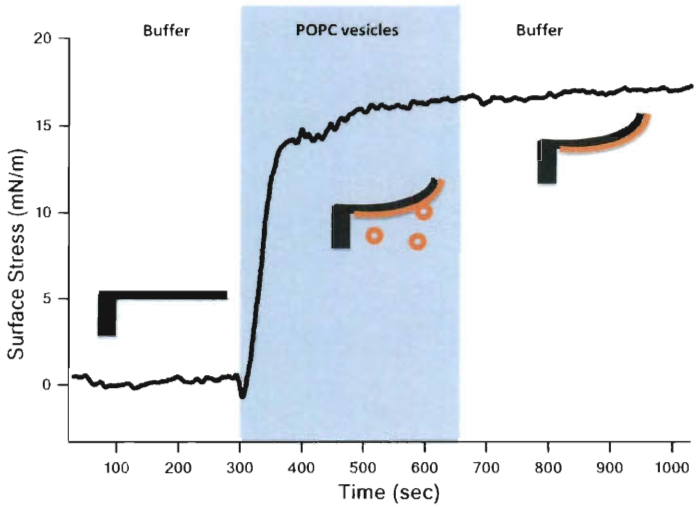

Figure 6.2. Detection of POPC SLB formation using the microcantilever sensor. SLB is formed on the SiO_2 surface of the microcantilever by the vesicle fusion method, leading to a deflection associated with the change in the surface free energy.

6.3.2.Lyso-lipids Insert into Supported Lipid Bilayer

Upon lyso-lipid injection, the microcantilevers bend away from the SLB coated side as a response to the compressive stress. Fig. 6.3 shows the surface stress change of microcantilevers upon the addition of lysoPC 14:0 and 12:0. This increased compressive stress indicates that the lyso-lipids generate an adsorption free energy, $\Delta G^0_{ads,\,lyso}$, which is released onto the SLB coating and transmitted to the SLB–solid interface. The lyso-lipid adsorption to the SLBs originates from the hydrophobic attraction between the lyso-lipids and the POPC lipids. To lower the total system free energy, the hydrophobic chains of the lyso-lipids prefer embedding themselves into the hydrophobic region of the SLBs, thus exposing less of the hydrophobic chains to water (for which the exposure is unfavorable). The hydrophobic insertion of lyso-lipids increases the membrane area more in the external leaflet (the monolayer which faces the bulk liquid) than in the inner leaflet (the monolayer which faces the solid substrate), and thus the bilayer dilates laterally and asymmetrically. In addition to the area change of the SLB, the collective adsorption free energy of lyso-lipids results in changes in the surface free energy of the SLB-coated microcantilevers and leads to an increased and more compressive surface stress. At concentrations below CMC, as shown by the grey lines in Fig. 6.3, once buffer is reintroduced to the system, the lyso-lipids are desorbed from the SLB causing the surface stress to return to its initial baseline value, indicating that the bilayer remained intact. The measured surface stress, $\Delta\sigma_{ads,lyso}$, after SLB saturation with the lyso-lipids is plotted with the concentration of each lyso-lipid in Fig. 6.4. A linear relation between the surface stress and concentration is observed for each of the two lyso-lipids and analyzed in the following section.

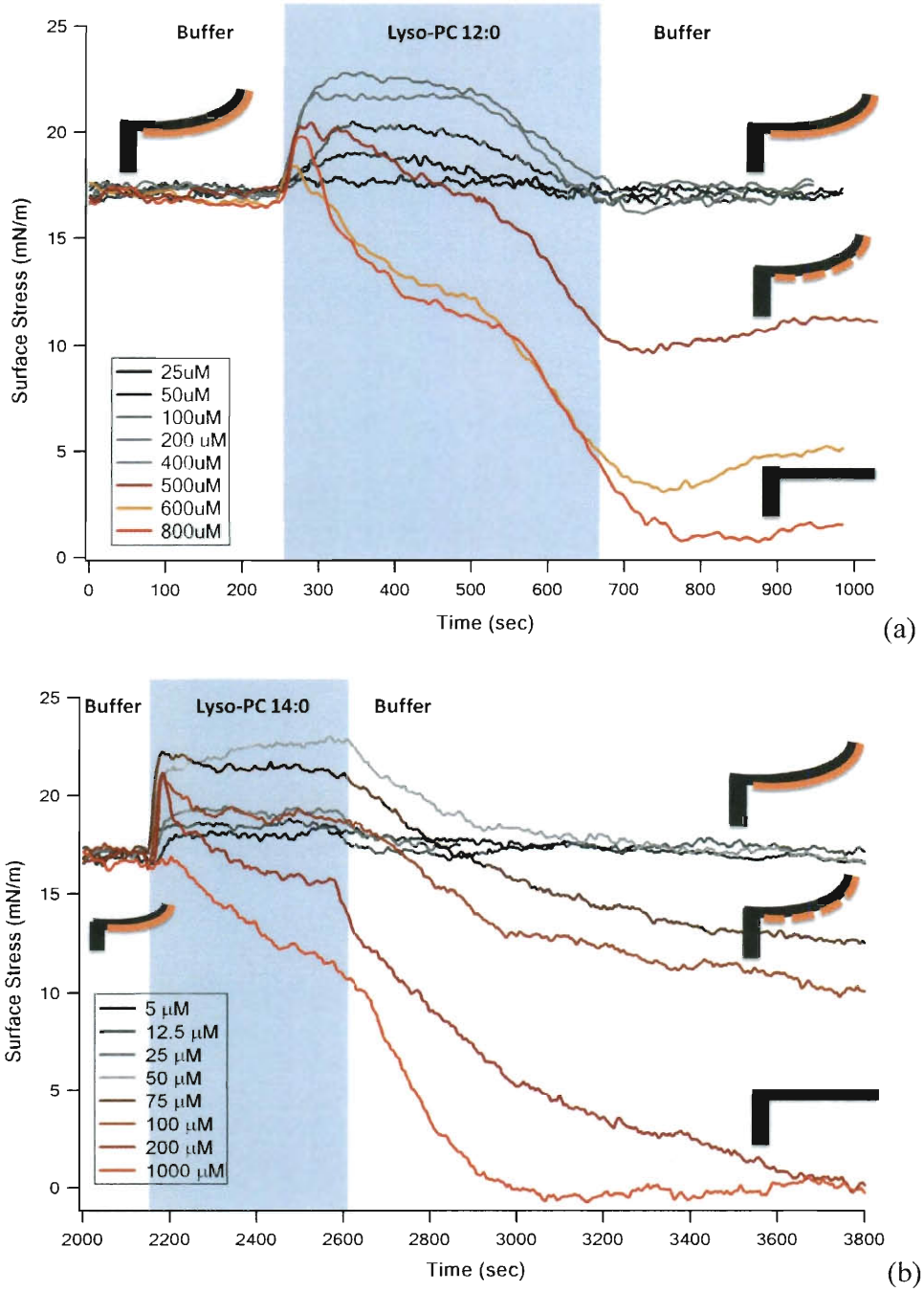

Figure 6.3. Comparison of the response of SLB-coated microcantilever to the lyso-lipids with different aliphatic chain lengths: (a) LysoPC 12:0 and (b) LysoPC 14:0. Below or close to CMC (shown by the grey lines), each lyso-lipid reversibly adsorbs to and desorbs from the SLBs. Above the CMC (shown in color), the changes in surface stress induced by lysoPC 14:0 and 12:0 show that the SLBs are removed.

6.3.3. Gibbs Free Energy of Adsorption

The adsorption of lyso-lipids or other amphiphiles to a lipid membrane is governed by thermodynamic equilibrium. The changes in Gibbs free energy are related experimentally to the partition coefficient, K, at equilibrium: [11]

$$K = \frac{C_p}{C_L C_f}, \tag{6.1}$$

where C_p is the concentration of lyso-lipids partitioned into the SLBs, C_L is the concentration of lipids in the SLBs, and C_f is the concentration of free lyso-lipids in the bulk solution. For lyso-lipids at low concentration, the ratio of C_p to C_L is approximated as the ratio of the changes in adsorption free energy of lyso-lipids adsorption to that of SLBs adsorption. [23] Thus, C_p/C_L is approximated as $\Delta\sigma_{ads,lyso}/\Delta\sigma_{ads,SLB}$:

$$\frac{C_p}{C_L}\frac{\mathbf{1}}{C_f} = \frac{\Delta G^{\mathbf{0}}_{ads,lyso} A_{lipid}}{\Delta G^{\mathbf{0}}_{ads,SLB} A_{lsyo}}\frac{\mathbf{1}}{C_f} = \frac{\Delta\sigma_{ads,lyso}}{\Delta\sigma_{ads,SLB}}\frac{\mathbf{1}}{C_f}. \tag{6.2}$$

A_{lipid} and A_{lyso} are the head area per lipid molecule, and $\Delta\sigma_{ads,SLB}$ is known from the SLB adsorption experiment. Assuming an infinitely dilute solution, the Gibbs free energy of partitioning is written as[17, 26]

$$\Delta G^{\mathbf{0}} = -RT\ln\left(K \cdot C_w\right). \tag{6.3}$$

Where ΔG^0 is the molar free energy cost of transferring the lyso-lipids from the bulk aqueous solution onto the supported membrane surface. C_w is the molar concentration of water (C_w = 55.5 M); R is the ideal gas constant and T is temperature. As shown in Fig. 6.4, the surface stress increases with concentration. The ΔG^0 can be derived from the slope of the surface stress versus concentration plot in Fig. 6.4 and is listed in Table 6.1. Our results for the free energy of

partitioning of a POPC SLB is the same order of magnitude of that found by Høyrup et al. and Henriksen et al. for POPC vesicles.[17, 27] Note that the free energy of partitioning, ΔG^0, decreases as the number of aliphatic carbons increase in the lyso-lipid. This is expected since the lyso-lipid partitioning is driven by the hydrophobic effect; thus the longer the carbon chain of a lyso-lipid is, the more free energy is released. Interestingly, the partition coefficient values for a SLB are three times larger than those for vesicles. There are a couple of possible explanations. The first is that our assumption that the surface stress change is solely due to the adsorption free energy. It is possible that lateral expansion of the membrane also contributes to the surface free energy. Additionally, we suspect that the difference in membrane tension between small unilamellar vesicles (SUVs) and SLBs may also account for the difference in lyso-lipid partitioning, but further studies varying membrane tension are required. The adsorption of lyso-PC 16:0 and 18:0 at concentrations below their CMC was also studied; however, no observable cantilever deflection was detected. Changes in surface stress due to lyso-lipid adsorptions at concentrations below 5 μM are difficult to distinguish.

	lysoPC 18:0	lysoPC 16:0	lysoPC 14:0	lysoPC 12:0
CMC [μM][§]	0.4	4 – 8.3	43 – 90	400 – 900
K [M^{-1}]	–	–	6470 ± 647	1470 ± 70.6
K [M^{-1}] from Henriksen[17]	–	12500 ± 3900	1750 ± 94	460 ± 50
ΔG^0 [kJ/mol]	–	–	-31.7 ± 0.236	-28.0 ± 0.116
K·CMC	–	–	0.278 – 0.582	0.588 – 1.323

Table 6.1. Calculation of partition coefficient, K, and the free energy of partitioning, ΔG^0. All data are derived under 25 °C. [§]Values provided by Avanti Polar Lipids, AL.

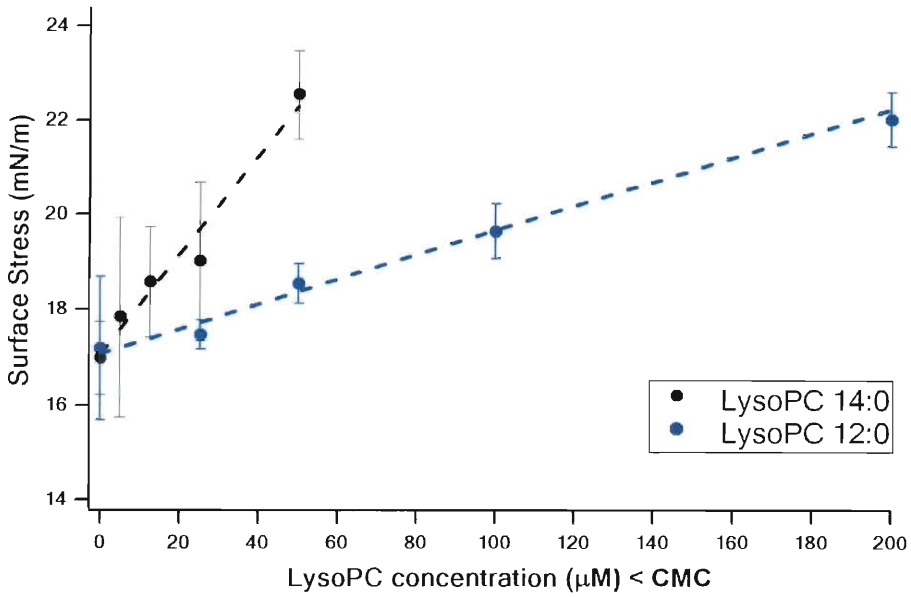

Figure 6.4. Plot of the changes in surface stress measured by microcantilever sensors as a function of the lyso-lipid bulk concentration (<CMC). Linear relation between the surface stress increase and the concentration of lyso-lipids are observed. Lines represent fitting of Eq. (6.3).

6.3.4.Solubilization of the SLB

Once the lyso-lipid concentration exceeds its CMC, the lyso-lipids form micelles and other morphologies. Above its CMC, the lyso-lipids start to remove lipids from the SLBs. As shown by the colored lines in Fig. 6.3 for lyso-PC 12:0 and 14:0 and Fig. 6.5 for lyso-PC 16:0 and 18:0, the extent of membrane solubilization varies for different lyso-lipids. As the lyso-lipids adsorb to the SLBs, they start to saturate the SLB and reach a threshold at which the SLBs are not capable of taking up more lyso-lipids. The monomers of lyso-lipids start to aggregate into adsorbed micelles at concentrations higher than CMC. As the micelles interact with the lipid bilayers, the detergency nature of the amphipathic lyso-lipids can cause the micelles to take up lipids from the lipid bilayer. The stronger the detergency nature of the lyso-lipid is, the easier the lipids tend to incorporate into the micelles. Lyso-lipids can also transfer from the micelles into

the bilayer because the lyso-lipids expose more of their aliphatic chains to water in the micelles than in the planar SLBs. Transferring the lyso-lipids from micelles to the SLB can reduce the system free energy.[13, 26, 28-31]

Note that the lysoPCs with different aliphatic chain lengths behave differently on the SLBs in terms of the solubilization ability. Lyso-lipids of the same headgroups but with different aliphatic chain lengths show different detergency toward the SLBs. Fig. 6.3 shows that lysoPC 14:0 (CMC ~ 43 to 90 μM) and 12:0 (CMC ~ 400 to 900 μM) with concentrations above their CMCs (colored lines) are able to solubilize the SLBs on the silicon dioxide surface. In this case, after the injection of lysoPC 14:0 and 12:0, the surface stresses of the microcantilevers drop from 17 mN/m to lower, even to 0 mN/m at high concentration close to 1000 μM. The drop in surface stress indicates that the SLBs are removed away from the solid surface, leaving the surface with patchy SLBs or even blank as it was before the POPC SLBs were formed. However, as shown in Fig. 6.5 for lysoPC 18:0 (CMC ~ 0.4 μM) and 16:0 (CMC ~ 4 to 8.3 μM), no surface stress drop is observed. Instead, increasing the concentration lysoPC 18:0 to 100 μM (well above its CMC) leads to a large compressive stress of more than 100 mN/m. Compared to the surface stress of 17 ± 1.4 mN/m induced by a SLB, the increase of surface stress induced by lysoPC 18:0 adsorbing to the SLBs indicates that a thick layer of lysoPC 18:0 aggregates is depositing onto the SLBs. Whether the SLBs stay on the solid surface is not clear, but the thick layer is possibly composed of aggregates of mixed POPC lipids and lysoPC 18:0. For lysoPC 16:0 at the concentration higher than CMC, lysoPC 16:0 does not cause solubilization of the SLB. Instead, lysoPCs 16:0 adsorb to the SLBs and increases the surface stress by 2 to 3 mN/m even after switching to the PBS buffer. Surface free energy change is a good indicator of whether the SLBs stay adsorbed on the microcantilever surface or are solubilized by the detergents.

The effect of lyso-lipids acting on solubilization of lipid membranes is complex. The lipid membrane solubilization is determined not only by how strong the detergency nature of the lyso-lipid is, but also by the interaction between the lyso-lipids and the POPC lipids. Other groups have determined that lysoPC 18:0 > 16:0 > 14:0 > 12:0 in its detergency strength ranking, determined by K·CMC.[17, 26] However, on the contrary, our results show that lysoPC 14:0 and 12:0 solubilize the lipid membrane, while lysoPC 18:0 and 16:0 do not. LysoPC 18:0 and 16:0 do not solubilize the POPC SLB because of the stronger hydrophobic affinity between the POPC and each of the two lysoPCs, 18:0 and 16:0. POPC is a lipid composed of two alkyl chains of palmitoyl (16:0) and oleoyl (18:1) groups, which match with the length of lysoPC 18:0 and 16:0. The aliphatic chain length mismatch between POPC lipids and lysoPCs 12:0 and 14:0 results in large membrane curvature perturbation, and thus solubilization of the lipid membrane occurs. Heriksen et al. have also shown that membrane solubilization only occurs when there is a mismatch between the lyso-lipid and membrane lipid chain lengths.[17] Along with detergency strength, the aliphatic chain length of the lyso-lipid is an important factor in determining the membrane solubilization.

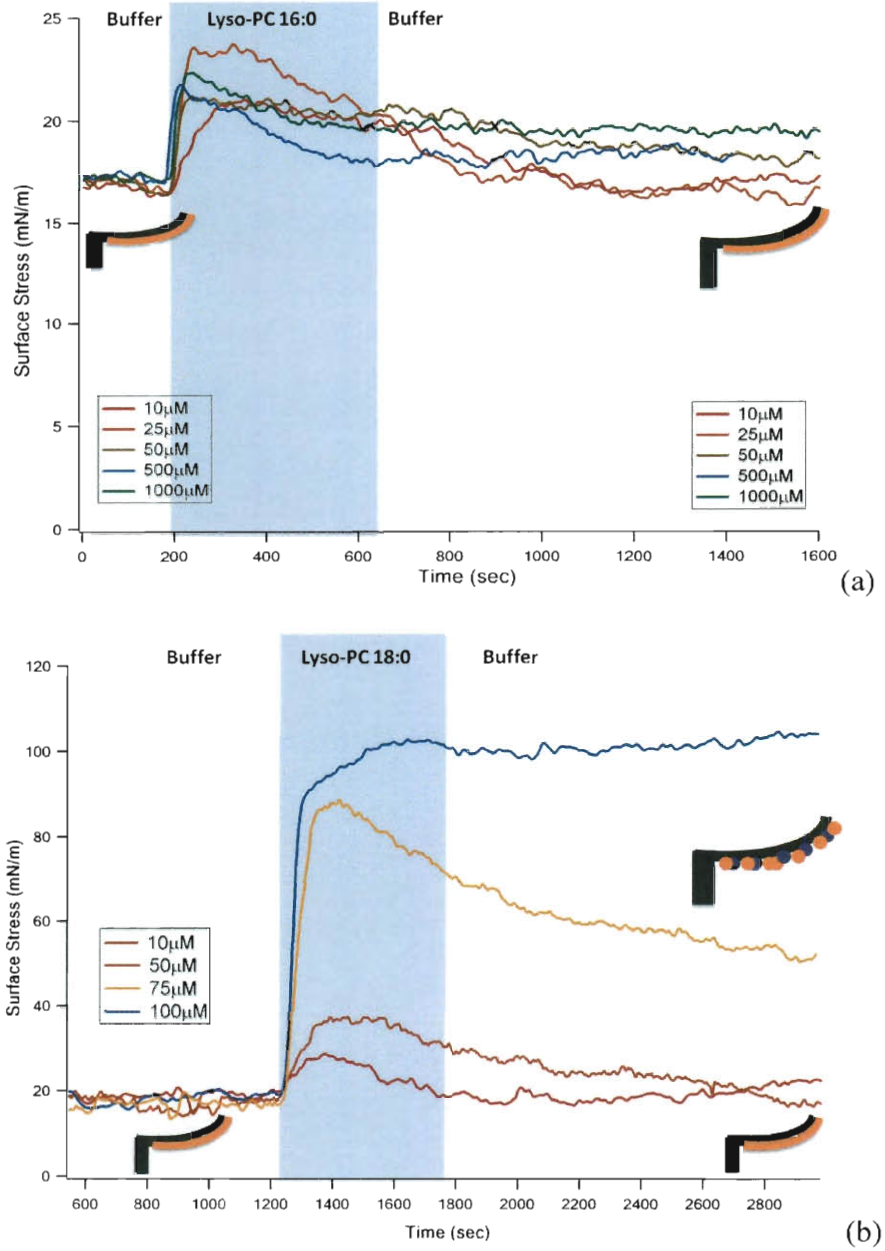

Figure 6.5. Comparison of the response of SLB-coated microcantilever to the lyso-lipids with different aliphatic chain lengths: (a) lysoPC 16:0 and (b) lysoPC 18:0. Above CMC, the changes in surface stress induced by lysoPC 18:0 and 16:0 indicate no SLB solubilization.

6.4. Conclusions

From our experiments we are able to monitor the interactions between SLBs and lyso-

lipids and extract thermodynamic parameters. Using the microcantilevers we observed both the lyso-lipid insertion and the membrane solubilization, and the deflecting distance and direction of the microcantilevers quantify the minute changes in lipid membrane. The effects of lyso-lipids on lipid membranes depend on the concentration and aliphatic chain length of the lyso-lipids and also on their hydrophobic match with the lipids. At the concentration smaller than CMC, lyso-lipids insert reversibly into the lipid membranes, and we calculate the free energy of partitioning of lyso-lipids with different chain lengths. At concentration higher than CMC, the lyso-lipid micelles either solubilize the lipid membrane or form lipid-surfactant mixed micelles physisorbed on the solid surface, depending on the extent of the perturbation in the lipid membrane caused by the mixed lyso-lipid micelles. Therefore, we have demonstrated that membrane-coated microcantilevers are useful surface analytical biosensors to characterize and probe the subtle changes in supported lipid bilayers caused by amphipathic molecules.

6.5. Reference

(1) Ly, H. V.; Longo, M. L. *Biophys. J.* **2004**, *87*, 1013-1033.

(2) Martinac, B.; Adler, J.; Kung, C. *Nature* **1990**, *348*, 261-263.

(3) Fuller, N.; Rand, R. P. *Biophys. J.* **2001**, *81*, 243-254.

(4) Zhelev, D. V. *Biophys. J.* **1998**, *75*, 321-330.

(5) Seddon, A. M.; Lorch, M.; Ces, O.; Templer, R. H.; Macrae, F.; Booth, P. J. *J. Mol. Biol.* **2008**, *380*, 548-556.

(6) Traikia, M.; Warschawski, D. E.; Lambert, O.; Rigaud, J. L.; Devaux, P. F. *Biophys. J.* **2002**, *83*, 1443-1454.

(7) Booth, P. J. *Curr. Opin. Struct. Biol.* **2005**, *15*, 435-440.

(8) Keller, S.; Heerklotz, H.; Jahnke, N.; Blume, A. *Biophys. J.* **2006**, *90*, 4509-4521.

(9) Artyukhin, A. B.; Stroeve, P. *Ind. Eng. Chem. Res.* **2003**, *42*, 2156-2162.

(10) Lichtenberg, D. *Biochim. Biophys. Acta* **1985**, *821*, 470-478.

(11) Nagarajan, R. *Curr. Opin. Colloid Interface Sci.* **1996**, *1*, 391-401.

(12) Helenius, A.; Simons, K. *Biochim. Biophys. Acta* **1975**, *415*, 29-79.

(13) Almgren, M. *Biochim. Biophys. Acta-Biomembr.* **2000**, *1508*, 146-163.

(14) Needham, D.; Stoicheva, N.; Zhelev, D. V. *Biophys. J.* **1997**, *73*, 2615-2629.

(15) Needham, D.; Zhelev, D. V. *Ann. Biomed. Eng.* **1995**, *23*, 287-298.

(16) Raphael, R. M.; Waugh, R. E. *Biophys. J.* **1996**, *71*, 1374-1388.

(17) Henriksen, J. R.; Andresen, T. L.; Feldborg, L. N.; Duelund, L.; Ipsen, J. H. *Biophys. J.*, *98*, 2199-2205.

(18) Fritz, J.; Baller, M. K.; Lang, H. P.; Rothuizen, H.; Vettiger, P.; Meyer, E.; Guntherodt, H. J.; Gerber, C.; Gimzewski, J. K. *Science* **2000**, *288*, 316-318.

(19) Raiteri, R.; Grattarola, M.; Butt, H. J.; Skladal, P. *Sens. Actuator B-Chem.* **2001**, *79*, 115-126.

(20) Thundat, T.; Oden, P. I.; Warmack, R. J. *Microscale Thermophys. Eng.* **1997**, *1*, 185.

(21) Yan, X. D.; Ji, H. F.; Thundat, T. *Curr. Anal. Chem.* **2006**, *2*, 297-307.

(22) Biswal, S. L.; Raorane, D.; Chaiken, A.; Birecki, H.; Majumdar, A. *Anal. Chem.* **2006**, *78*, 7104-7109.

(23) Thundat, T.; Majumdar, A. In *Sensors and Sensing in Biology and Engineering*; Barth, F. G., Humphrey, J. A., Seecomb, T. W., Eds.; Springer: Verlag Wien, 2003, pp 337-355.

(24) Liu, K. W.; Biswal, S. L. *Anal. Chem.* **2010**, *82*, 7527-7532.

(25) Hope, M. J.; Bally, M. B.; Webb, G.; Cullis, P. R. *Biochim. Biophys. Acta,* **1985**, *812*, 55-65.

(26) Heerklotz, H.; Seelig, J. *Biophys. J.* **2000**, *78*, 2435-2440.

(27) Hoyrup, P.; Davidsen, J.; Jorgensen, K. *J. Phys. Chem. B* **2001**, *105*, 2649-2657.

(28) Reinl, H. M.; Bayerl, T. M. *Biochemistry* **1994**, *33*, 14091-14099.

(29) Jahnig, F. *Biophys. J.* **1984**, *46*, 687-694.

(30) Lichtenberg, D.; Opatowski, E.; Kozlov, M. M. *Biochim. Biophys. Acta-Biomembr.* **2000**, *1508*, 1-19.

(31) Koynova, R.; Tenchov, B. *Curr. Opin. Colloid Interface Sci.* **2001**, *6*, 277-286.

Chapter 7

Probing Peptide-Membrane Interactions Using Lipid Membrane-coated Microcantilever

7.1.Introduction

Understanding peptide-membrane interactions is important in elucidating biomolecular mechanisms, such as membrane fusion, cell signaling, and therapeutic approach of antibiotic and antiviral drugs. Membrane-active peptides are proteins that are known for their association with lipid membranes. They may interact predominantly with the hydrocarbon region of the lipid membrane, the polar headgroup region, or both regions of the bilayer, depending on the peptide's hydropathicity. An amphipathic helix (AH) peptide that is of great interest is the AH segment derived from the N-terminal end of the Hepatitis C Virus's nonstructural protein NS5A. The Hepatitis C Virus (HCV) infects more than 170 million people worldwide and those who are exposed risk chronic liver disease. [1, 2] So far no vaccine for preventing HCV infection exists, and HCV infection is difficult to diagnose because most of the patients do not exhibit obvious symptoms. Understanding the infectious mechanism of HCV is thus of great need.

The association of the NS5A-derived AH peptide with lipid membranes is an essential step in the HCV viral infection. This step is followed by RNA replication of the virus in liver cells. The AH viral attack is able to induce lysis of lipid membranes. Blocking the membrane binding pathway of the AH is a promising therapeutic strategy. [3] Cho et al. and Chah et al. investigated the binding mechanism of this AH peptide interacting with model lipid membranes, either lipid vesicle (LUVs) or supported lipid membranes (SLBs), with analytical tools, such as

quartz crystal microbalance with dissipation (QCM-D), dynamic light scattering (DLS), reflectometry and atomic force microscopy (AFM). [4-8] The NS5A-derived AH peptide is thought to bind parallel to the lipid membrane surface and penetrate into the lipid membrane, leading to expansion of the outer leaflet. Cho's AFM images showed that sequential introduction of AH onto the SLBs causes a membrane thinning at a threshold AH concentration (1.63 – 3.25 μM), which indicates that the membrane laterally expands, according to Huang's geometric model. [6] In addition to insights into the binding mechanisms, the virus-mimetic attack of NS5A-derived AH for rupturing lipid membranes provides a novel SLB pattering approach onto surfaces that do not easily rupture vesicles, such as gold and TiO_2 surfaces, which are known for difficulties in forming SLBs spontaneously without external forces. [8, 9]

Instead of laboriously purifying this AH segment of the NS5A protein from HCVs, we use a synthetic analogue, PEP1 (synthesized by AnaSpec, CA). Similar to the natural NS5A-derived AH, PEP1 exhibits typical amphipathic characteristics by partially penetrating the lipid bilayer and interacting with both polar hydrophilic lipid headgroups and hydrophobic tails. Several binding and disruption processes have been proposed empirically, however a physical understanding is still lacking. [6] Compared to PEP1, other well characterized amphipathic helical peptides belongs to the family of antibacterial peptides, such as melittin and magainin. [10-14] They are known for adsorbing onto lipid membranes and reorienting to form transmembrane pores, leading to higher membrane permeability or even disruption. We refer to theories and models developed for these antibacterial peptides to explain the membrane binding and possible pore formation of PEP1. More specifically, we are interested in extracting the membrane lateral expansion caused by the PEP1, because it is an indicator of foreign molecules insertion into the membrane.

This chapter explores the membrane lateral expansion caused by peptide adsorption and pore formation, using the microcantilevers. Previously it has been shown that microcantilevers are useful in sensing peptide binding and reconstruction on surfaces; for example, the amyloid fibrils of insulin grow in the in-plane direction and generate a tensile surface stress of 20 mN/m within two hours on microcantilever surfaces. [15, 16] Ghatkesar et al. observed melittin molecules binding to lipid vesicle membranes deposited on gold surfaces of the microcantilevers. [17] These findings open up possible techniques to monitor protein aggregations using microcantilevers; however, there have not been a quantitative explanation of how the surface stress can be related to changes in the surface-bound proteins. This chapter establishes a method for quantifying the peptide-induced mechanical response of the microcantilevers.

In Chapter 4, a systematic characterization of the SLBs adsorption on the microcantilever surface and analysis of the electrostatic and hydrophobic contributions that take parts in the changes in adsorption free energy are performed. [18] In addition, the insertion and solubilization effects of amphiphilic surfactants on SLBs were detected using the lipid membrane-coated microcantilevers in Chapter 6. In particular, herein is a practical application of our previously developed lipid membrane-coated cantilever sensors in biomolecular recognition at model membrane interfaces. The lipid membrane-coated microcantilever has the potential to probe membrane motions in the lateral directions, thus adding more information other than thickness and bound mass that are studied with ellipsometry or quartz crystal microbalance. We will unravel the affinity differences between AHs and phospholipid membranes. The response of the lipid membrane-coated cantilevers is analyzed based on the free energy change of this interaction between model membranes and peptides.

7.2.Experimental Section

7.2.1. Lipid Vesicle Preparation

A zwitterionic lipid, 1-palmitoyl-2-oleoyl-*sn*-glycero-3-phosphocholine (POPC), was used to form a neutral lipid bilayer. The lipids were purchased from Avanti Polar Lipids (Alabaster, AL). Vesicles were prepared by the extrusion method. [19] Briefly, lipids were dissolved at 5 mg/mL in chloroform. The chloroform was evaporated under a nitrogen stream. The resulting lipid film was then dried in a vacuum chamber for 2 h and then hydrated in a solution composed of 0.5:99.5 (v%) of DMSO and 0.25 mL pH 7.4 phosphate buffered saline (PBS, Sigma-Aldrich) solutions made in ultrapure deionized water (Barnstead Nanopure system, Thermo Fisher Scientific), followed by vortexing the solution. The solution was then extruded 40 times through a 100 nm polycarbonate membrane using a mini-extruder (Avanti Polar Lipids, AL), resulting in a translucent solution of large unilamellar vesicles (LUVs) approximately 100 nm in size. The vesicle solution was further diluted with 9 parts of PBS to 1 part of the freshly extruded vesicle solution and stored at 4 °C until use. Note that the final vesicle concentration may be lower than initially desired due to lipid loss on filter membranes after extrusion; however, the concentration was well above the threshold needed to achieve full surface coverage of SLB.

7.2.2. Amphipathic Helix Peptide Preparation

The peptide, PEP1, was synthesized by AnaSpec (San Jose, CA). PEP1 has 31 amino acids (MW= 3804.3 g/mol), with the sequence: H–Ser–Gly–Ser–Trp–Leu–Arg–Asp–Val–Trp–Asp–Trp–Ile–Cys–Thr–Val–Leu–Thr–Asp–Phe–Lys–Thr–Trp–Leu–Gln–Ser–Lys–Leu–Asp–Tyr– Lys–Asp–NH_2. It was used as delivered without further purification. The peptide was dissolved in a small amount of dimethyl sulfoxide (DMSO, $(CH_3)_2SO$, MW=78.14, EMD Chemicals, USA) and then slowly diluted in phosphate buffered saline (PBS, Sigma-Aldrich,

USA). The final peptide solution was prepared in an eluent mixture of DMSO and PBS (0.5:99.5 v%). The peptide solution was kept refrigerated at 4°C no more than three days prior the experiments. PEP1 is an amphipathic helix peptide that forms a helix structure when adsorbed onto lipid membranes. Fig. 7.1 shows the helical wheel diagram that illustrates the hydrophilic and hydrophobic surfaces on PEP1.

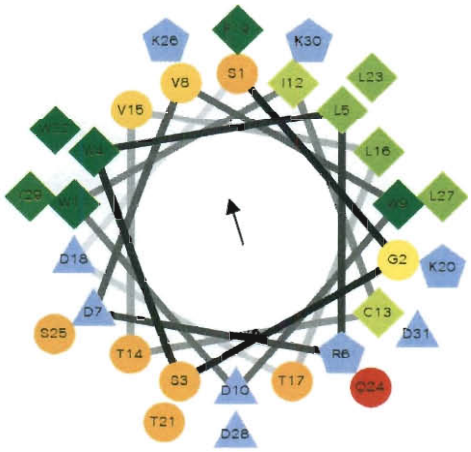

Figure 7.1. The helical wheel diagram of the 31 residue alpha helix peptide, PEP1, with the amino acid sequence: SGSWLRDVWDWICTVLTDFKTWLQ SKLDYKD-NH2. The diagram is used to illustrate the hydrophilicity of the peptide. (See TABLE 7.1 for the color code of this diagram) The PEP1 shows a hydrophobic face as indicated by the arrow and a hydrophilic face on the other side. The plot is generated from the program on the website: http://rzlab.ucr.edu/scripts/wheel/wheel.cgi

7.2.3.Microcantilever Preparation and Measurement

Cantilever chips were purchased from Concentris GmbH (Basel, Switzerland). The cantilevers are 500 μm in length, 100 μm in width, and 1 μm thick. Each chip contains eight rectangular silicon cantilevers, each with a spring constant of 0.026 N/m. The cantilevers were coated with 3 nm titanium followed by 20 nm gold layer, resulting in a bimetallic structure. The

cantilever arrays were placed in an UV ozone cleaner for 5 min under 5 psi oxygen to clean the gold surface on the front surface and generate a hydrophilic silicon dioxide surface on the back surface. Each cantilever was individually functionalized using glass microcapillaries. The surface functionalization typically proceeded for two hours. To prevent binding preferentially to the gold side of the cantilever beam, polyethylene glycol (PEG) polymers were used. A dithiolaromatic–PEG molecule ($C_{25}H_{44}O_6S_2$, MW=504.74 g/mol, Sensopath Technologies, Bozeman, MT) was used to prevent vesicle adsorption to the gold surface of the cantilever. A good blocking agent, bovine casein (Alfa Aesar, MA, USA) solution, was used to prevent lipid bilayer and peptide adsorption on the silicon dioxide surface of the cantilever. Aqueous solution saturated with casein was filtered with a syringe filter of 0.22 μm pore size to remove undissolved protein aggregates. A reference cantilever was functionalized with both the dithiolaromatic–PEG and casein. The microcantilever will be used to probe the interactions between the peptide and the lipid membrane, as illustrated in Fig. 7.2.

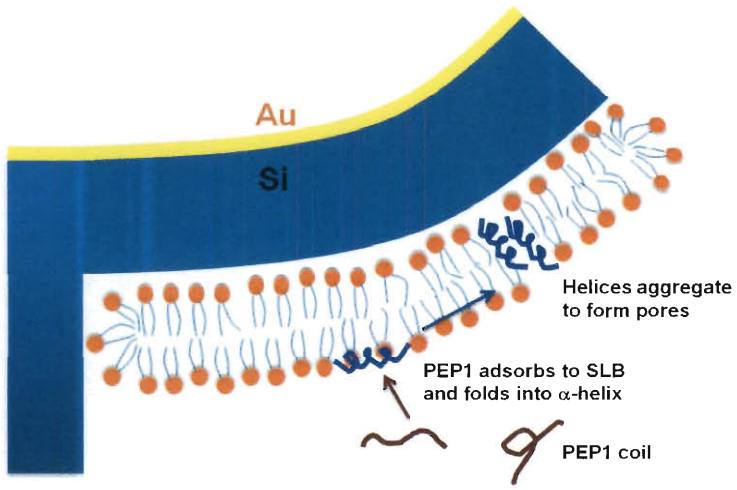

Figure 7.2. Schematic of the use of the lipid membrane–coated microcantilever for sensing the peptide adsorption and insertion. These interactions generate compressive stress on the microcantilevers and lead the microcantilever to bend toward the gold side.

7.3. Results and Discussions

7.3.1. Lipid Deposition onto Functionalized Microcantilever Surfaces

Upon injection of the POPC vesicle solution into the flow chamber, the cantilevers undergo a surface stress change and deflect. Vesicles are attracted by the negatively charged SiO_2 surface of the microcantilevers and fuse onto the surface to form SLBs. This surface stress change is compressive; therefore the cantilevers bend away from the side of SLB formation. The microcantilever bends with a deflection of 73 ± 6.0 nm. Thus, the measured surface stress, $\Delta\sigma_{ads,SLB}$, for SLB formation on SiO_2 is 17 ± 1.4 mN/m. Note that the vesicle solution flowed for 7 min (as indicated with shaded area in Figure 4), after which, the valve was switched back to the PBS buffer port. Since the bilayer's adsorption is irreversible over this time scale, the cantilevers remain deflected from 300 to 650 s. The SLBs are stable for at least two hours of observation time and do not desorb after the solution is switched to buffer. After the SLBs are prepared on the SiO_2 surfaces of the microcantilevers, PEP1 is then introduced onto the SLBs.

7.3.2. PEP1s Adsorb onto POPC SLBs

As shown in Fig. 7.3, at bulk PEP1 concentrations lower than 4 μM, the surface stress readily increases with the concentration in a linear fashion. For this concentration range, the PEP1 peptides adsorb to the membrane surfaces parallel to the membrane plane and create an area increment in the outer leaflet of the membrane. At bulk PEP1 concentration higher than 4 μM but below 15μM, the surface stress does not show any apparent increase and remains at 25~28 mN/m. The adsorbed PEP1 peptides saturate the lipid membrane at this bulk concentration, so that the membrane does not take up more PEP1 than its maximum capacity

even when the bulk PEP1 concentration increases. It is also possible that the surface bound PEP1 and membrane pores created by the PEP1 coexist at this bulk concentration. Fig. 7.4 compares the adsorption curve of PEP1 on the SLB coated microcantilevers with that of a casein coated cantilever. On the casein coated microcantilever, the surface stress remains zero or small after the introduction of POPC vesicles and PEP1 onto the surface. Though there is some disturbance of surface stress after contacting the PEP1, it is thought that the PEP1 peptides non-specifically adsorb to casein through hydrophobic interactions.

In addition, after immersing the membrane-coated microcantilevers in PEP1 solution for 7 minutes for enough contact time, as shown in Fig. 7.4 by the shaded area, the surfaces are rinsed with buffer. There is no drop in surface stress observed, which indicates the PEP1 adsorption onto lipid membranes is irreversible, and no PEP1 desorption from membrane to bulk buffer occurs.

The total surface area of the membrane–peptide complex expands by the total area of adsorbed peptides and results in an internal stress in the lipid membranes. The model membrane is thought a soft material that can be elastically deformed, thus the increase in membrane surface area (or membrane strain in surface area) can be related to the internal stress by the membrane's stretch modulus K_A. The membrane internal stress, $\Delta\sigma_{mem}$, accounts for the lateral interactions between the lipid-lipid and lipid-peptide in the SLB. The other source of surface stress, $\Delta\sigma_{ads}$, comes from the lipid–surface interactions, which is the chemical potential gained from adsorption.

$$\Delta\sigma_{mem} = K_A \frac{A_P}{A_L} \frac{P}{L}. \tag{7.1}$$

Thus the total surface stress, $\Delta\sigma_{total}$, measured on the microcantilevers is comprised of the contributions from lipid–lipid and lipid-peptide ($\Delta\sigma_{mem}$) and lipid–surface interactions ($\Delta\sigma_{ads}$):

$$\Delta\sigma_{total} = \Delta\sigma_{ads} + \Delta\sigma_{mem} = \Delta\sigma_{ads} + K_A \cdot \frac{A_P}{A_L}\frac{P}{L} \tag{7.2}$$

where A_P and A_L represent the molecular area of the peptide and the lipid, respectively. P/L is the number ratio of membrane bound peptide to lipid. The membrane internal stress is estimated from Eq. (7.1) by taking the K_A to be 240 mN/m, A_P be 360 Å^2, [20] and A_L be 65 Å^2 for lipid membranes in a fluid state. [6] Huang et al. predicted that the typical value for $\Delta\sigma_{mem}$ at concentration when pore formation occurs is 5 ~ 15mN/m, which is close to the surface stress measurement derived from the microcantilevers, which is ~ 13 mN/m. By excluding the PEP1 adsorption term ($\Delta\sigma_{ads}$) and only taking the membrane internal stress term ($\Delta\sigma_{mem}$) for the calculation of the total measured surface stress, the P/L value will be estimated to be 1/102, which indicates that one PEP1 is surrounded by 102 lipid molecules. The real P/L might be smaller because the adsorption term ($\Delta\sigma_{ads}$) has to be taken into consideration. However the $\Delta\sigma_{ads}$ value is difficult to predict here and must be estimated from other measurements.

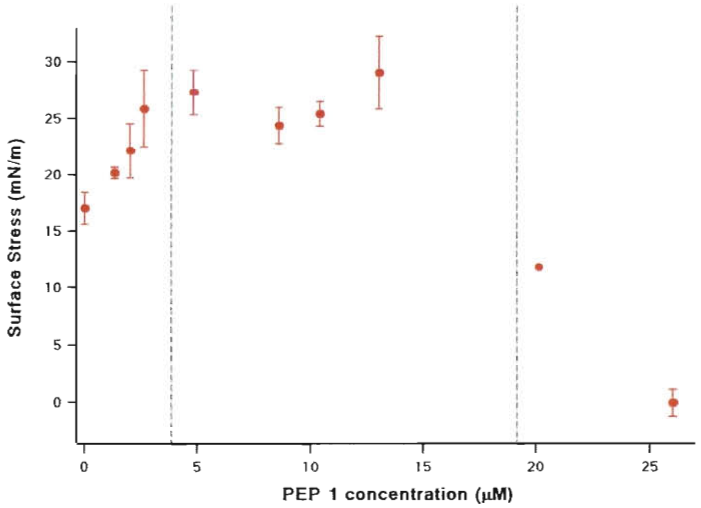

Figure 7.3. Surface stress generated on microcantilevers after the PEP1 solution is introduced onto the SLBs on SiO_2 surface. Three regions are separated by dash lines. At concentration < 4μM, the increasing trend of the surface stress is near to a linear relation to the PEP1 concentration; at concentration > 4μM, the PEP1s saturate the membrane surface, the surface stress does not show obvious increase. At high concentration (26 μM), the membrane is completely solubilized, leaving a blank SiO_2 surface and a zero surface stress.

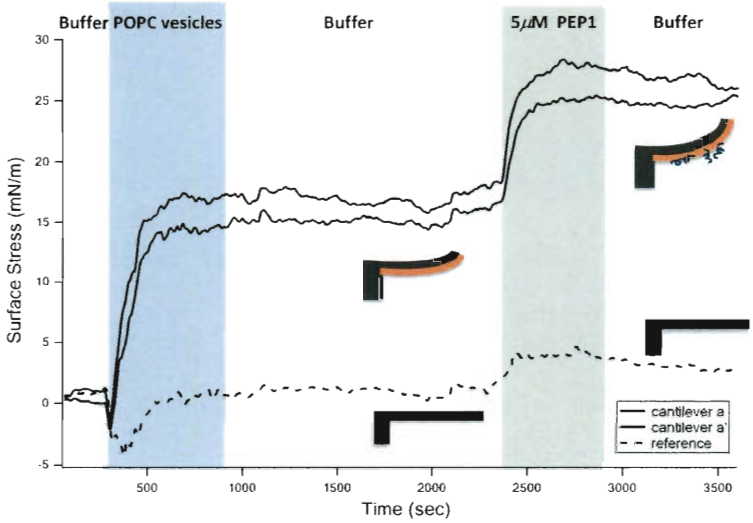

Figure 7.4. PEP1s insert into POPC SLBs. Experimental cantilevers (solid lines) on the same chip are shown. The SiO_2 surface of the reference cantilever (dash line) is blocked by casein, thus no lipid membrane adsorbs on it. Note that after injecting the PEP1 solution, there is a slight surface stress change on the reference cantilever, caused by a minute PEP1 adsorption on casein.

7.3.3. High Surface Concentration of PEP1 Leads to POPC SLBs Lysis

As a larger concentration of peptides aggregate into the membrane, there is an increase in the number of pores, leading to instability of the membrane. When the membrane internal stress accumulates and reaches a value where it cannot be counterbalanced by the membrane tension at the edges of pores, the membrane lyses. We monitor the real-time surface process of the lysis of a SLB when in contact with higher PEP1 concentrations. The microcantilevers show that the SLBs completely lyse on native SiO_2 surfaces. The surface stress drop from 17 ± 1.4 mN/m to zero, which indicates the SLB is perturbed and readily desorbs after contacting with PEP1 at 26 μM, as shown in Fig. 7.5. It has been previously proven that lipid vesicles rupture due to PEP1 at higher concentration (13 μM). [5, 8, 9] Other groups have observed using QCM-D and SPR that the vesicles rupture upon PEP1 exposure and a supported membrane remains adsorbed onto the gold and TiO_2 surfaces. [8, 9]

Contradictory to our results, Cho and coworkers did not observe SLB lyses on SiO2 surfaces using QCM-D. [7]. It is thought that the solubilization of supported lipid membranes is dependent of the surface properties of the SiO_2 support. On our microcantilevers, the 3 nm native SiO_2 thin film forms naturally at the Si surface, while the SiO_2 surface of the quartz crystals used for QCM-D measurements is a 100 nm thick film prepared by sputtering. The native SiO_2 may be less attractive to the SLB. As a result, once the membranes rupture, the membrane patches desorb immediately from the native SiO_2 surface; while on the sputtered SiO_2 the disrupted membrane patches remain adsorbed. In addition, comparing the response of the PEP1 adsorption on POPC SLBs using the microcantilever sensors and QCM-D, the peptide partitioning into lipid membrane is more responsive in surface stress than in mass. For a P/L ratio of 1/100 for the

adsorption of PEP1 to lipid membranes, the frequency change measured on QCM-D will be estimated to be 1.25 Hz, while frequency change for the SLB formation is 25~26 Hz. On microcantilevers, the maximum surface stress change induced by the PEP1 is 13 mN/m, while that induced by the SLB formation is 17 mN/m. Thus, the microcantilever sensor is more sensitive to small molecule adsorption to membranes and to interactions that are involved with lateral membrane internal stress change.

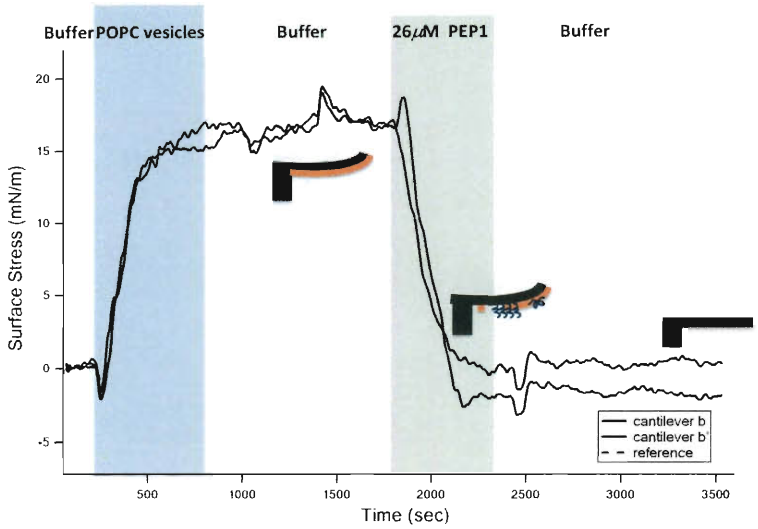

Figure 7.5. POPC SLB is solubilized readily after contacting with a high concentration of PEP1.

7.4. Conclusion

The bending motion of lipid membrane-coated microcantilevers is a direct surface measurement of surface stress change as the PEP1 molecules bind to the membrane. Interactions between PEP1 and the lipid membranes are measured for different peptide concentrations. From the plot of surface stress versus PEP1 concentration, three regions of different interactions are observed. At concentration < 4μM, the amount of the PEP1 peptides adsorbed to the membrane is linear with the bulk concentration. At concentration > 4μM but < 15μM, the PEP1 peptides

saturate the membrane and reach a plateau in surface stress. At higher concentration of PEP1, membrane lysis begins. Compared to other surface-sensitive tools, such as QCM-D, the microcantilever sensor is more sensitive in probing small molecules adsorption because the membrane internal stress change can also be detected instead of just peptide adsorption. Thus the lipid membrane-coated microcantilever sensor is capable of characterizing the kinetics and dynamics of membrane-peptide interactions with good sensitivity.

7.5. Note on the Helical Wheel Diagram

In Fig. 1, the helical wheel diagram is coded by shape and color. The greenish colors indicate more hydrophobic residues on the amino acids and the reddish colors indicate more hydrophilic residues. The program to generate the plot is created by Don Armstrong and Raphael Zidovetzki (Department of Cell Biology and Neuroscience, University of California Riverside)

Shapes	Hydrophilic : circle Hydrophobic: diamond Potentially negatively charged: triangle Potentially positively charged: pentagon
Colors	Hydrophobic residue: green Zero hydrophobicity: yellow. Hydrophilic: red (uncharged) and light blue (charged)

TABLE 7.1. The representative codes of the helical wheel diagram used in Fig. 7.1.

7.6. Reference

(1) Di Bisceglie, A. M. *Hepatology* **2000**, *31*, 1014-1018.

(2) Cheng, G.; Montero, A.; Gastaminza, P.; Whitten-Bauer, C.; Wieland, S. F.; Isogawa, M.; Fredericksen, B.; Selvarajah, S.; Gallay, P. A.; Ghadiri, M. R.; Chisari, F. V. *Proc. Natl. Acad. Sci. U. S. A.* **2008**, *105*, 3088-3093.

(3) Elazar, M.; Cheong, K. H.; Liu, P.; Greenberg, H. B.; Rice, C. M.; Glenn, J. S. *J. Virol.* **2003**, *77*, 6055-6061.

(4) Cho, N. J.; Dvory-Sobol, H.; Xiong, A. M.; Cho, S. J.; Frank, C. W.; Glenn, J. S. *ACS Chem. Biol.* **2009**, *4*, 1061-1067.

(5) Cho, N. J.; Wang, G. L.; Edvardsson, M.; Glenn, J. S.; Hook, F.; Frank, C. W. *Anal. Chem.* **2009**, *81*, 4752-4761.

(6) Cho, N. J.; Cho, S. J.; Hardesty, J. O.; Glenn, J. S.; Frank, C. W. *Langmuir* **2007**, *23*, 10855-10863.

(7) Cho, N. J.; Cheong, K. H.; Lee, C.; Frank, C. W.; Glenn, J. S. *J. Virol.* **2007**, *81*, 6682-6689.

(8) Chah, S.; Zare, R. N. *Phys. Chem. Chem. Phys.* **2008**, *10*, 3203-3208.

(9)Cho, N. J.; Cho, S. J.; Cheong, K. H.; Glenn, J. S.; Frank, C. W. *J. Am. Chem. Soc.* **2007**, *129*, 10050.

(10)Huang, H. W.; Chen, F. Y.; Lee, M. T. *Phys. Rev. Lett.* **2004**, *92*.

(11)Lee, M. T.; Chen, F. Y.; Huang, H. W. *Biochemistry* **2004**, *43*, 3590-3599.

(12)Lee, M. T.; Hung, W. C.; Chen, F. Y.; Huang, H. W. *Proc. Natl. Acad. Sci. U. S. A.* **2008**, *105*, 5087-5092.

(13)Ludtke, S. J.; He, K.; Heller, W. T.; Harroun, T. A.; Yang, L.; Huang, H. W. *Biochemistry* **1996**, *35*, 13723-13728.

(14)van den Bogaart, G.; Guzman, J. V.; Mika, J. T.; Poolman, B. *J. Biol. Chem.* **2008**, *283*, 33854-33857.

(15)Knowles, T. P. J.; Shu, W.; Huber, F.; Lang, H. P.; Gerber, C.; Dobson, C. M.; Welland, M. E. *Nanotechnology* **2008**, *19*.

(16)White, D. A.; Buell, A. K.; Dobson, C. M.; Welland, M. E.; Knowles, T. P. J. *FEBS Lett.* **2009**, *583*, 2587-2592.

(17)Ghatkesar, M. K.; Lang, H.-P.; Gerber, C.; Hegner, M.; Braun, T. *PLoS One* **2008**, *3*, e3610.

(18)Liu, K. W.; Biswal, S. L. *Anal. Chem.* **2010**, *82*, 7527-7532.

(19)Hope, M. J.; Bally, M. B.; Webb, G.; Cullis, P. R. *Biochim. Biophys. Acta,* **1985**, *812*, 55-65.

(20)Rawicz, W.; Olbrich, K. C.; McIntosh, T.; Needham, D.; Evans, E. *Biophysical Journal* **2000**, *79*, 328-339.

Chapter 8

Monitoring DNA Binding to *Escherichia coli* Lactose Repressor Using Microcantilevers and Quartz Crystal Microbalance with Dissipation

8.1. Introduction

Immobilized biomolecules are greatly influenced by the solid surfaces used to support them. Characterizing the effect of a solid surface on the conformation and recognition functions of biomolecules thus requires surface sensitive techniques. In addition to the solid–supported lipid bilayers described in Chapters 4-7, this chapter provides one example of surface–immobilized proteins bound on gold surfaces, which recognize and bind to a specific DNA sequence.

Lactose repressor protein (LacI) serves as a negative transcription regulator in *E. coli*,[1] binding to the operator DNA sequence within the *lac* operon to prevent the transcription of downstream structural genes by RNA polymerase. [2] LacI binding to a metabolite of lactose, allolactose, generates a conformational change that diminishes the high affinity of repressor for operator, allowing initiation and transcription of the structural genes. [3] Termed inducers, synthetic galactosides, *e.g.* IPTG, function similarly to release operator DNA. [4]

Structurally, LacI is a homotetramer, assembled as "a dimer of dimers" (Fig. 8.1). Each monomer contains an inducer binding site, whereas dimer is required to bind the operator DNA. [5-8] The structure of LacI comprises the N-terminal DNA binding domain (amino acids 1-50), the hinge helix (amino acids 51-60), the core inducer-binding domain (amino acids 61-330), and the

leucine heptad repeat tetramerization domain (amino acids 331-360) at the C-terminus (Fig. 8.1). [7, 8] Binding to inducer does not impact the C-terminal core subdomain or the tetramerization domain, but reorients the core N-subdomain interface, in turn disrupting DNA binding. [6-9]

Several methods have been used to study ligand-surface and protein-DNA interactions, including *in situ* surface plasmon resonance (SPR), reflectance FTIR, and *in situ* ellipsometry. [10, 11] In particular, SPR has been a useful tool for studying the kinetics of binding. [12] However, the above-mentioned techniques do not provide conformational properties, such as elasticity, of the resulting film. The application of microcantilevers and quartz crystal microbalance with dissipation (QCM-D) provides analytical methods to directly detect the binding of a small ligand to an immobilized protein. [13-15] Microcantilever sensors transduce changes in surface free energy and internal stress of the surface-immobilized film at solid-liquid or solid-gas interfaces into mechanical readout. The proteins motion are detectable for microcantilevers in two aspects. One is that the protein binding onto surfaces adds up the chemical potential at the interfaces as well as the surface free energy. Also, the lateral attraction or repulsion of the surface-bound proteins creates internal stress in the protein film. Few of other techniques can access to the internal stress of a surface-bound soft film at the nanoscale. In addition to microcantilevers, QCM-D is capable of simultaneously measuring the change in mass and *in situ* viscoelastic properties of the protein film bound to the quartz crystal. [16] Höök and coworkers were some of the earliest to study the structural changes of proteins with QCM-D. [17, 18] Recently, Fernandez and coworkers studied reversibility of protein adsorption as well as the rigidity of the protein layers using QCM-D. [19] Thus far, QCM-D has been used to measure binding of small molecules, DNA binding, as well as cell adhesion. [13, 14, 20] QCM-D has become increasingly popular to study biomolecular interactions due to its ease of use and high-throughput analysis.

A very effective mode of protein immobilization to the sensor is through a strong

gold-sulfur covalent bond. In order to measure a binding event by QCM, the receptor protein must be attached with an orientation that allows binding to its ligands. For this purpose, cysteine has been introduced into a protein at a position distant from the functional site and active site to insure retention of binding properties upon immobilization. For example, binding of bacterial periplasmic binding proteins (PBPs) to small ligands and the associated conformational change were successfully detected by QCM-D. [20]

In this study, microcantilevers and QCM-D have been utilized to detect ligand binding and allosteric response in LacI. Previous work shows that binding affinity of wild-type LacI for DNA is diminished when bound to a gold surface, indicating the repressor uses its highly basic DNA binding site for gold conjugation. [21] A specific orientation of bound protein via a direct sulfur-gold linkage was obtained using a mutant LacI, T334C. This designed substitution was engineered with a solvent-exposed thiol located at the C – terminus, distant from the N-terminal DNA binding domain and the core inducer binding site. [21] Here, we explore the applicability of microcantilevers and QCM-D in detection of ligand binding and ligand-induced conformational change of LacI using this variant T334C protein.

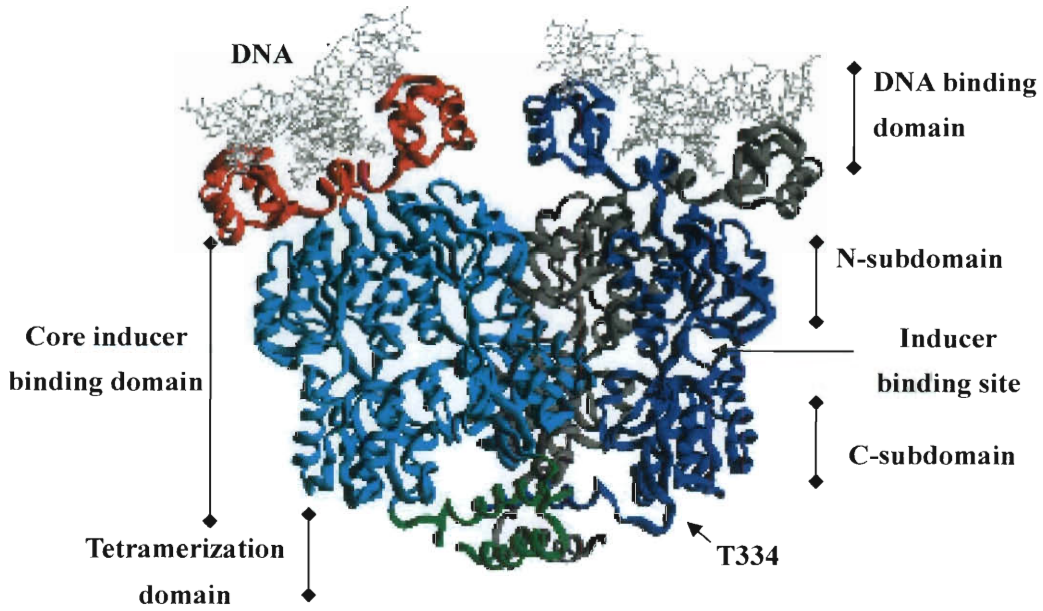

Figure 8.1. The crystal structure of tetrameric LacI showing the position of residue T334 (pdb file 1LBI [6]). In the left dimer, different colors show the three main regions of LacI (red, DNA binding domain; cyan, core domain; green, tetramerization domain); two monomers are displayed in distinct colors (blue, gray) in the right dimer. Operator DNA is shown in light gray. The position of threonine 334 is shown by an arrow on the monomer depicted in blue. Position 334 was chosen for the cysteine mutation because of its solvent exposure and distance from both the inducer and the DNA binding sites.

8.2. Materials and Methods

8.2.1. Protein expression and purification

The T334C mutation in LacI [21] was produced on plasmid pLS1, [22] which contains the complete LacI sequence. Plasmid DNA was purified by Qiagen miniprep Kit. Full sequencing (SeqWright) of the coding region for LacI in the T334C mutant plasmid verified the presence of only the expected mutation.

Protein expression and purification were carried out with small modifications to accommodate the presence of solvent-exposed cysteine. [21, 22] Briefly, wild-type and T334C LacI

were expressed using *E. coli* BLIM cells. [23] Cells transformed with a specific plasmid were grown in 2 × YT liquid media at 37 °C for 20-24 hrs. The cells were collected by centrifugation and resuspended in lysis buffer (0.2 M Tris-HCl, pH 7.6, 0.2 M KCl, 0.01 M Mg acetate, 5% glucose, 10 mM DTT and 0.3 μM PMSF). The lysis supernatant was fractionated using 37% ammonium sulfate, and the precipitate was collected by centrifugation. All buffers contain ~10 mM DTT to prevent oxidization and aggregation. Protease inhibitor tabs (Roche) were added to inhibit the degradation of the proteins. The resuspended cell pellet was dialyzed in three 20 min steps and was loaded onto a phosphocellulose column and eluted with a gradient from 0.12–0.30 M potassium phosphate buffer (pH 7.5). Fractions containing LacI were confirmed by SDS-PAGE, and the concentration of the protein was determined by absorbance at 280 nm (ε = 0.6 $cm^{-1}(mg/ml)^{-1}$).

8.2.2. Microcantilever Preparation and Measurement

Cantilever chips were purchased from Concentris GmbH (Basel, Switzerland). The cantilevers are 500 μm in length, 100 μm in width, and 1 μm thick. Each chip contains eight rectangular silicon cantilevers, each with a spring constant of 0.026 N/m. The cantilever arrays were placed in an UV ozone cleaner for 5 minutes under 5 psi oxygen. This resulted in a cantilever with a clean gold surface on the frontside and a hydrophilic silicon dioxide surface on the backside. The reference cantilevers were individually functionalized using glass microcapillaries for two hours. To prevent proteins binding to gold side of the cantilevers, hydrophilic polyethylene glycol (PEG) polymers were utilized. A dithiolaromatic-PEG molecule ($C_{25}H_{44}O_6S_2$, MW=504.74 g/mol, Sensopath Technologies, Bozeman, MT) was used to prevent vesicle adsorption to the gold surface of the cantilever. The silicon dioxide surface was left unmodified because the binding of proteins to the SiO_2 surface was minor compare to gold surfaces. After use, the cantilevers were once again placed in the UV ozone cleaner for 5 minutes

under 5 psi oxygen and then refunctionalized as described above.

All measurements were performed with a Cantisens Research System (Concentris GmbH, Basel, Switzerland). The cantilevers were mounted in a liquid chamber in which solutions were pumped past the cantilever chip via a syringe pump. The chamber was temperature controlled and for all reported experiments the chip was held at 25 ^{o}C. Prior to the introduction of vesicle solutions, the cantilever signals were set to a zero baseline value. Each sample injection consisted of flowing 0.2 mL of protein or DNA solution at a flow rate of 0.42 μL/sec. Excess liquid was pumped to the waste reservoir via a syringe pump. Real-time deflection of microcantilevers was monitored via a scanning laser diode aligned to the tip of the microcantilevers. The position of the reflected laser beam was captured using a position-sensitive-detector (PSD), with a sampling frequency of 1 Hz. The average thermomechanical sensitivity of the cantilevers was measured to be 73 ± 11 nm/K. [24] Due to small differences in material properties of the cantilevers such as stiffness or thickness variation of the evaporated gold layer, the deflections of the cantilevers were normalized using each cantilever's thermomechanical sensitivity. After normalization, the signal difference between the experimental cantilever and the reference cantilever was calculated to allow us to measure the cantilever deflection due to the vesicle rupture into a SLB.

8.2.3. QCM-D measurement

QCM-D measures changes in adsorbed mass and viscoelastic properties of adsorbed material by monitoring changes in the frequency and decay of oscillation of a quartz crystal. [25, 26] The frequency corresponds to the deposited mass, and the energy decay is described by the dissipation factor D, which is the sum of all losses in the system. The dissipation factor D is defined as the ratio of energy dissipated per oscillation over total energy stored in system over 2π.

The QCM-D measurements were conducted on a Qsense E4 (Q-Sense AB, Gothenburg, Sweden) with an axial flow chamber. The quartz crystal is driven at its resonance frequency of 5 MHz, with measurements at subsequent overtones: 15, 25 and 35 MHz. For sufficiently rigid films (dissipation value $< 1 \times 10^{-6}$), changes in frequency can be related to changes in adsorbed mass per area according to the Sauerbrey relation: [27]

$$\Delta m = -\frac{C}{t}\Delta f \tag{8.1}$$

Where C is a constant of 17.7 ng/cm^2, and t is the overtone. The following frequency shifts reported in this thesis are all normalized to $\Delta f/t$. Thus, a frequency shift of 1 Hz corresponds to a mass of 17.7 ng/cm^2 deposited onto the crystal. The system allows for simultaneous measurements of frequency change and energy dissipation by periodically switching off the power to the crystal and recording the decay of the damped oscillation. Front side gold coated AT-cut quartz crystals (Q-sense), with a mass sensitivity of 2 ng/cm^2 are used for protein immobilization. The gold-coated quartz crystals were first treated using UV ozone (Novascan PSD-UV) for 10 minutes followed by an ammonia and hydrogen peroxide treatment (a 5:1:1 mixture by volume of DI water, H_2O_2 and NH_3) at 70°C for 5 minutes. The crystals were then thoroughly rinsed and stored in purified DI water (water resistively of 18.2 MΩ·cm) until use.

Flow of solution was controlled at a rate of 50 µl/min with a peristaltic pump. The temperature of the chamber was maintained at 25°C at all times. FB buffer (0.01 M Tris-HCl, pH 7.4, 0.15 M KCl, 0.3 mM DTT, 0.1 mM EDTA, and 5% DMSO) was used as a baseline. After equilibrating with buffer, the protein solution was flowed through the measurement chamber until surface saturation was achieved, after which the flow was switched back to the FB buffer solution. Other solutions (DNA, IPTG and ONPF) were introduced at the same flow rate onto the bound protein layer. IPTG is Isopropyl β-D-1-thiogalactoside, and ONPF is o-nitrophenyl-β

-D-fucoside and a counterpart of IPTG. Both reagents were purchased from Sigma Aldrich.

8.2.4. Operator binding assay

Operator binding experiments were performed by nitrocellulose filter binding assay using a 96-well dot blot apparatus. [28] The 40 bp natural operator O^1 (5' – TGTTGTGTGGAATTGTGAGCGGATAACAATTTCACACAGG – 3') (Invitrogen) was used for these measurements. This assay was carried out in FB buffer with 100 μg/mL of bovine serum albumin. Protein at various dilutions from 1×10^{-13} to 5×10^{-9} M was mixed with [^{32}P]-labeled O^1 (~1.5×10^{-12}M), and the mixtures were filtered through nitrocellulose after ~20 min incubation. The filter membrane was exposed to a Fuji phosphorimaging plate overnight. The plate was read by a Fuji phosphorimager, and the retained radioactivity was analyzed by Igor Pro (Wavcemetrics). The binding affinities of various repressors were determined by the following equation:

$$Y_{obs} = Y_{max}\left(\frac{[IPTG]^n}{K_d{}^n + [IPTG]^n}\right) + c \qquad (8.2)$$

where Y_{obs} is the observed level of retained radioactivity at a given protein concentration, Y_{max} is the level of radioactivity at saturation, c is the background when no repressor is present, and K_d is the equilibrium dissociation constant. The value of the Hill coefficient, n, is generally ~1 for LacI.

8.3. Results and Discussion

8.3.1. Assessing DNA binding for single mutant T334C

To confirm function for single mutant T334C, to be used along with wild-type LacI in QCM-D assays, both operator binding affinity and response to IPTG binding were measured by filter binding assay. The O^1-binding behavior of T334C is similar to that for wild-type LacI (K_d

~1.5 × 10^{-11}M) (Fig. 8.2). In the presence of 1 mM IPTG, T334C affinity for operator DNA is diminished comparably to wild-type LacI. T334C therefore presents essential wild-type properties and provides features that allow study by QCM-D.

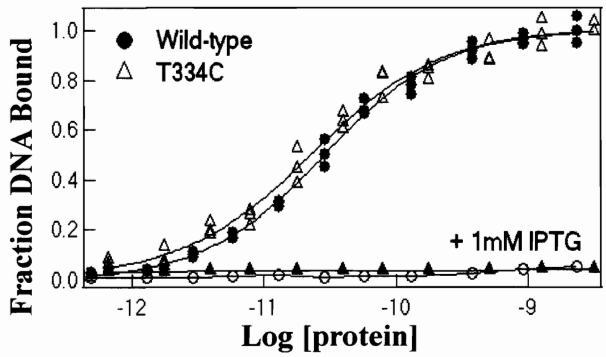

Figure 8.2. Operator binding curves for wild-type LacI and T334C. The operator binding experiment was conducted by filter binding assay as described in Materials and Methods. Fraction DNA bound in the absence of IPTG is shown by filled circles for wild-type and open triangles for T334C. In the presence of 1 mM IPTG, wild-type is represented by open circles and T334C by filled triangles. The curves shown were generated by fitting the data using Igor Pro.

8.3.2. Testing Binding of Single mutant T334C to Gold and Protein-DNA Recognition on Microcantilevers

After the mutant T334C LacI protein comes in contact with the microcantilever surfaces, they bind with gold surface through the gold-cysteine bond and generate a large compressive stress on the gold surface. The experimental microcantilevers (denoted as stat 1, 2, 3, 4, 5, and 7) deflect ~ 1200 nm toward the Si side and slowly relax to reach a final equilibrium value. The relax process is oftentimes observed for proteins adsorbing to solid surfaces because the proteins change their configurations at the solid surfaces, trying to relax to a structure with a minimum free energy. Among the eight cantilevers shown in Fig. 8.3(a), the cantilevers with PEG-blocked gold surface (stat 6 and 8) show no obvious deflection due to the binding on the gold side.

However some nonspecific adsorption on the Si side causes the two cantilevers to bend slightly toward the gold side. In addition, the neighbor cantilevers closest to cantilever 6 and 8 (stat 5 and 7) are affected by the blocking PEG-thiol vapor, so they deflect not as much as those of cantilever 1~4.

The micron scale deflection of the microcantilevers due to the chemical linkage of cysteine on the protein and gold surface is huge, compared to the nano-scale deflection due to physical sorption of a lipid membrane on SiO_2 surface described in the previous chapters. The formation of chemical bonds of thiol-gold is highly endothermic and stresses the surface heavily. In addition, the proteins move from the free space and crowd solid-liquid interface, which leads to a lateral force in between surface bound proteins. Though it is not clear whether the lateral force between LacI proteins, the steric and electrostatic forces between the LacI proteins are likely to add up repulsions in between the proteins. Summing up these two sources of surface energy, the overall resultant is a compressive surface stress of ~ 280 mN/m on the gold surface.

After the LacI proteins are immobilized on the gold surfaces, the O^1 DNA molecules are introduced. All experimental microcantilevers bend toward the Si side between 100 to 200 nm, as shown in Fig. 8.3(b), indicating that O^1 DNAs bind to the DNA-binding domains of the immobilized LacI T334C mutants. In addition, the O^1 DNA operators create compressive stress to the cantilever surfaces. The sources of the compressive stress may come from the (i) binding free energy of the O^1 DNA to the T334C mutants that transforms to the surface free energy or (ii) the steric and electrostatic repulsions between each LacI protein complexes. Beside the experimental cantilevers, the reference cantilevers remain un-deflected because there are no LacI proteins immobilized on the surface to recognize the DNA and neither DNA binding to the Si and gold surfaces.

After the O^1 DNA operators are added, IPTG molecules are introduced. However, the

microcantilevers fail to detect changes caused by the IPTG binding to the immobilized T334C mutants. There is no difference in the deflection before and after the IPTG solution is introduced. It is thought that the surface stress of the microcantilevers does not change significantly as the IPTG molecules bind to the T334C mutants and release the DNA allosterically. Moreover, for complicated macromolecular complexes bound on the surfaces of microcantilevers, the sensitivity of the microcantilevers may decay when the binding position is several nanometers away from the surface and hardly generate enough surface stress to be detected. In the following experiments, an alternative sensor, the QCM-D, is used for the binding assays.

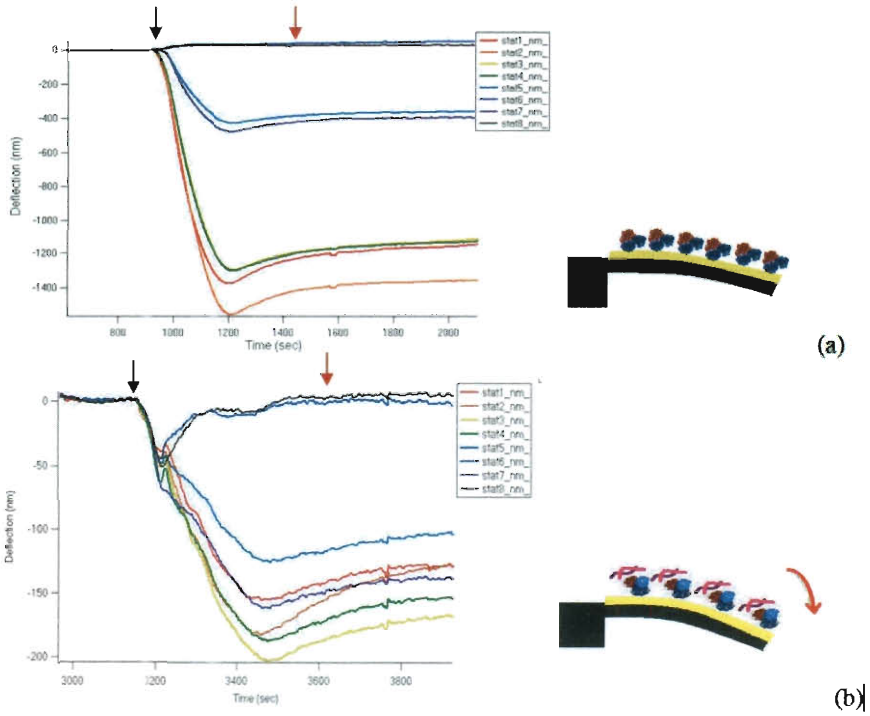

Figure 8.3. Microcantilevers deflect due to (a) immobilization of single mutant T334C to gold, followed by (b) protein – O^1 DNA binding recognition. The black arrows indicate the time of sample injection, and the red arrows indicate the time of switching the sample solutions to buffer.

8.3.3. Binding of wild-type LacI and single mutant T334C in QCM experiments

Wild-type LacI was used as a control in the QCM assay with the expectation from prior

experiments that DNA binding would be blocked by interaction of the LacI N-terminal DNA binding domain with the gold surface. [21] After introducing wild-type LacI, a large frequency change is detected (Fig. 8.4(a)) corresponding to the adsorption of LacI to the gold surface. Following a buffer wash, introduction of the operator O^1 results in minimal change in mass for the wild-type LacI, indicating little binding of the DNA sequence. Addition of IPTG at high concentrations also generates little change in frequency. These results are consistent with previous experiments that indicate wild-type LacI physically binds to gold through its DNA-binding domain, which is attracted by the highly polarized gold surface[21]. However, the mass of IPTG appears too small to be observed on the microbalance, since wild-type LacI should still be able to bind IPTG.

The single mutant T334C, modified with introduction of a solvent-exposed cysteine at the C-terminus for each monomer (Fig. 8.1), is expected to bind the gold surface with a specific orientation mediated by sulfhydryl interaction with gold. Upon introduction of T334C to the crystal surface, changes in the frequency are comparable to those observed for wild-type LacI. With the addition of operator O^1, further mass changes are observed, which are reversed when IPTG is flowed through the cell, with the signal returning to that for T334C alone (Fig. 8.4(b)). This shift is consistent with release of the operator DNA from the repressor by IPTG binding. The results demonstrate that immobilized T334C can bind operator DNA and IPTG. Thus, the results confirm that the mutated LacI, T334C, can perform its normal functions, including both operator and IPTG binding and allosteric release of operator in the presence of IPTG when bound to a surface. Fitting the frequency changes to a viscoelastic Kevin-Voigt model and applying the Sauerbrey relation, we obtain the adsorbed mass, which in turn can be converted to number of proteins by multiplying the protein's molecular weight and Avogadro's number. An average binding area can then be calculated by dividing the crystal surface area by the number of

proteins. We find that the T334C molecules are in a more highly packed arrangement: average binding area 19 ± 1.6 nm^2 per T334C protein mutant compared to 33 ± 0.83 nm^2 per wild-type protein (Table 8.1). These results highlight the importance of protein orientation on the surface for retention of function when pursuing surface immobilization.

Examination of the dissipation response reveals differences in the protein conformation of wild-type LacI and T334C on the crystal surface (Fig. 8.4; Table 8.1). Wild-type LacI binds tightly to gold and yields little change in the dissipation coefficient, $\Delta D = (0.068 \pm 0.021) \cdot 10^{-6}$, whereas T334C binding to the crystal surface results in a $\Delta D = (1.3 \pm 0.14) \cdot 10^{-6}$. This strong differential can be explained by the fact that wild-type LacI binds to the gold surface through its highly basic DNA-binding domain. In contrast, T334C binds to the gold surface primarily through the sulfur-gold covalent bond at position 334, leaving the highly flexible arms of the DNA-binding domains to freely rotate and stretch. The latter arrangement forms a "softer" protein layer; thus, the measured dissipation is about 20 times larger than for its wild-type analog. These results are consistent with NMR data that indicate that the DNA binding domains, when unliganded, have significant mobility. [29]

From the differences in frequency and dissipation changes, it is clear that the surface arrangement of T334C mutant differs from that for the wild-type LacI. To remove the time dependency of the data, we can relate the observed changes in D to changes in f, by plotting ΔD vs. Δf (Fig. 8.6). Large ΔD vs. Δf ratios indicate flexible conformations of an extended structure or loose binding between interacting groups. [18] In the ΔD vs. Δf plot, wild-type LacI binding exhibits a small slope change ($\Delta D / \Delta f = (0.0033 \pm 0.00040) \cdot 10^{-6}$/Hz), indicating wild-type LacI forms a rigid protein film (Fig. 8.6(a)). Interestingly, the T334C mutant generates a slope change near Δf = -40 Hz. Above -40 Hz, the slope is not significantly different from that for the wild-type LacI ($\Delta D/\Delta f = (-0.0084 \pm 0.00084) \cdot 10^{-6}$/Hz (Fig. 8.6(a)). In contrast, below -40 Hz

the slope increases significantly, $\Delta D/\Delta f$ = (-0.027± 0.0025)·10^{-6}/Hz (Fig. 8.6(b)). A potential rationale for this transition is that the binding mechanism is a competition between the highly basic DNA-binding domains and the C-terminal cysteine to interact with gold crystal. For T334C proteins on the gold surface, reorientation may occur spontaneously until the gold-sulfur bond forms. Above -40 Hz where protein adsorption is low, the T334C population on the surface may bind through a mix of electrostatic interaction at the N-terminus and gold-sulfur binding at the C-terminus. Below -40 Hz, as the proteins become more crowded on the surface, binding of the DNA domains may be impeded in favor of the covalent Au-S bond. The T334C binding mechanism is thus a competition between two binding sites: ionic interactions with the DNA-binding domain and the Au-S bond by the designed cysteine. The latter interaction ultimately dominates to generate the formation of a surface bound protein layer with the DNA-binding domain exposed to the bulk solution.

	Wild-type	T334C
Δf (Hz)	-44 ± 1.1	-78 ± 6.7
ΔD (10^{-6})	0.068 ± 0.021	1.3 ± 0.14
Binding area (nm^2 / protein)	33 ± 0.83	19 ± 1.6

Table 8.1. Summary of frequency change (Δf) and rigidity (ΔD) for wild-type LacI and T334C.

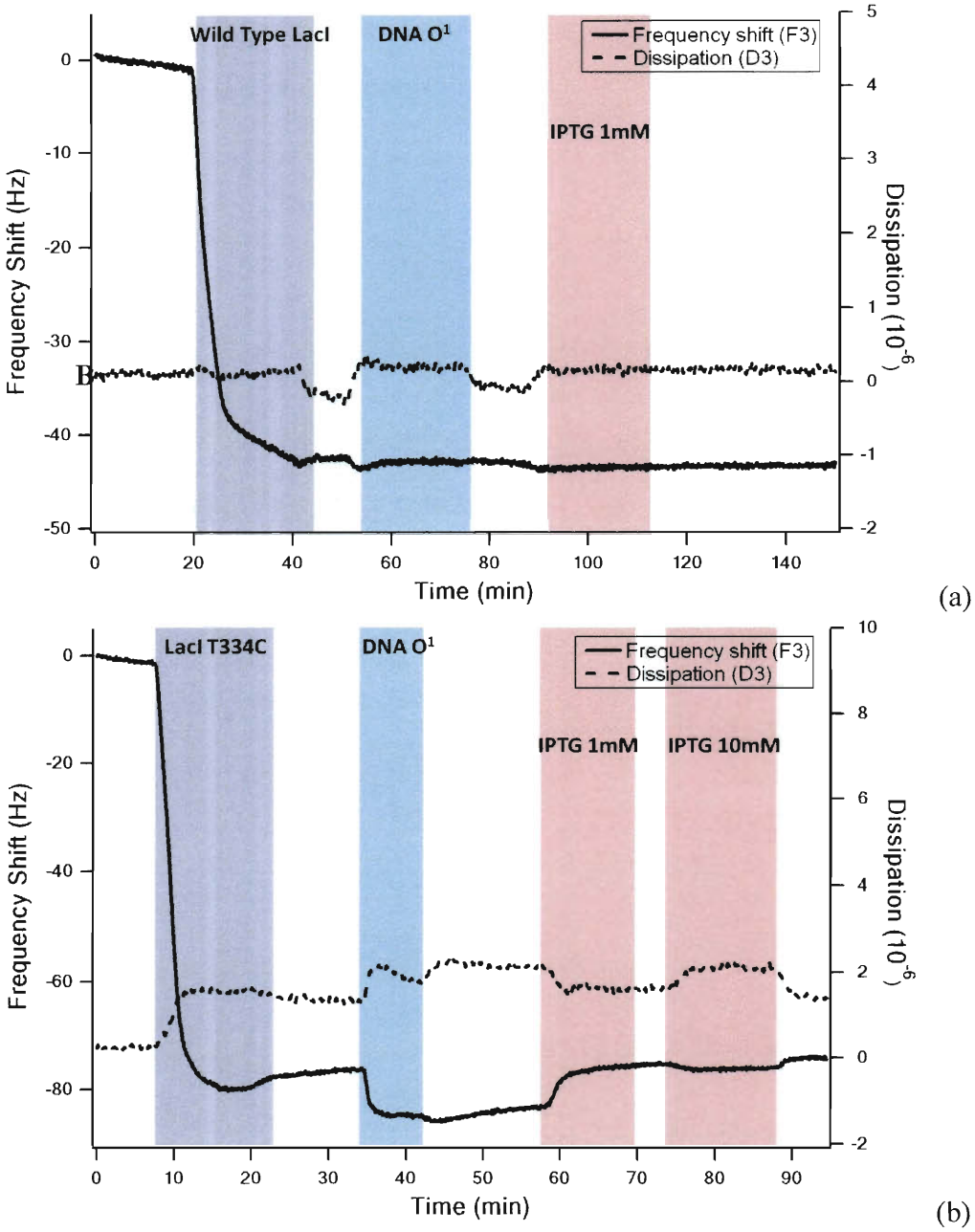

Figure 8.4. The frequency and dissipation results from the third overtone for the natural operator O^1 and inducer IPTG binding to (a) wild-type LacI and (b) T334C. The concentrations used in the assay are protein, 400 nM; DNA, 950 nM; and IPTG, 1 mM. The purple, blue and pink blocks represent time periods when protein, DNA and IPTG flow over the gold-coated quartz crystals, respectively.

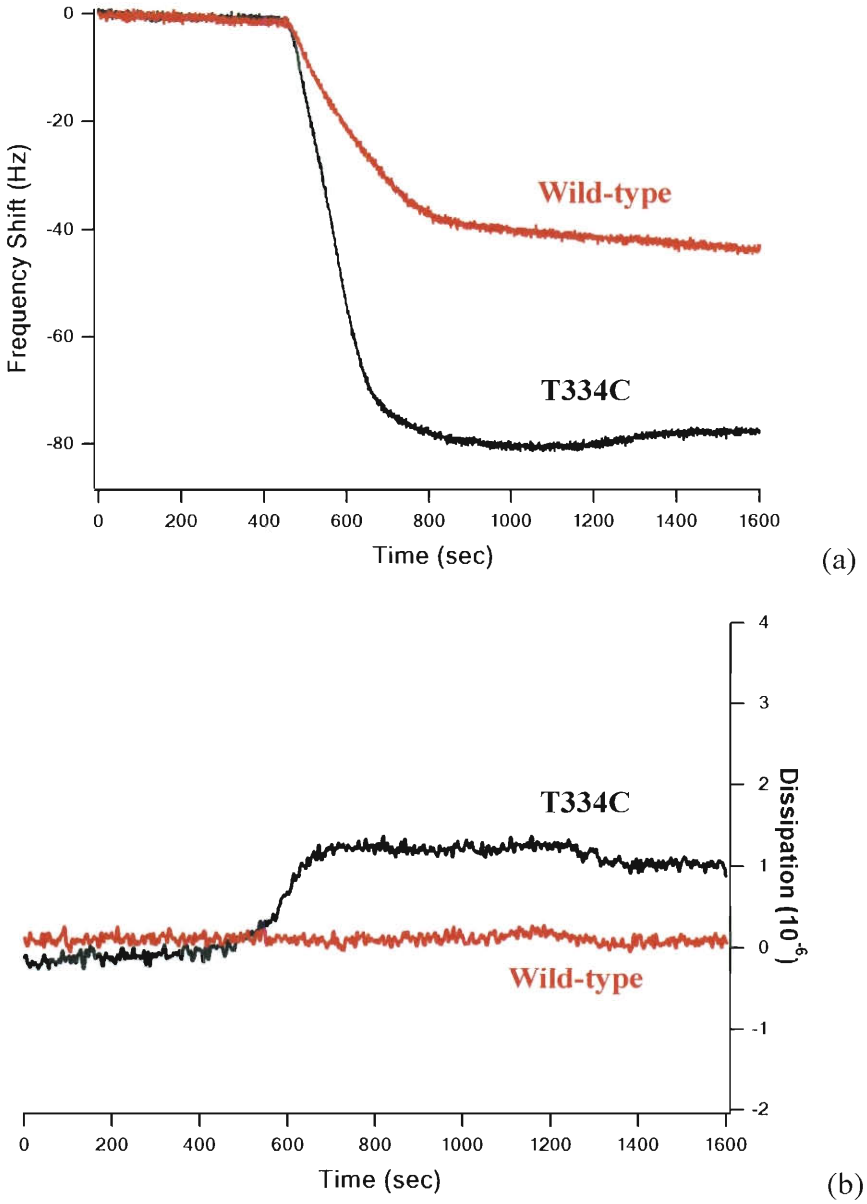

Figure 8.5. (a) Frequency change and (b) Dissipation change for wild-type LacI (red) and T334C (black). The difference between wild-type LacI and T334C reveals that they bind to the gold surface using different regions of the structure: DNA-binding domain for wild-type and position 334 through the sulfur-gold covalent bond for T334C.

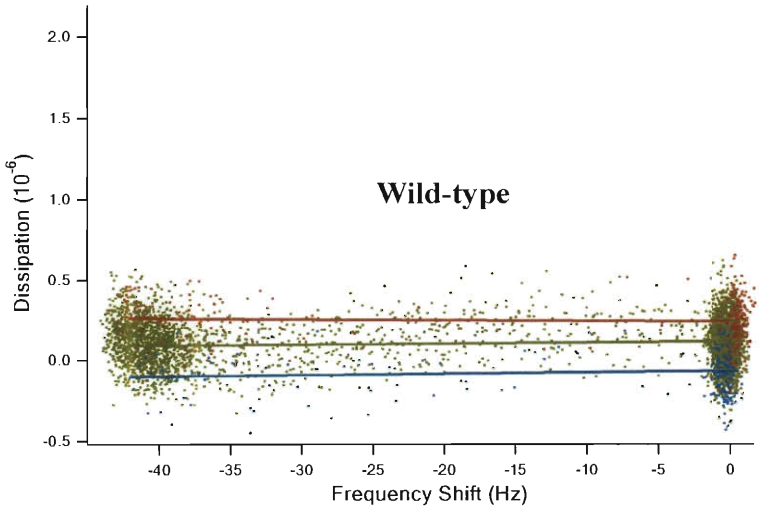

(a)

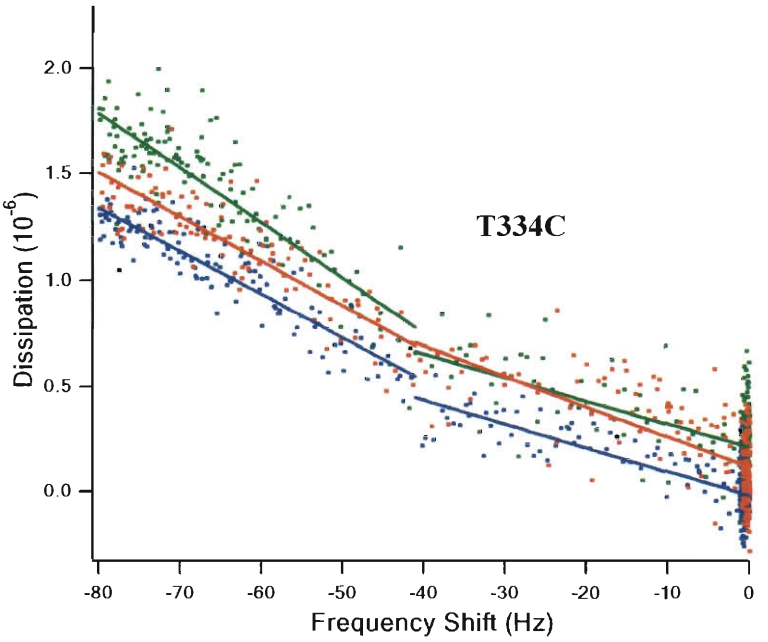

(b)

Figure 8.6. ΔD-Δf plot for wild-type LacI (a) and T334C (b). The slopes for wild-type LacI and T334C are different, indicating distinct binding mechanisms for these two proteins.

8.3.4. Protein-DNA binding recognition and response to effectors

Because T334C binds to the gold surface through a direct sulfur-gold linkage and retains wild-type binding affinities to both operator and IPTG, this system could be applied to monitor

binding to various DNA sequences as well as response to multiple effectors. In QCM-D, results can be visualized directly, which provides opportunity to compare results under different conditions simultaneously. We have compared the natural operator (O^1), a symmetric operator DNA sequence (O^{sym}), and a nonspecific DNA sequence (O^{ns}) in this system. The O^{sym} sequence is known to bind LacI ~10-fold more tightly than O^1, [30]whereas O^{ns} exhibits substantially weaker affinity. The experimental results are consistent with the known binding behaviors: the repressor binds to O^{sym} more strongly than O^1 (Fig. 8.6), although the established 10-fold difference in DNA binding affinity cannot be easily distinguished. For the nonspecific DNA sequence, the results show no detectable binding between T334C and O^{ns} (Fig. 8.6).

Compared to diminished DNA binding affinity in response to IPTG binding, the affinity for DNA is slightly increased following binding to the "anti-inducer" ONPF, which stabilizes LacI binding to operator. [4] The responses to the inducer IPTG and the anti-inducer ONPF observed in the QCM-D experiments are consistent with the expected behavior. Minimal mass change was found following ONPF binding to the mutant T334C for both repressor-O^1 and repressor-O^{sym} mixture, suggesting there is no detectable dissociation of DNA sequences from the ONPF-bound repressor (Fig. 8.6). Upon IPTG addition, a change in mass is observed consistent with release of both O^1 and O^{sym} from the repressor (Fig. 8.7). Thus, the QCM-D data reflect the anticipated behavior of LacI in binding to DNA and sugar ligands. Based on these results, other residue(s) of interest can be introduced in addition to T334C, and valuable binding information can be obtained efficiently by QCM-D prior to detailed biochemical and biophysical examination.

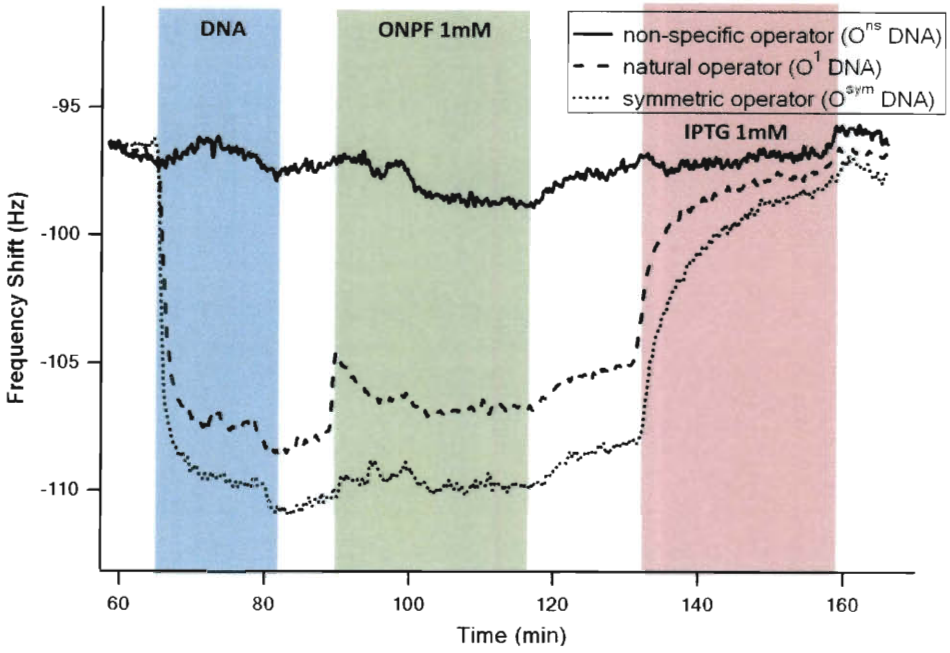

Figure 8.7. QCM-D Experimental results for T334C binding to O^1, O^{sym} and O^{ns} as well as response to anti-inducer ONPF and inducer IPTG binding. T334C was bound to the gold surface before introducing the three different DNA sequences. The concentrations used in the assay are T334C, 400 nM; DNA, 950 nM; ONPF, 1 mM; IPTG, 1 mM. The blue, green and pink blocks represent time periods when DNA, ONPF and IPTG flow over the gold-coated quartz crystals, respectively.

8.4. Conclusion

QCM-D has successfully detected T334C repressor binding to multiple DNA sequences and ligands. The changes in frequency and dissipation are consistent with expected responses to both inducer and anti-inducer binding to LacI. Whereas wild-type LacI is unable to bind DNA once immobilized to a gold surface, using LacI with a designed cysteine mutation for covalent interaction with gold restores protein-DNA binding capacity. Based on these results, we propose that substitutions at other locations of interest on the surface of this protein could be quickly screened for mutants that might have effects on operator binding, IPTG binding, and/or the

allosteric response to inducer. Indeed, several conditions can be examined simultaneously with protein binding to the gold surface of the crystals in the orientation that allows DNA binding. Furthermore, these results indicate that QCM-D can be applied to many other ligand-binding proteins to obtain rapid binding information. For proteins where structural information is not available and ligand binding is not observed after attachment to the gold surface, random introduction of cysteine residues at intervals across the sequence suggestive of surface exposure and subsequent measurement of binding would be a feasible approach.

Complimentary experiments are also performed on microcantilever sensors. Both the T334C repressor binding to gold surface and DNA binding to T334C repressors, which are covalently linked on the gold surface, generates a surface stress change that can be measured on microcantilevers. However, the allosteric binding of IPTG to T334C repressor is not observable; neither is the release of DNA from the T334C repressors. It is thought that the microcantilever sensors fail to detect the reaction if the resultant change in surface stress is not obvious.

8.5. References

(1) Jacob, F.; Monod, J. *Journal of Molecular Biology* 1961, *3*, 318.

(2) Gilbert, W.; Mullerhi.B *Proceedings of the National Academy of Sciences of the United States of America* 1966, *56*, 1891-&.

(3) Jobe, A.; Bourgeoi.S *Journal of Molecular Biology* 1972, *69*, 397-&.

(4) Barkley, M. D.; Riggs, A. D.; Jobe, A.; Bourgeois, S. *Biochemistry* 1975, *14*, 1700-1712.

(5) Matthews, K. S.; Nichols, J. C. *Progress in Nucleic Acid Research and Molecular Biology, Vol 58* 1998, *58*, 127-164.

(6) Lewis, M.; Chang, G.; Horton, N. C.; Kercher, M. A.; Pace, H. C.; Schumacher, M. A.; Brennan, R. G.; Lu, P. Z. *Science* 1996, *271*, 1247-1254.

(7) Bell, C. E.; Lewis, M. *Nature Structural Biology* 2000, *7*, 209-214.

(8) Friedman, A. M.; Fischmann, T. O.; Steitz, T. A. *Science* 1995, *268*, 1721-1727.

(9) Flynn, T. C.; Swint-Kruse, L.; Kong, Y. F.; Booth, C.; Matthews, K. S.; Ma, J. P. *Protein Science* 2003, *12*, 2523-2541.

(10) Brockman, J. M.; Frutos, A. G.; Corn, R. M. *Journal of the American Chemical Society* 1999, *121*, 8044-8051.

(11) Rigler, P.; Ulrich, W. P.; Hoffmann, P.; Mayer, M.; Vogel, H. *Chemphyschem* 2003, *4*, 268-275.

(12) Hao, D. Y.; Ohme-Takagi, M.; Yamasaki, K. *Febs Letters* 2003, *536*, 151-156.

(13) Höök, F.; Kasemo, B.; Nylander, T.; Fant, C.; Sott, K.; Elwing, H. *Analytical Chemistry* 2001, *73*, 5796-5804.

(14) O'Sullivan, C. K.; Guilbault, G. G. *Biosensors & Bioelectronics* 1999, *14*, 663-670.

(15) Peh, W. Y. X.; Reimhult, E.; Teh, H. F.; Thomsen, J. S.; Su, X. D. *Biophysical Journal* 2007, *92*, 4415-4423.

(16) Rodahl, M.; Hook, F.; Fredriksson, C.; Keller, C. A.; Krozer, A.; Brzezinski, P.; Voinova, M.; Kasemo, B. *Faraday Discussions* 1997, 229-246.

(17) Höök, F.; Rodahl, M.; Brzezinski, P.; Kasemo, B. *Langmuir* 1998, *14*, 729-734.

(18) Höök, F.; Rodahl, M.; Kasemo, B.; Brzezinski, P. *Proc. Natl. Acad. Sci. U. S. A.* 1998, *95*, 12271-12276.

(19) Jordan, J. L.; Fernandez, E. J. *Biotechnology and Bioengineering* 2008, *101*, 837-842.

(20) Carmon, K. S.; Baltus, R. E.; Luck, L. A. *Biochemistry* 2004, *43*, 14249-14256.

(21) Calabretta, M. K.; Matthews, K. S.; Colvin, V. L. *Bioconjugate Chemistry* 2006, *17*, 1156-1161.

(22) Swint-Kruse, L.; Elam, C. R.; Lin, J. W.; Wycuff, D. R.; Matthews, K. S. *Protein Science* 2001, *10*, 262-276.

(23) Wycuff, D. R.; Matthews, K. S. *Analytical Biochemistry* 2000, *277*, 67-73.

(24) Yue, M.; Lin, H.; Dedrick, D. E.; Satyanarayana, S.; Majumdar, A.; Bedekar, A. S.; Jenkins, J. W.; Sundaram, S. *J. Microelectromech. Syst.* 2004, *13*, 290-299.

(25) Rodahl, M.; Hook, F.; Krozer, A.; Brzezinski, P.; Kasemo, B. *Review of Scientific Instruments* 1995, *66*, 3924-3930.

(26) Rodahl, M.; Hook, F.; Kasemo, B. *Analytical Chemistry* 1996, *68*, 2219-2227.

(27) Sauerbrey, G. *Zeitschrift Fur Physik* 1959, *155*, 206-222.

(28) Falcon, C. M.; Matthews, K. S. *Journal of Biological Chemistry* 1999, *274*, 30849-30857.

(29) Wadejardetzky, N.; Bray, R. P.; Conover, W. W.; Jardetzky, O.; Geisler, N.; Weber, K. *Journal of Molecular Biology* 1979, *128*, 259-264.

(30) Sadler, J. R.; Sasmor, H.; Betz, J. L. *Proceedings of the National Academy of Sciences of the United States of America-Biological Sciences* 1983, *80*, 6785-6789.

Chapter 9

Conclusions and Future Work

9.1. Summary

The immobilization of SLBs onto a SiO_2 surface involves an adsorption free energy change, which takes place on the solid substrate. Microcantilever sensors transduce the surface free energy into a measurable mechanical motion. Analyzing free energy changes on solid supports, which are tuned by varying the lipid compositions (Chapter 4) and lipid phases (Chapter 5), has proved a useful method to probe the collective interactions between lipid membranes and a substrate. Higher affinity, as a result of electrostatic attractions, between the SLBs and solid surfaces indicates higher surface free energy change and thus cause the microcantilevers to bend further to accommodate the increase in free energy. Besides SLB – substrate interactions, membrane-active molecules interact with lipid membranes with extensive possibilities and perplexities. Amphiphilic or amphipathic surfactants (Chapter 6) and peptides (Chapter 7) interact with lipid membranes through different mechanisms and also take part in altering the free energy on the solid surfaces which are used to support the SLB. Experimental observations conclude that the insertion of surfactants and peptides into SLBs not only raises the adsorption free energy but also the internal membrane stress in the SLBs. Both of these effects generate a large enough surface free energies change to be detected by the microcantilever transducer as a compressive surface stresses. Surfactants and peptides at high concentrations are toxic to SLBs and can strip the SLBs from surfaces, thus the *in situ* free energy, which corresponds to the solid – SLB interactions, diminishes to zero. Correlating the free energy changes on the solid surfaces with surfactants and peptides' functions on lipid membranes will

add knowledge to understanding the interactions of small molecules with SLBs and expands the array of molecules that can be studied with microcantilever sensors.

Natural proteins have hierarchical structures which oftentimes interact with solid surfaces in an unknown manner. A model protein studied in this thesis, the *Lac* repressor (LacI), compares how a modified T334C mutant that includes a cysteine group to orient the protein relative to the gold surface through a covalent sulfur bonds retains it binding capabilities over that of wild type LacI. QCM-D is used to measure the "weight" of the proteins on Au surfaces and probe the viscoelastic properties of the protein layer. What was discovered new about this T334C LacI mutant is that (i) the surface binding density of the protein is higher compared to the wild-type; (ii) the T334C protein layer is softer and thicker than the tightly bound wild-type layer; (iii) the DNA binding kinetics of T334C mutant is observed in real-time and is comparable to that observed in solution, while that of a wild-type is completely inactive; and (iii) the binding process of T334C to Au is likely to undergo two steps: from non-specific to directed binding to Au.

Concluding the experimental observations of surface bound lipid bilayers and LacI proteins, this thesis provides a quantitative method and a starting point to understand biomolecules at the liquid – solid interface. However, there are questions that remain unanswered. Particularly, each type of sensor used in this thesis has limits and is sensible to a specific physical property or a set of collective interrelated interactions. For example, on the microcantilever surfaces, the observed surface stress change is a coupling of both the material strain and the chemical reactions. Theoretical calculations of the mechanical strain and the chemical free energy should be able to decouple the effects to probe only the chemical reaction contribution. Despite the fact that the mechanical strain effect is neglected in this thesis, the measurements are

reasonably accurate. Nevertheless, some proposed ideas that can continue the work of this thesis are written in the following section 9.2.

9.2. Future Work

9.2.1. Using Microcantilevers to Detect Surface Process of Proteins on Lipid Membranes

Surface sensitive sensors provide a unique method for biomolecular analysis and are particular appropriate for analyzing and improving immobilized biosystems. Using lipid membrane-coated microcantilevers for probing interactions with membrane-active molecules also has potential in extensive biophysical and biochemical research. In one way, an explicit model to describe the relation between the lateral membrane tension and the measured surface stress of the microcantilever is required in order to quantify the free energy of small molecules interacting with the SLBs. This thesis initiated the experimental and empirical explanations for the magnitude and the direction of the surface stress induced by the small molecular interactions, which are relatively simple; however, for complicated molecules that interact with lipid membranes dynamically, such as proteins and enzymatic substances, the measurement and interpretation could be rather challenging. Several interesting proteins that can (i) induce local curvature of lipid membranes, such as N-BAR domains (see Fig. 9.1(a)), (ii) hydrolyze lipids of the upper leaflet of the SLB, such as Phospholipase A2 (PLA_2) and leave a SLB composed of one layer of lyso-lipids and one layer of intact lipids (see Fig. 9.1(b)), and (iii) fold at/in the SLB, such as β-barrel outer membrane protein A (OmpA) (see Fig. 9.1(c)). Lipid membrane-coated microcantilevers may add additional information of those interactions.

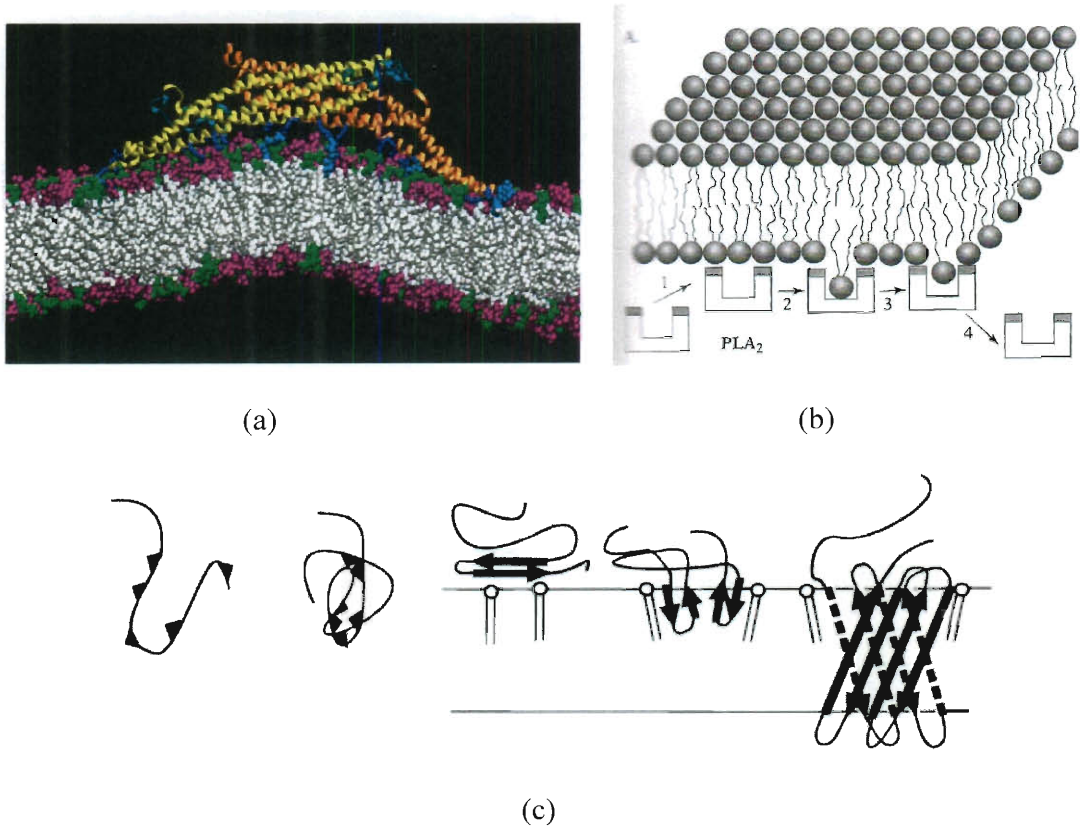

(a) (b)

(c)

Figure 9.1. (a) N-BAR domains [1] (b) Phospholipase A2, or PLA_2 [2] (c) β-barrel outer membrane protein A (OmpA) [3]

9.2.2. Numerically Solving the Asymmetrical Force Field of SLBs

Physical properties of SLBs differ from free-standing membranes in surface tension and lipid mobility due to the SLBs' asymmetrical force distribution. Coarse grained simulations of SLBs near a wall have been performed by several groups and have shown that a huge fluctuation of membrane tension is present. [4] However, the coupling effect of the interfacial tension of the solid-liquid-membrane interfaces with the solid has not been explored. Understanding the stress coupling between the membrane film and the solid lattice is important because such a theoretical explanation can be used to predict the surface stress of the solids and the deflection values of the

microcantilevers which are coated with SLBs. A preliminary simulation of the stress profile near a solid wall which supports a SLB is provided in this section.

The following figures illustrate the simulation results of the density profile of the lipid bilayer near a wall. When the wall is still far (~ 1/2 bilayer thickness), the bilayer density profile is as symmetrical as that of a free standing lipid bilayer, as shown in Fig. 9.2. As the lipid bilayer gets closer to the wall (bilayer-wall distance ~ 1/5 bilayer thickness), the density profile of the lipid bilayer is altered and shows asymmetrical distribution, as shown in Fig. 3. The large perturbation in the stress profile near the wall is consistent with the asymmetrical lateral pressure profile of a SLB found by Xing et al. [4]

In Fig. 9.3, the stress profile is defined as:

$$\gamma = \Omega^{ex} = \frac{\{\Delta\Omega[\rho(\mathbf{r})] - \Delta\Omega^{s}\}}{A} \quad . \tag{9.1}$$

Where $\Delta\Omega$-$\Delta\Omega^s$ is the force difference between the pure solvent and the homogeneous reservoir. The stress profile can be calculated by integrating the lateral pressure tensor of the system s(x) in each layer along the x direction:

$$\gamma = \int_{-\infty}^{\infty} dx\, s(x) = \int_{-\infty}^{\infty} dx[P_N(x) - P_T(x)] \tag{9.2}$$

Where $P_N(x)$ is the normal component of the pressure tensor, and $P_T(x)$ is the tangential component of the pressure tensor. The very negative stress value at the inner head layer represents either a strong compression or contraction while the outer head layer has similar values as bulk. This asymmetrical membrane lateral pressure of a SLB indicates an internal stress in the membrane coating on microcantilever surfaces and may contribute to some extent of bending of the microcantilever. A connection of this stress profile above the solid surface with

the surface free energy on the solid surfaces is needed to be confirmed in the future work.

This preliminary work is cooperation with Zhengzheng Feng, Chapman group, Department of Chemical and Biomolecular Engineering, Rice University.

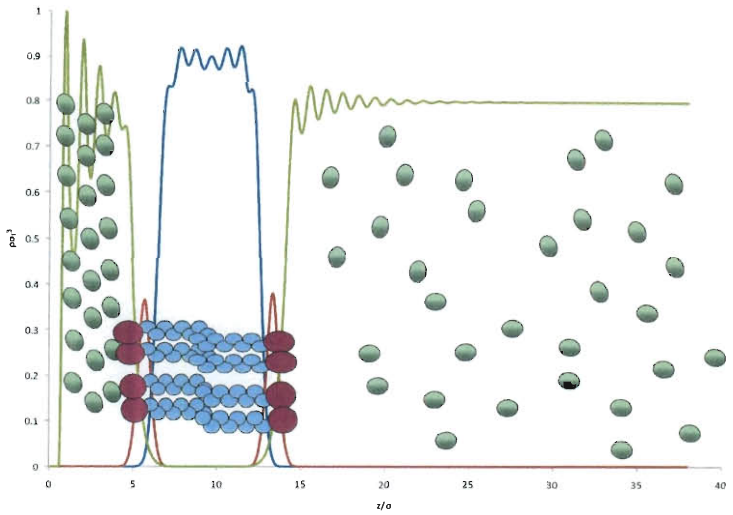

Figure 9.2. When a thick layer of water is present in between the lipid bilayer and the wall, the density profile of the lipid bilayer is affected. The x-axis indicates the distance of the lipid bilayer surface from the wall, and the y-axis the density profile. The blue line represents the density profile of lipid tail; red, lipid head; green, solvent. In this plot, the lipid bilayer is not close to the wall enough (the distance ~ ½ bilayer thickness), thus the density profile of lipid heads and tails are symmetrical along the bilayer center. (ref: Zhengzheng Feng)

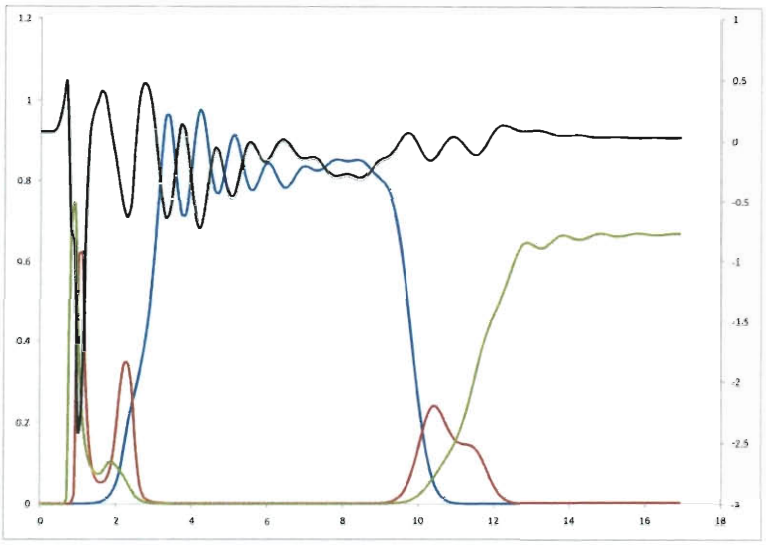

Figure 9.3. As the bilayer is close enough to the wall (bilayer-wall distance ~ 1/5 bilayer thickness), the density profiles of both lipid head and lipid tail are greatly altered by the boundary condition. The black line represents stress profile. (ref: Zhengzheng Feng)

Parameters and models used in this simulation:

Component order to be: 1-Lipid Tail, 2-Lipid Head, 3-Solvent

Fluid-fluid potential: Lenard-Jones 12-6 model

Wall-fluid potential: Lenard-Jones 9-3 model

Size matrix (sigma): lipid tail: 1.0, lipid head: 1.44, solvent: 1.0

Fluid interaction matrix: $(\varepsilon_j/kT) = \begin{bmatrix} 1.0 & 0.22 & 0.22 \\ 0.22 & 1.42857142 & 1.42857142 \\ 0.22 & 1.42857142 & 1.42857142 \end{bmatrix}$

Fluid-surface interaction matrix: $(\varepsilon_i/kT) = [0.72 \quad 1.36 \quad 1.36]$ (similar as fluid interaction, weak attraction for tail, strong for head/solvent)

Cutoff in both potential (sigma): 2.5

Domain size (sigma): 40

9.2.3. Assembly of Giant Unilamellar Vesicles into Chains Using Magnetic Fields

Studying the interactions between lipid membranes and membrane deformations can add insights in vesicular adsorption, aggregation, and fusion. [5] To force two lipid membranes to contact, applying a uniform force field to a suspension of giant unilamellar vesicles (GUVs) is a convenient way to control the attraction between lipid membranes with a tunable and precise manner. This approach can be done by immersing GUVs into a ferro-fluid (a dispersion of ferromagnetic nanoparticles) causing the GUVs to assemble side-by-side into chains by applying a magnetic field, as demonstrated in Fig. 9.4.

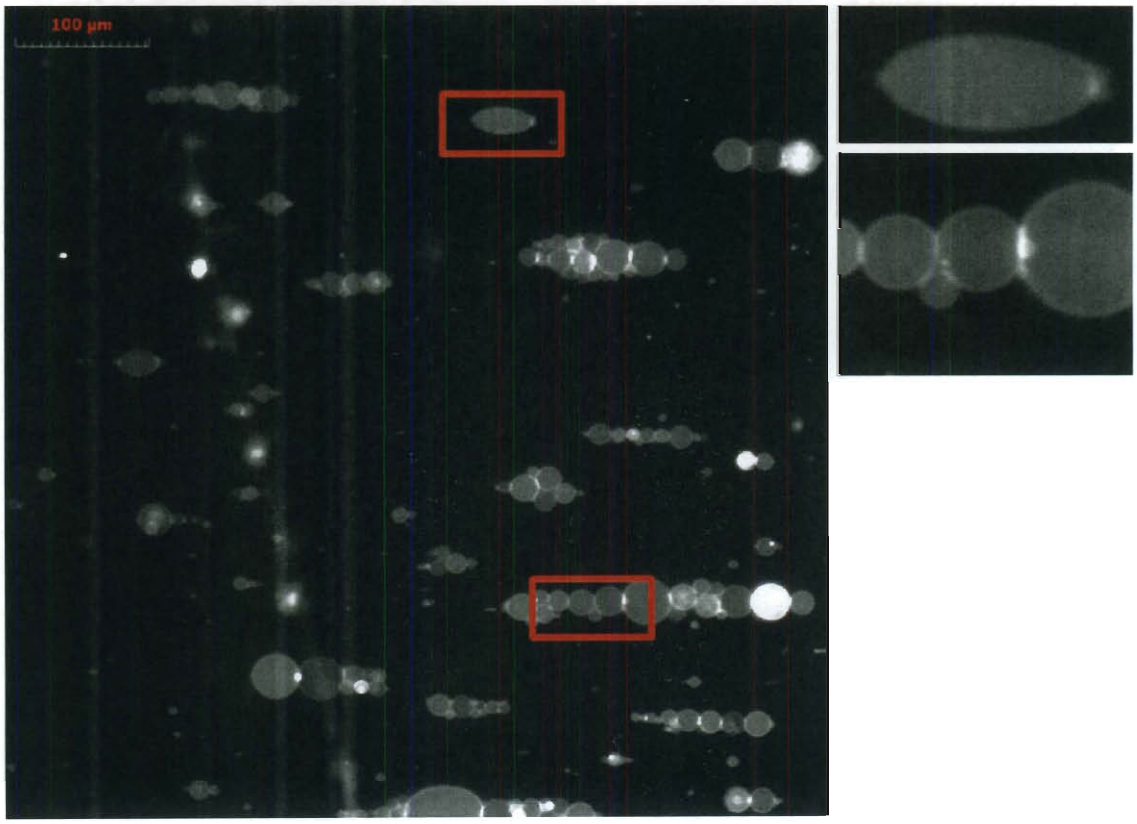

Figure 9.4. GUV chains. When a magnetic field is applied, the ferrofluid in the surrounding bulk solution direct the GUVs to chain structures. GUVs of various sizes may stack together to form spindle shape vesicle aggregates. The stacking condition can be eliminated by homogenizing GUVs' sizes (the protocol is described in Appendix A.5). Elongation of a big GUV along the direction of the magnetic field is observed in the upper right figure.

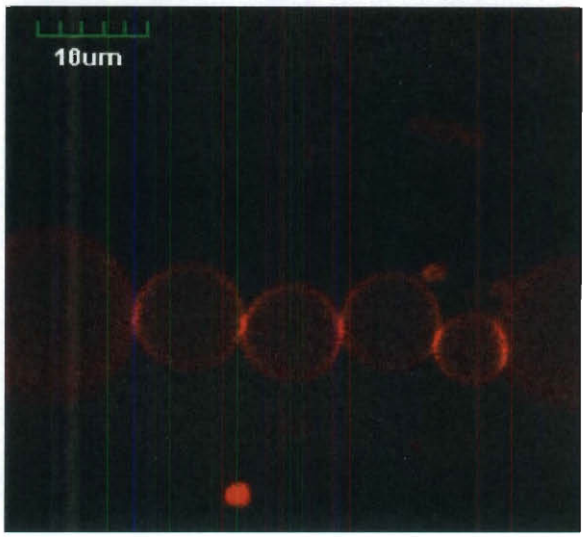

Figure 9.5. Confocal image of a GUV chain. The contact lines of the membranes are brighter because they contain two bilayers and are with higher fluorophore density.

Similar to spherical non-magnetic particles dispersed in ferrofluid, these GUVs are non-magnetic cavities inside a magnetized medium. When a magnetic field is applied, the dipole-dipole interactions will lead to the formation of linear chains of GUVs oriented along the direction of the external field. Future work in this area may provide a fundamental model for membrane-membrane interactions and elongations. [6] Also, linking GUVs into chains provides a simplified model for Krebs et al.'s work of using magnetic force to link human cells into chains for possible applications in tissue engineering. [7]

9.3. Conclusion

This thesis has developed a number of methods that make use of surface-sensitive sensors to characterize (i) the effect of solid surfaces on the function of immobilized bio-macromolecules and (ii) the interaction and recognition between immobilized bio-macromolecules and their target ligands. By examining the mass and the adsorption free energy of these bio-macromolecules, information about the structure, orientation, and binding affinity to either the surface or reactive agents can be explored. Specifically, two classes of immobilized bio-macromolecules, the supported lipid bilayer (SLB) and the *Lac* repressor protein (LacI), are characterized using microcantilever sensors and QCM-D.

9.4.References

(1) Blood, P. D.; Swenson, R. D.; Voth, G. A. *Biophys. J.* **2008**, *95*, 1866-1876.

(2) Luckey, M. *Membrane Structural Biology - With Biochemical and Biophysical Foundations*; Cambridge University Press, 2008.

(3) Kleinschmidt, J. H.; Tamm, L. K. *Biochemistry* **1996**, *35*, 12993-13000.

(4) Xing, C. Y.; Faller, R. *J. Phys. Chem. B* **2008**, *112*, 7086-7094.

(5) Lis, L. J.; McAlister, M.; Fuller, N.; Rand, R. P.; Parsegian, V. A. *Biophysical Journal* **1982**, *37*, 657-665.

(6) Bacri, J. -C.; Cabuil, V.; Cebers, A.; Menager, C.; Perzynski, R. *Europhys. Lett.*, **1996,** 33 235

(7) Krebs, M. D.; Erb, R. M.; Yellen, B. B.; Samanta, B.; Bajaj, A.; Rotello, V. M.; Alsberg, E. *Nano Lett.* **2009,** 13, 1812–1817.

Appendix A

Structure, Preparation and Characterization of Materials

A.1 Molecular Structures

A.3.1 Lipids

Name	Molecular Structure
16:0-18:1 PC (POPC) 1-palmitoyl-2-oleoyl-sn-glycero-3-phosphocholine	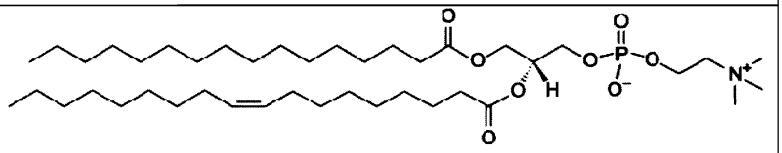
14:0-16:0 PC (MPPC) 1-myristoyl-2-palmitoyl-sn-glycero-3-phosphocholine	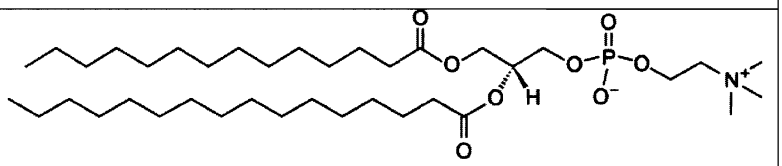
18:1 TAP (DOTAP) 1,2-dioleoyl-3-trimethylammonium-propane (chloride salt)	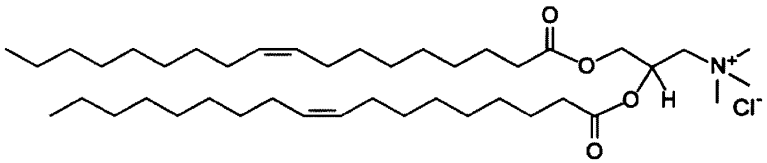
16:0-18:1 PS (POPS) 1-hexadecanoyl-2-(9Z-octadecenoyl)-sn-glycero-3-phospho-L-serine (sodium salt)	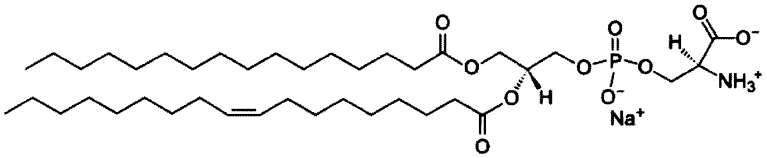

Reference: Avanti Polar Lipids, http://www.avantilipids.com/

A.3.2 Cholesterol

Name	Molecular Structure
Cholesterol (from ovine wool, >98%)	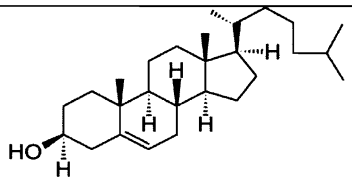

Reference: Avanti Polar Lipids, http://www.avantilipids.com/

A.3.3 Lyso-lipids

Name	Molecular Structure
12:0 Lyso PC ; CMC=400-900 μM 1-lauroyl-2-hydroxy-*sn*-glycero-3-phosphocholine	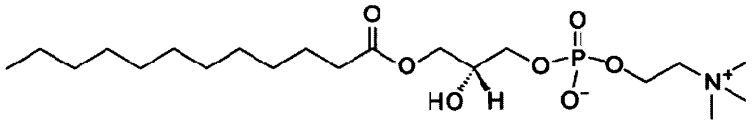
14:0 Lyso PC ; CMC=40-90 μM 1-myristoyl-2-hydroxy-sn-glycero-3-phosphocholine	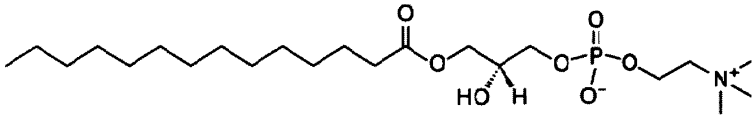
16:0 Lyso PC ; CMC=4-8 μM 1-palmitoyl-2-hydroxy-sn-glycero-3-phosphocholine	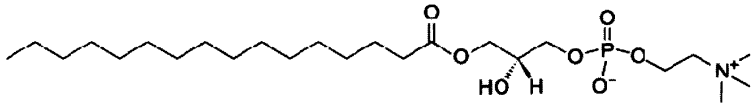
18:0 Lyso PC ; CMC = 0.4 μM 1-stearoyl-2-hydroxy-sn-glycero-3-phosphocholine	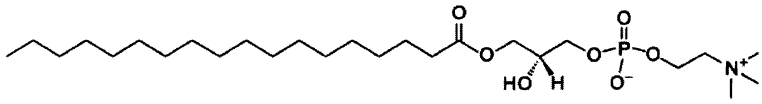
18:1 Lyso PC ; CMC=3-5 μM 1-oleoyl-2-hydroxy-sn-glycero-3-phosphocholine (MOPC)	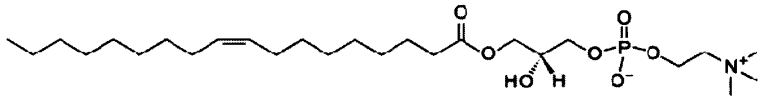

Reference: Avanti Polar Lipids, http://www.avantilipids.com/

A.3.4 Polyethylene glycol (PEG)

Name	Molecular Structure
Dithiolaromatic-PEG ; MW=504.74 g/mol $C_{25}H_{44}O_6S_2$	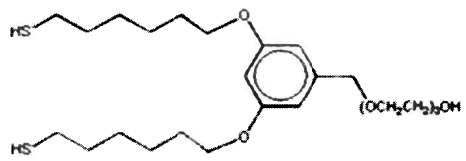 PEG-thiol
2- [methoxy-(polyethyleneoxy)propyl]-trimethoxysilane ; MW= 326.46 g/mol $C_{13}H_{30}O_7Si$ T_g = -54°C (amorphous at room temp)	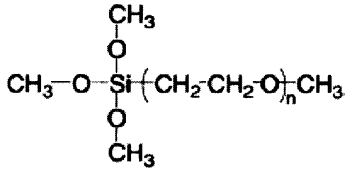 *2-[methoxy (polyethyleneoxy) propyl] trimethoxy silane (Gelest)* *PEO(375)-Silane, n=6-9*

Reference: Sensopath Technologies ; Gelest Inc.

A.2 Lipid Vesicle Size Determined by Dynamic Light Scattering (DLS)

A.2.1 Freeze-thaw and extrusion derived lipid vesicles

The freeze-thaw method is a protocol to break lipid vesicles into smaller pieces and to make the vesicles unilamellar. The freeze-thaw protocol starts from a solution of multilamellar vesicles (MLVs). Freeze the solution by dipping the vial into a liquid nitrogen bath (Caution! Careful handling and protective gloves are required at the extreme temperature at -273 K. Use PVC vial if possible; glass vials might fracture.) for 3 minutes and then take the vial out and thaw it in a water bath of 60 ^{o}C for 3 minutes until all the ice in the vial melts down to liquid solution. Repeat the freeze-thaw process for 20 times to achieve unilamellar vesicles. The vesicle size is determined by dynamic light scattering (DLS). The resulted size differs and depends on the lipid constitutes and buffer kind. The trial samples are made as follows: Sample set 1: freeze-thawed 20~25 times; sample set 2: then freeze-thawed 3 more times and then extruded 30 times through 100 nm pore-size polycarbonate membranes; sample set 3: then extruded 30 times through 30 nm pore-size polycarbonate membranes. The results are concluded in Fig. A.1.

The trends observed in Fig. A.1 show that for vesicles made right after the freeze-thaw process (sample set 1), the size is still far from nanometer sizes, but for vesicles containing charged lipids, the size could be smaller than 300 nm. Adding charged lipids can lower the average size of sample set 1, however this effect is not seen in sample set 2 and 3. Ion types in the buffer may also make difference in vesicle sizes. TBS (Tris Buffered Saline), which contains cationic tris ions, may stabilize and decrease the size of negatively charged vesicles (DOPA doped) than PBS may do, as shown in Fig. A.1 (c).

Extrusion is the step that really reduces the vesicle size into the nanometer size scale. All the vesicles prepared by extruding through a polycarbonate membrane of 100 nm pore size show significant decrease in size. For example, the average size of POPC vesicle is 140 nm. The extrusion method is useful for all the lipid composition and buffer tested. However, extruding these vesicles through a smaller pore-size polycarbonate membrane of 30 nm pore size doesn't help shrink down the size to smaller. The average size is no significant difference before and after the second extrusion with smaller pores. The possible reason is that the lipid membrane is soft and deformable, thus the vesicles can still pass a pore that is smaller than the vesicle itself, by deforming as an elliptic shape. This phenomenon is also documented in the literature.[1, 2] In addition, when using extrusion method, 100 nm pore-size polycarbonate membranes are more applicable than larger pore-size ones in producing unilamellar vesicles, because the MLV extruded through the 200 nm and 400 nm filters retain multilamellar.

The experiments are done on a Zeiss LSM410 confocal microscopy. A spot is photobleached by a mercury lamp light source, and the fluorescence of the spot and surrounding area is monitored with a laser source which corresponds to the emission wavelength of the fluorescent tag (Texas-red is used here). The spot was bleached for <3 minutes after which the area was watched for 20 minutes with 200 pictures being taken, one every 6 seconds. For this trial, the gain was set at 640. In Fig A.3, the experimental fluorescence is shown. The experiment is performed in a PDMS microfluidic channel, which adheres to an annealed glass slide. LUVs are made from 1 mg/mL POPC lipid doped with 0.5 mol% Texas-red DHPE dye. The fluorescence fraction, calculated from the equation:

$$f(t) = \frac{F(t) - F(0)}{F(\infty) - F(0)}, \tag{A.1}$$

is found to be 0.714. The half life time was 233.42 seconds. The long half time is due to the large size of the bleached area, which is 300 μm here. The diffusion coefficient was calculated using the equation:

$$D_f = \frac{0.22\, r^2}{\tau_{1/2}}, \tag{A.2}$$

where r is the radius of the bleached spot and $\tau_{1/2}$ is the half life time. The diffusion coefficient was found to be 1.825 $\mu m^2/s$.

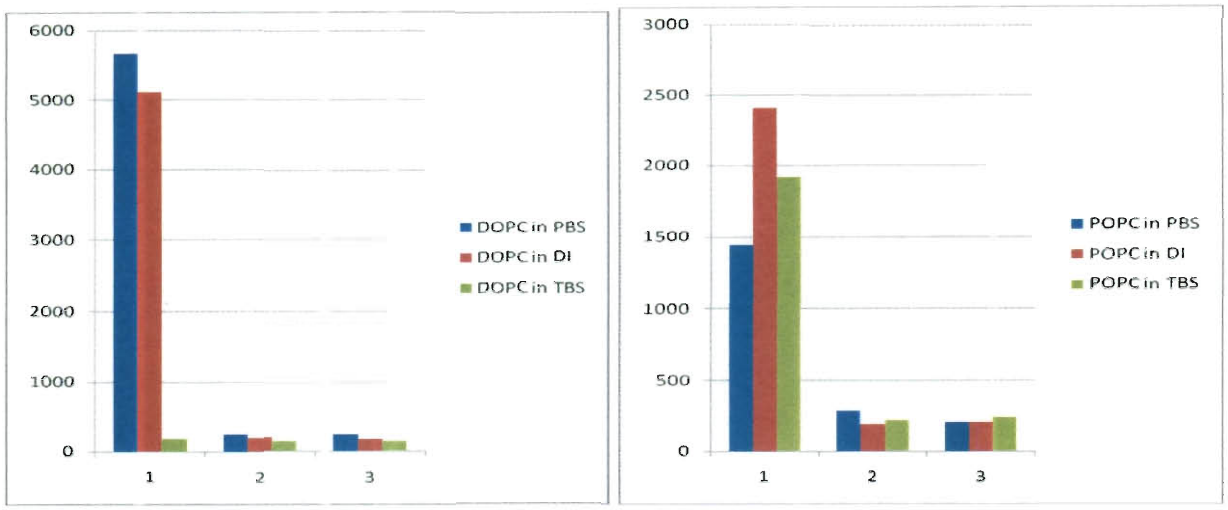

(a) (b)

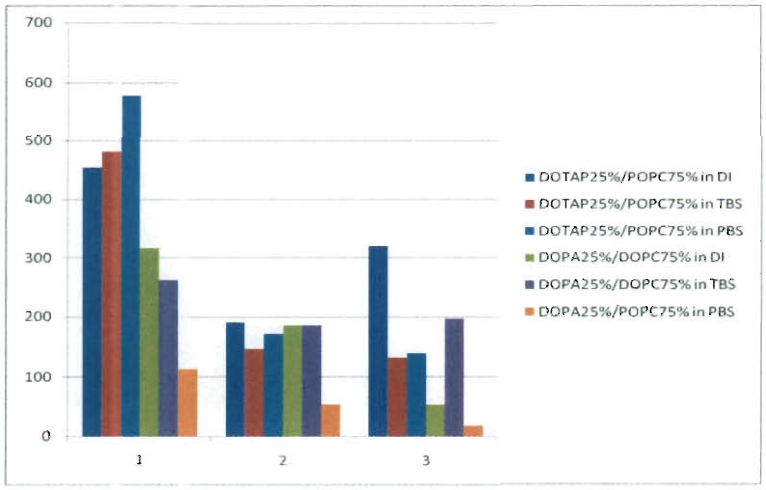

(c)

Figure A.1. Lipid vesicle size determined by DLS. DLS results for zwitterionic lipids (POPC and DOPC), cationic lipid (DOTAP) and anionic lipid (DOPA) are shown. Thses vesicle samples are made using freeze-thaw method. The y-axis stands for the measusred hydrodynamic size in nm, and x-ais stands for the sequential sample number (1: freeze-thawed 20~25 times; 2: then freeze-thawed 3 more times and then extruded 30 times through 100 nm pore-size polycarbonate membranes; 3: then extruded 30 times through 30 nm pore-size polycarbonate membranes).

A.2.2 Vesicles of mixed POPC and lyso-lipid

To make controllable vesicle size with smaller diameter (to achieve SUVs with diameter smaller 60 nm), the attempt to alter the curvature is made by adding cone-shape lyso-lipid in the POPC vesicles. The result is shown in Fig.A.2. The vesicle size is decreased for vesicles with lysoPC 18:1 (MOPC), and the amount of lysoPC 18:1 ranging from 17% to 50% in the POPC vesicle does not make a significant size difference. It is thought that the lyso-lipids prefer to stay in the outer leaflet of the membrane because of the geometry effect. As a result, incorporating cone-shape lyso-lipids into the membrane can increase the membrane tolerance to higher curvature, which indicates smaller sized vesicles can be obtained.

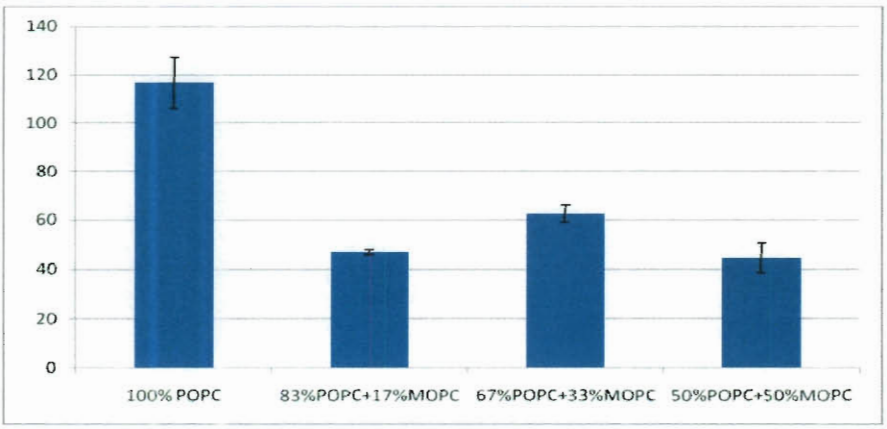

Figure A.2. Lipid vesicle size determined by DLS. Thses vesicle samples are made using extrusion method (extruded 30 times through 100 nm pore-size polycarbonate membranes) in PBS buffer. The y-axis stands for the measusred hydrodynamic size in nm, and x-ais stands for the sample constitutes.

A.3 Techniques to Characterize SLBs

A.3.1 SLB Fluidity Determined by Fluorescence Recovery After Photobleaching (FRAP)

A.3.1.1 POPC SLB on Glass

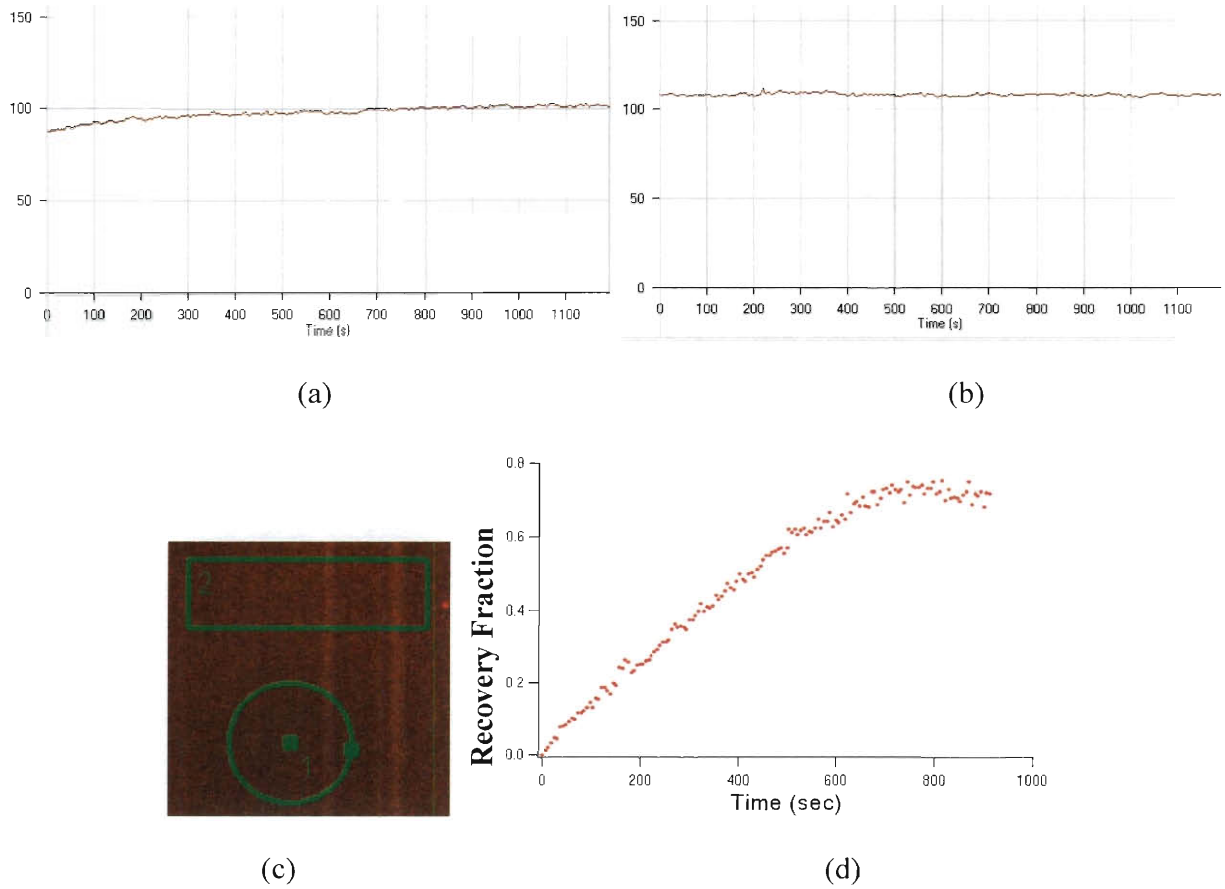

Figure A.3. Fluorescence Recovery After Photobleaching (FRAP) experiment for POPC SLB on a glass slide. (a) and (b) are the fluorescence intensity of the region of interest (ROI) 1 and 2 in (c). ROI 1 is the bleached region, while ROI 2 is the reference. (d) Recovery fraction over time.

A.3.1.2 POPC SLB Penetrated by C_{60} Nano-aggregates on Glass

As a simple trial experiment, carbon nanoparticles (C_{60}) are added onto the SLBs to see if the C_{60} can change the fluidity of the SLBs. It is thought that after contacting with lipid membranes, C_{60} may penetrate into the hydrophobic region of the bilayer and perturb the configuration of lipid alkyl chains. The C_{60} particle solution is a kind gift from Ping Zhang from the Thomson group (Civil and Environmental Engineering, Rice University) and is dissolved in

toluene as received. It is then sonicated for 30 min in pure water and diluted by 20 same volumes of 2 mM PBS buffer. The C_{60} aggregates are determined to have a diameter of 35.2 nm and zeta potential of -6.19 mV. After flowing through the lipid bilayer, the $C6_0$ solution was held inside the chamber for 20 minutes. The FRAP results (Fig. A.4) show that the C_{60} nanoparticles can enhance the recovery percentage by 20%, while the diffusion coefficient remains similar to a pure POPC SLB. The calculated values are: $t_{1/2}$=294.33 sec, D_f=1.47 and R=0.95. It is thought that the C_{60} nanoaggregates penetrate into the hydrophobic region of the bilayer and perturb the tight packing of the lipid alkyl chains. Thus the bilayer with C60 nanoaggregates has higher lateral mobility than the bilayer without. [3-5]

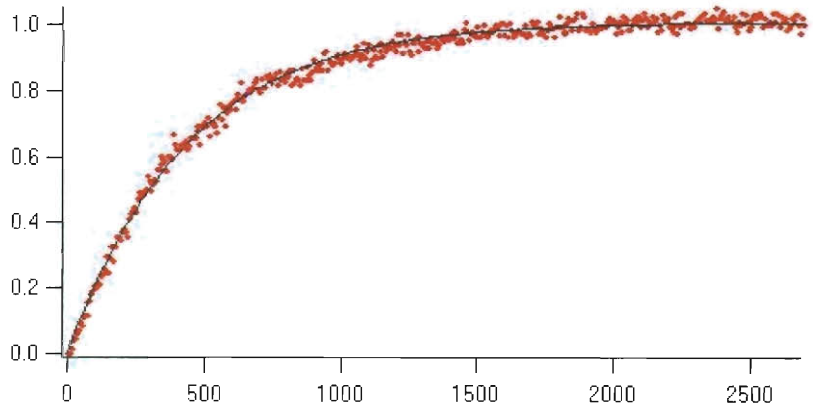

Figure A.4. FRAP experiment for POPC–C_{60} nanoparticle aggregates SLB on a glass slide.

A.3.2 SLB Thickness Determined by Imaging Ellipsometry (IE)

Ellipsometor can achieve angstrom resolution in z-direction and is suitable for measuring supported lipid bilayers which have thickness in nanometer scale. The working principles are described in Chapter 3. To measure the thickness of a SLB in an aqueous environment, a fluid

cell is used for the setup. The SLB is formed by vesicle fusion method and immersed in water in a fluid cell of 3 ml volume (Nanofilm Technologie, Göttingen, Germany), and the substrate used in the fluid cell is silicon wafer pre-cleaned with piranha for the formation of SLBs. On the top chamber of the fluid cell there are two glass windows for focusing the incoming laser beams on the silicon substrate. A peristaltic pump is used to control the inlet and outlet fluid which pass through the fluid cell.

The detector measures the R_p/R_s values using null method and obtains Δ and Ψ. Scanning the surface with varying wavelengths of light can give characteristic plots for both Δ and Ψ, as shown in Fig. A.5.

The imaging ellipsometry combines capabilities of classical ellipsometry and microscopy together and provides film thickness not only at a point but a 2-D plane. Thus, the imaging ellipsometry uses CCD as it detector and has advantages over the traditional ellipsometry in visualizing a film when surface morphologies and surface patterns of the film are of interest. The imaging ellipsometor used here is an Elli2000 model and is developed by Nanofilm (merged to Accurion GmbH; Göttingen, Germany). It has has an xy-resolution of approximatly 1 μm. Integrating the 2-D plane of region of interest with the thickness of each point, a 3-D contour plot is shown in Fig. A.6.

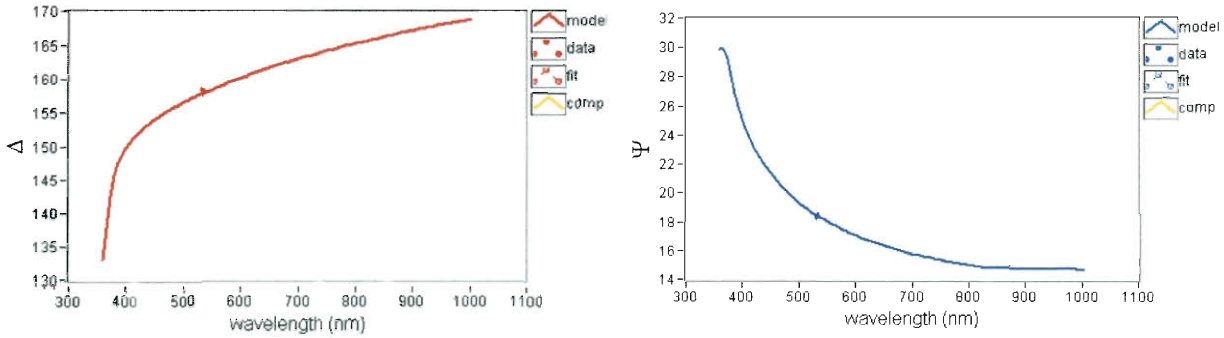

Figure A.5. Nulling 1-zone result of the Δ and Ψ of the water/SLB/SiO_2/Si layered film at 532 nm light source. The datum dot in each figure is fitted with the theory, which predicts the Δ and Ψ for the laser wavelengths from 380 ~ 1000 nm. The fitting result converges and gives a SLB thickness and the refractive index of the SLB.

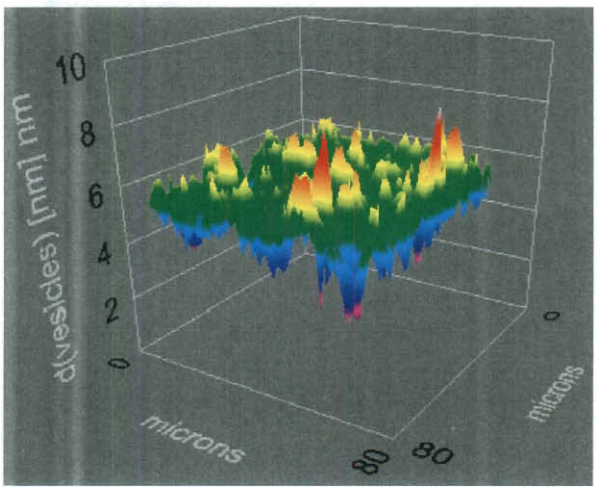

Figure A.6. Fitted image of a POPC SLB supported on a silicon wafer obtained by imaging elliposometry. Along bilayer xy plane, dimension is 80 μm by 80 μm; while in z axis, the scale is down to nanometer. The average thickness is close to 5 nm. Several spikes on the membrane surface indicate either defects or vesicles not fully fusing onto the silicon wafer surface pre-treated with acid piranha solution.

A.3.3 SLB Mass Determined by Quartz Crystal Microbalance with Dissipation (QCM-D)

Using the QCM-D to detect the mass of supported lipid bilayers is a convenient way to check the integrity of the bilayers on different surfaces. The working principles of QCM-D are described in Chapter 3. On the SiO_2 surface, the characteristic curves of a good SLB is shown in Fig. A.7. A frequency change of 25~26 Hz indicates a SLB which full covers the SiO_2 surface of the crystal, and the small dissipation ($<10^{-6}$) indicates a thin SLB without adsorbed vesicles which are not ruptured. During the first 10 min, the overtones of the fundamental resonance split due to the mixed lipid vesicle and bilayer on the surface. The overtones overlap after 10 min of the introduction of lipid vesicles, and the SLB is complete. The SLBs are stable for hours on the SiO_2 surface of the quartz crystals

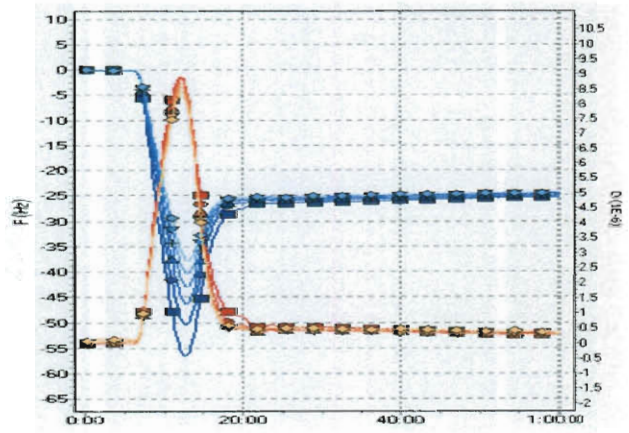

Figure A.7. Characteristic frequency (blue lines) and dissipation (red lines) curves of SLB formation on SiO_2 surfaces sensed by the QCM-D. Overlaped curves are overtones of the fundamental resonance of the quartz crystals.

A.4 Preparation of Microcantilevers

A.4.1 Thermosensitivity

Considering the bimetallic effect in the microcantilevers, the two composite materials, a

thin gold film evaporated uniformly on the substrate, and a silicon substrate. The deflection-temperature relation is derived as follows: [6-8]

$$\Delta z = \frac{3(\alpha_f - \alpha_s)L^2(t_s + x)}{t_s C}\Delta T \text{, where the constant } C = 6 + 6x + 4x^2 + \frac{E_f}{E_s}x^3 + \frac{E_s}{E_f x}. \quad \text{(A.3)}$$

The x is the ratio of thin film thickness t_a to the substrate thickness t_s. E_f, and E_s are the Young's modulus for the film and the substrate, and α_f and α_s are the thermal expansion coefficients. For the microcantilever used in this thesis, the values for the parameters are:

$\alpha_{gold} = 14.2 \times 10^{-6}\ K^{-1}$

$\alpha_{silicon} = 2.59 \times 10^{-6}\ K^{-1}$

$E_{gold} = 79$ GPa

$E_{silicon} = 169$ GPa

$t_{gold} = 20$ nm

$t_{silicon} = 1$ μm

L = cantilever length.

Cantilevers of 500 and 750 μm long can be obtained from Concentris, while the 500 μm one is used throughout the thesis. The C constant is calculated to be 113.1. The thermosensitivity is defined as the deflection value changed per 1 K of temperature change. Following the equations above, the calculated thermosensitivity for cantilevers of 500 and 750 μm long are listed in TableA.1:

L (μm)	Δz /ΔT (nm/K) calculated	Δz /ΔT (nm/K) experimental
500	78.54	-75.52 ± 4.50
750	176.7	-

TABLE A.1. Comparison of calculated and experimental thermosensitivity for 500 and 750 μm long microcantilevers.

Using the material properties of gold and silicon, 1 K temperature change causes the surface stress change of 18.38 mJ/m^2 (or mN/m) for a 500 μm long cantilever, which is converted from the deflection value, 78.54 nm. The cantilevers are tested for thermomechanical properties under water (PBS buffer at pH7.4). Experimental thermosensitivity measurements are shown in Fig. A.8 and are close to calculated values.

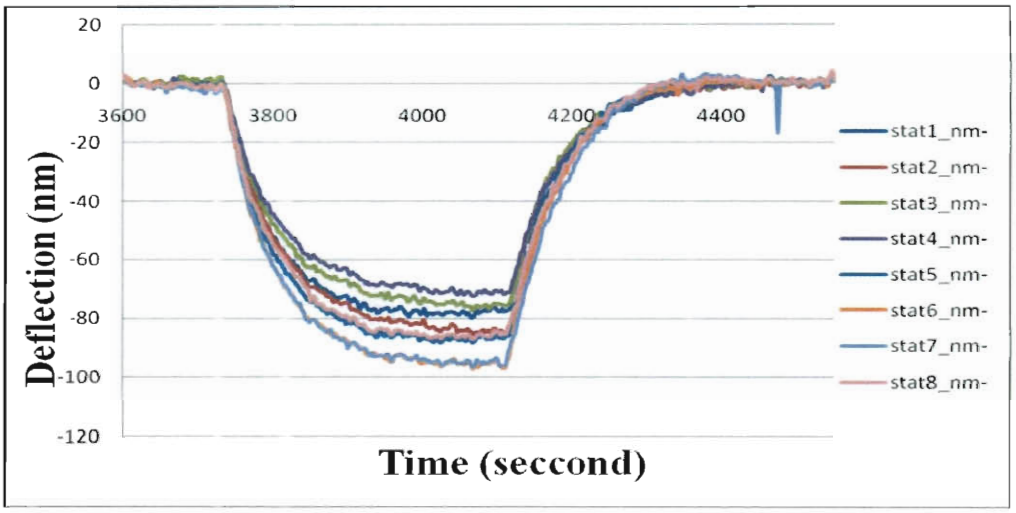

Figure A.8. Themperature response of a 500 μm long microcantilever array of eight cantilevers (stat1 ~ stat 8) for temperature change from 25 °C to 26 °C (ΔT = 1 K). Data for obtaining the averaged thermomechanical sensitivity for each cantilever are taken when the deflection values stabilized. For example, during 4050 ~ 4100 sec.

A.4.2 Functionalization of Microcantilevers

Functionalization of individual cantilevers are done using microcapillaries (See Fig. A.9) Each cantilever is alighed with the desinated microcapillary using a micromanipulator. Then insert the desired cantilever into a capillary filled with reagent. It is recommanded to avoid using

solvent with high volatility, because the vapor can cross-contaminate the neighbor cantielvers. The functionalization time usually lapse for 1~2 hours. For reagent solution with volatility higher than water, it is recommanded to slide the cantilevers in only cover 2/3 length of the capillary to prevent solution overflowing to the adjecent cantilevers.

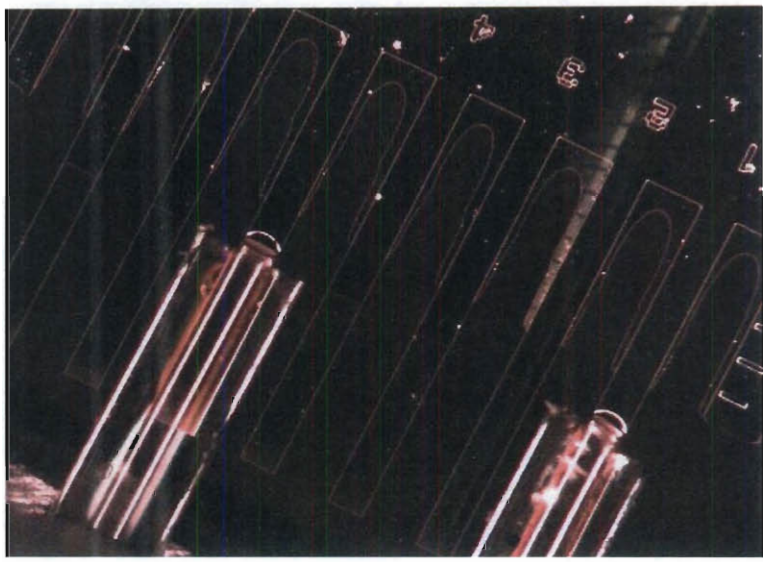

Figure A.9. of microcantilever array ndividual cantilevers are alighed with each microcapillary on a micromanipulator and then immerse in the grafting molecules in the microcapillaries for 1~2 hours.

A.4.3 Regeneration of Used Microcantilevers

The steps for regenerating used microcantilevers:

1.Etch the gold film by Dip the used cantilevers into pure gold etchant for 10 seconds. Dry it with a paper towel.

2. Clean the SiO_2 side. The cantilever array is then plunged into warm piranha solution (H_2SO_4:H_2O_2 = 7:1 at 90°C) for 10 seconds using a Teflon tweezer. Then dip it into DI

water for cleaning.

3. Arrange the cantilevers on a glass slide and paste them on the surface with single-side tapes. Use clean-room compatible tape.
4. Evaporate 3nm of Ti or Cr film on the front side of the cantilever arrays followed by new 20nm gold film in an E-BEAM evaporator in the clean room.
5. Take the microcantilever arrays out from the tape, and the microcantilevers are ready to use.

A.5 Protocol of Preparing Giant Unilamellar Vesicles (GUVs) by Electroformation

The steps for preparing GUVs by electroformation are: (main ref: Robert Raphael Lab and Huey Huang Lab, Rice University) [9]

1. Prepare 200 mM sucrose solution (1.37 g of sucrose in 20 mL water) and 200 mM glucose solution (0.68 g in 20 mL water). The sucrose is going to be encapsulated inside GUVs, while the glucose is outside the GUVs. The density difference can precipitate the GUVs down to the bottom of the observation chamber. Also, the reflective index difference between sucrose and glucose solutions will enhance the image contrast (otherwise, the GUVs are invisible under microscopes). If intending to let GUVs float freely, use only water, inside and outside of GUVs. Use syringe filters to get rid of impurities.
2. Prepare the ~0.5 mg/mL lipid solution dissolved in chloroform: Tetrafluoroethylene (TFE) = 1:1 v%. (ex. 50μL of stock 25 mg/mL DOPC in chloroform + TFE 1mL + chloroform 1 mL).
3. Coat two ITO-coated glass slides with 40 μL of solution 2 on each. Let the lipid film

dry evenly. Then place the two ITO slides in vacuum for 20 minutes.

**To make monodispersed size of GUVs, modify step 3 by:

(i) Prepare a PDMS stamp with circular pillar patterns of 20 μm (soft lithography).

(ii) Form a thick lipid film on a regular glass slide.

(iii) Transfer the lipid film from the glass slide to two ITO slides using the stamp, as shown in Fig. A.11.

4. Assemble the o-ring chamber as shown in Fig. A.10. Glue one side of o-ring with silicone glue, and then sandwich the three pieces with clips. Filled the o-ring chamber with sucrose solution, as prepared in step 1, before champ the sandwich with clips.
5. Clip each ITO slides with alligator clips. Apply AC current through the ITO slides. The protocol for DOPC is: 10 Hz for 80 min, then 5 Hz for 20 min, and finally 1 Hz for 20 min.
6. Disassemble the chamber. Pipette out the solution from the o-ring chamber into glucose solution prepared in step 1.

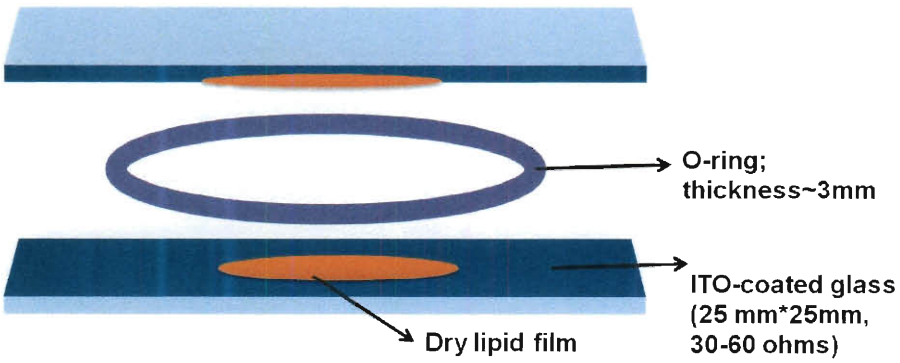

Figure A.10. Chamber for GUV electroformation. An alternative chamber can be made using PDMS of similar shape instead of using o-rings.

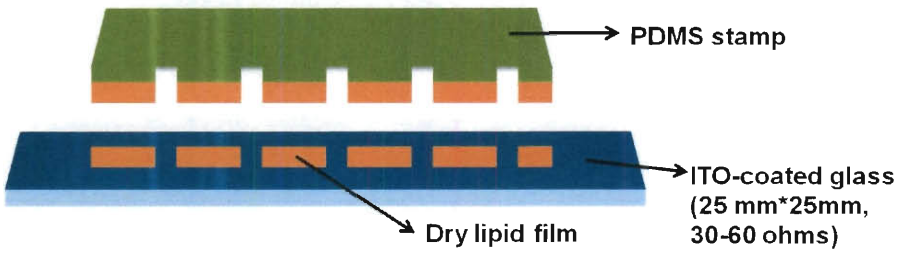

Figure A.11. Soft lithography method used to pattern dry lipid films with same sizes. This method will lead to monodispersed GUVs.

A.6 References

(1)Mayer, L. D.; Hope, M. J.; Cullis, P. R. *Biochim. Biophys. Acta* **1986**, *858*, 161-168.

(2)Hope, M. J.; Bally, M. B.; Webb, G.; Cullis, P. R. *Biochim. Biophys. Acta,* **1985**, *812*, 55-65.

(3)Qiao, R.; Roberts, A. P.; Mount, A. S.; Klaine, S. J.; Ke, P. C. *Nano Letters* **2007**, *7*, 614-619.

(4)Spurlin, T. A.; Gewirth, A. A. *Nano Letters* **2007**, *7*, 531-535.

(5)Wong-Ekkabut, J.; Baoukina, S.; Triampo, W.; Tang, I. M.; Tieleman, D. P.; Monticelli, L. *Nature Nanotechnology* **2008**, *3*, 363-368.

(6)Thundat, T.; Warmack, R. J.; Chen, G. Y.; Allison, D. P. *Appl. Phys. Lett.* **1994**, *64*, 2894-2896.

(7)Mertens, J.; Finot, E.; Thundat, T.; Fabre, A.; Nadal, M. H.; Eyraud, V.; Bourillot, E. *Ultramicroscopy* **2003**, *97*, 119-126.

(8)Barnes, J. R.; Stephenson, R. J.; Woodburn, C. N.; Oshea, S. J.; Welland, M. E.; Rayment, T.; Gimzewski, J. K.; Gerber, C. *Rev. Sci. Instrum.* **1994**, *65*, 3793-3798.

(9)Angelova, M. I.; Soléau, S.; Méléard, P.; F., F.; P., B. *Progr Colloid Polym Sci* **1992**, *89*, 127-131.